University of Cape Town

Department of Human Biology
Division of Biomedical Engineering
in association with the
Cardiovascular Research Unit
Chris Barnard Division of Cardiothoracic Surgery

High Porosity Electrospun Scaffolds for Small Diameter Vascular Graft Applications

Submitted to the University of Cape Town
In fulfilment of the requirements for the degree
MSc(Med) in Biomedical Engineering

Author: Jason Voorneveld

Supervisor: Assoc. Prof. Deon Bezuidenhout
Co-Supervisor: Assoc. Prof. Thomas Franz

Submitted: April 16, 2015

Abstract

Porosity, pore size and pore interconnectivity have been shown to be critical factors for cellular infiltration into vascular grafts. While electrospinning has been shown to produce many promising characteristics for the fabrication of vascular graft scaffolds, it has yet to create sufficient porosity for transmural endothelial in-growth. This study was aimed at using dual electrospinning with sacrificial fibre extraction to produce scaffolds with controllable porosity characteristics while maintaining sufficient structural strength to resist deformation during implantation. Scaffolds were subsequently covalently grafted with heparin, a known anti-coagulant with growth-factor binding properties.

Poly(ethylene oxide) (PEO) and Pellethane® (PU) were spun simultaneously and subsequently PEO was selectively extracted to create additional void space within the fibrous structure. Low, medium and high porosity scaffolds (76%±0.2%, 83%±0.5% and 90%±1.0% respectively) along with their heparinized versions were analysed *in vitro* for pore size, porosity, fibre morphology and mechanical properties; and *in vivo* for cellular infiltration, vascularisation, collagen deposition and inflammation subcutaneously in male Wistar rats (7,14 and 28 days, n = 6).

The tensile strength ($\sigma_t = -44P + 41$ MPa, r^2=0.96) and elastic modulus ($E = -9.2P + 9.0$ MPa, r^2=0.97) of the constructs decreased linearly with increasing porosity (P) (post PEO removal) and the heparinization process resulted in decreased strength (8.4±4.9MPa to 2.2±1.1 MPa, p<0.02) but slightly increased stiffness (9.0±0.6 MPa to 9.7±1.2 MPa, p<0.001) when compared to non-heparinized scaffolds (100% PU). Calculated compliance values increased with increases in sacrificial fibre fraction ($C_{d[PU]} = -0.078FF_{PU} + 10.3$ %/100mmHg, $r^2 = 0.72$, p<0.001 and $C_{d[PU+Hep]} = -0.038FF_{PU} + 6.93$ %/100mmHg, $r^2 = 0.45$, p<0.05) and closely matched the compliance values of the human popliteal artery reported in literature. Average pore-size for low, medium and high porosity scaffolds was 4.0±2.3µm, 9.9±4.2µm and 11.1±5.5µm (p<0.0001). Heparinization resulted in increased fibre diameter (3.6±1.1µm vs 1.8±0.8µm, p<0.0001) but did not influence pore-size (p>0.66).

Cellular infiltration for low, medium and high porosity scaffolds reached 33±7%, 77±20% and 98±1% of scaffold width respectively by day 28 of implantation (p<0001); heparinizа-

tion did not influence infiltration.

Electrospun grafts with selectively extracted sacrificial fibres allowed for tunable porosity and pore-size. Increasing porosity resulted both in predictable losses to mechanical strength and improvements to cellular infiltration which could prove to be a useful optimization parameter for vascular grafts. This method of electrospinning shows great promise for fabrication of synthetic vascular graft substitutes, for the purpose of producing spontaneous transmural endothelialisation, and warrants further study in a circulatory model.

Acknowledgements

The completion of this thesis, in all its multidisciplinary complexity, would not have been possible were it not for the diverse group of peers and mentors at the Cardiovascular Research Unit of UCT. I am sure that I have received assistance from every single person in the unit at least once during my stay but the people mentioned below have played an integral role in the success of this project and in my personal development.

Firstly, I would like to thank my supervisor, Deon Bezuidenhout, who enthusiastically captured me into the project and patiently mentored me through to its completion. I will not forget the time, energy and funding he dedicated to my development, even when each was in short supply, he still made a plan to make sure that I could carry on moving forward. If I ever make something of myself in this field, I have him to thank for it. I would also like to thank my co-supervisor, Thomas Franz, for his assistance in designing and interpreting the mechanical testing aspects of the project.

I would like to extend a special thanks to two people in the research unit, Anel Oosthuysen and Helen Ilsley for carrying out the heparinization process and histological processing respectively. These ladies not only carried me through large portions of my project but taught me a great deal about their fields, dedicating not days but weeks to myself and my project, for which I am truly thankful. I would also like to thank Dale McWilliam for his tireless dedication and precision in helping with the tensile testing experiments.

Another especially notable thanks must go to the FHS RAF team, specifically Rodney Lucas, Janet McCallum, Emma Alsop and Kim Tutt for their assistance with the animal experiments, another team who made it clear that they personally invest in the work that they do to ensure success.

With the broad range of imaging modalities used in this thesis I have come to rely on the expertise of many knowledgeable and patient individuals. Notably: Miranda Waldron for her assistance with SEM, Susan Cooper and Dirk Lang for the many hours they sat with me behind the confocal microscope, Anton Du Plessis and the NanoCT unit at the University of Stellenbosch who kindly offered scans of my scaffolds free-of-charge and finally Willem Swart from IMP Scientific & Precision and the team at Phenom World

for lending us their desktop SEM that is every electrospinner's dream. I would also like to thank Joel Du Toit, David Conradie, Johan Coetzee and Jandre De Villiers for their patience in explaining even the simplest aspects of polymer science to me. Similarly, I would like to thank Neil Davies for his assistance in analysing histological data.

Last, but certainly not least, I would like to thank my friends Danie Kritzinger and Jeandre Gerding for encouraging me to take the leap from a paid salary as an engineer to pursue my dreams of developing medical devices through the long and trying road of academic life. Who would I be if I did not give thanks to the extra special Jenna Diamond, who has paid the price of this Master's degree with me at every step. Finally, I give thanks to the person whom I owe every ounce of my success to, Anne Voorneveld, for instilling in me the idea that I can do anything I put my mind to.

I also acknowledge the National Research Foundation and the Cardiovascular Research Unit, University of Cape Town for funding this study, thereby making it all possible.

Declaration

I, **Jason Voorneveld**, hereby declare that the work on which this thesis/dissertation is based is my original work (except where acknowledgements indicate otherwise) and that neither the whole work nor any part of it has been, is being, or is to be submitted for another degree in this or any other university. I authorise the University to reproduce for the purpose of research either the whole or any portion of the contents in any manner whatsoever.

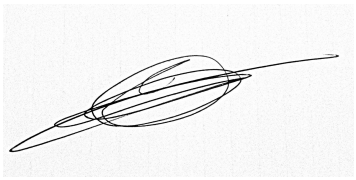

Signature: _____ Date: April 16, 2015

Table of Contents

List of Tables

List of Figures

Glossary

Ex Vivo	Testing in tissue that has been excised from a living organism.
In Vitro	"In Glass", Testing physiological phenomena outside of the physiological context.
In Vivo	Testing inside a living organism.
Abluminal	The outer surface of a hollow organ.
Allograft	Vessel transplanted between different individuals of the same species.
Anastomosis	Surgical union of two hollow organs, synthetic or biological..
Anisotropy	A property of being directionally dependant.
Atherosclerosis	Plaque deposition in the luminal surface of blood vessels causing vessel hardening and constricted blood flow.
Autograft	Vessel harvested from patients own body for transplant at a different site.
Biodegradable	The ability of a material to degrade under physiological conditions whether hydrolytically or enzymatically.
Dielectric Constant	A measure of the permittivity of a material expressed as a ratio relative to the permittivity of a vacuum.
Endothelium	A layer of epithelial-like cells lining the luminal surface of certain organ cavities, such as blood vessels.
Fibre Fraction	The ratio of structural fibres mass to total mass of the scaffold (including sacrificial fibres).
Gauge Length	The length of a specimen at no load conditions before being subjected to tensile strain.
Graft	A replacement for a blood vessel either biological or synthetic.
Hyperplasia	Abnormal growth caused by excessive proliferation of cells.
Luminal	The inside surface of a hollow organ.
Lyophilization	A dehydration process which dries frozen samples by process of sublimation under near-vacuum pressures.
Neovascularisation	Formation of functional microvascular networks.
Patency Rate	The percentage of grafts still patent after a given time period.
Patent	Refers to blood vessels that remain open and unblocked.
Permittivity	A measure of a materials resistance to an applied electric field.
Porogen	A particle used for creating pores within another substance / material / construct.
Proliferation	Dividing of a mother cell into two daughter cells.
Sacrificial Fibre	Refers to the group of fibres present in the scaffold which are removed to generate voids between structural fibre groups.

Structural Fibre	Refers to the group of fibres present in the scaffold which form the remaining architecture after sacrificial the fibre group's removal.
Thick Groups	Scaffolds where PEO fibres were spun using DCM as a solvent to produce thick sacrificial fibres.
Thin Groups	Scaffolds where PEO fibres were spun using EtOH as a solvent to produce thin sacrificial fibres.
Thrombosis	Formation of a thrombus.
Thrombus	A blood clot acting to partially or completely block a blood vessel.
Transanastomotic	Refers to events occurring over the anastomosis of the graft.
Transmural	Refers to events occurring through the wall of the graft.
Xenograft	Vessel transplanted between different species.

Acronyms

2D	Two Dimensional.
3D	Three Dimensional.
AA	Abdominal Aorta.
AAc	Acrylic Acid.
AAm	Acrylamide.
Acr	Acrylated.
AIB	Aortoiliac Bypass.
AIDS	Acquired Immune Deficiency Syndrome.
BPM	Beats Per Minute.
CAD	Computer-Aided Design.
CCA	Common Carotid Artery.
CD	Circumferential Direction.
CHD	Coronary Heart Disease.
CI	Confidence Interval.
Col	Collagen.
CT	Computed Tomography.
CV	Cardiovascular.
DI	Deionised Water.
DMF	Dimethylformamide.
EC	Endothelial cell.
EGV	Inferior Epigastric Vein.
ePTFE	Expanded Polytetrafluoroethlene.
ES	Electrospinning / Electrospun.
EtOH	Ethanol.
FA	Femoral Artery.
FF	Fibre Fraction.
FFA	Fluoroscein Free Acid.
FLA	Femptosecond Laser Ablation.
FLUF	Focused, Low density, Uncompressed nanoFibre.
FR	Flow Rate.
GL	Gauge Length.
H&E	Hemotoxylin and Eosin.
HDF	Human Dermal Fibroblast.

Hep Heparin surface modified.
hFOB Human Fetal Osteoblasts.
hMSC Human Mesenchymal Stem Cells.
HP High Porosity.
HUVEC Human Umbilical Endothelial Cell.
HVPS High Voltage Power Supply.
HVSC Human Vena Saphena Cell.
IND Inter-Nodal Distance.
LP Low Porosity.
LTE Low Temperature Electrospinning.
MDSC Muscle Derived Stem Cells.
MeOH Methanol.
MP Medium Porosity.
MS Musculoskeletal.
n Sample Size.
NA Not Applicable.
NADH Nitrous Acid De-aminated Heparin.
ND Not Determined.
NNC Neonatal Cardiomyocytes.
NR Not Reported.
PA Popliteal Artery.
PAD Peripheral Artery Disease.
PAN Polyacrylonitrile.
PBS Phosphate Buffered Saline (pH = 7.4).
PCL Poly(ϵ-caprolactone).
PDLA Poly(D,L-lactic acid).
PEG Polyethylene glycol.
PEO Polyethylene oxide.
PET Poly(Ethylene teraphthelate).
PGS Poly(glycerol sebacate).
PLA Poly(lactic acid).
PLCL Poly(L-lactide-co-ϵ-caprolactone).
PLGA Poly(DL-lactide-glycolide).
PLL Poly(L-lactide).
PLLA Poly(l-lactic acid).
PMMA Poly(methyl methacrylate).
PSR Picrosirius Red.
PTFE Polytetrafluoroethlene.
PU Polyurethane.
RM Regenerative Medicine.
RT Room Temperature.
SC Subcutaneous.

SD Standard Deviation.
SEM Scanning Electron Microscopy.
SF Silk Fibroin.
TD Transverse Direction.
TE Tissue Engineering.
THF Tetrahydrofuran.
TRI PCL/collagenI/hydroxyapatite.
US Ultrasonication.

Nomenclature

$\boldsymbol{C_d}$	Diametral Compliance.
$\boldsymbol{D_d}$	Inner Diameter at Diastolic Pressure.
$\boldsymbol{d_i}$	Inner Diameter.
$\boldsymbol{d_o}$	Outer Diameter.
$\boldsymbol{D_s}$	Inner Diameter at Systolic Pressure.
$\boldsymbol{d_t}$	Tissue Infiltration Depth.
$\boldsymbol{E}$	Young's Modulus.
$\boldsymbol{\epsilon}$	Strain.
$\boldsymbol{C}$	Concentration (mass/volume).
$\boldsymbol{Q}$	Volume Flow Rate.
$\boldsymbol{\eta}$	Efficiency Factor.
$\boldsymbol{FF_{PU}}$	Polyurethane Fibre Fraction.
kg	Kilogram.
$\boldsymbol{m}$	Mass.
$\boldsymbol{m_{after}}$	Mass of scaffold after sacrificial fibre removal.
$\boldsymbol{m_{before}}$	Mass of scaffold as spun / before sacrificial fibre removal.
µl	Microlitre.
mm	Millimetre.
µm	Micrometre.
ml	Millilitre.
mmHg	Millimetres Mercury.
MPa	Mega Pascal (N/mm^2).
$\boldsymbol{m_{PEO}}$	Mass of polyethylene oxide present in the scaffold.
$\boldsymbol{m_{PU}}$	Mass of polyurethane present in the scaffold.
$\boldsymbol{P}$	Porosity.
$\boldsymbol{P_d}$	Diastolic Pressure.
$\boldsymbol{P_i}$	Luminal Pressure.
$\boldsymbol{P_s}$	Systolic Pressure.
$\boldsymbol{\rho}$	Density.
$\boldsymbol{r_i}$	Abluminal Radius.
$\boldsymbol{r_o}$	Luminal Radius.
RPM	Revolutions per Minute.
$\boldsymbol{\sigma_h}$	Hoop Stress.

$\boldsymbol{\sigma_t}$	Tensile Stress.
$\boldsymbol{t_{systole}}$	Systolic Period.
$\boldsymbol{V_a}$	Volume after sacrificial fibre removal.
$\boldsymbol{V_b}$	Volume before sacrificial fibre removal.
$\boldsymbol{V_f}$	Fibre Volume.
$\boldsymbol{w_s}$	Scaffold Width.

Chapter 1

Introduction

1.1 Background

Atherosclerosis is the leading cause of death worldwide, causing nearly three quarters of all cardiovascular diseases [1]. Presently the most effective method of treating atherosclerosis is by surgical intervention whereby the afflicted artery is bypassed with a graft. There are three main categories under which vascular grafts can be divided: large calibre grafts with luminal diameters of 8mm or greater; medium calibre grafts with corresponding diameters between 6 and 8mm and small calibre grafts with diameters less than 6mm [2, 3].

For large calibre bypasses, synthetic grafts have been largely successful with the use of expanded Polytetrafluoroethlene (ePTFE) and Dacron® (PET, Poly(Ethylene Teraphthelate)) as graft materials. These same materials have had moderate success in medium calibre applications. However, all synthetic choices have failed dismally in the small calibre arena where the autograft remains the gold standard. The latter, however, is not always available or suitable for use which excludes surgical intervention, reducing life quality and expectancy [4]. This is disconcerting considering that the requirement for small and medium diameter grafts is much greater than for large diameter grafts. In the USA a 1999 study on clinical procedures involving vascular grafts showed that 71% consisted of small diameter vessels, 24% fitting in-between the small and medium diameter classification and only 5% required large diameter vessels [5, 6].

Considering that all coronary and lower extremity peripheral artery bypasses fall into the small to medium calibre classification it is important to note the following statistics:

1. An estimated 6.4% of United States (US) adults over the age of 20 have some form of coronary heart disease (CHD).

2. 2.9% of US adults have had CHD resulting in myocardial infarction.

3. CHD accounted for almost 1 in every 6 deaths in the US. [7]
4. Prevalence of peripheral arterial disease (PAD) is 10%-25% (age >55 years). [8]
5. Patients with PAD are at the same relative risk of death, from cardiovascular causes, as those with CHD or cerebrovascular disease. [8–11]

In South Africa 195 people died per day from some form of cardiovascular disease between 1997 and 2004. This statistic was projected to increase by 41% between 2000 and 2030 despite the overwhelming death rate caused by AIDS [12]. A separate study on rural black South Africans determined that PAD prevalence in the population (542 patients) was significantly higher than global averages [11]. Given these morbid statistics it can be seen that a readily available, small diameter, off-the-shelf prosthetic graft with a satisfactory patency rate would be a welcome addition to the arsenal of tools in the fight against PAD and CHD.

In terms of treatment, a patient has three different options depending on the extent of atherosclerosis present in the artery and the stability of the patient [13]. Pharmacological therapy and risk factor modification is a first choice to patients who have stable, minor lesions. If pharmacological therapy is ineffective then minimally-invasive procedures such as balloon angioplasty, stenting, rotoblation and cutting balloons can be performed. These procedures are minimally invasive due to the use of catheters but require specialized equipment, a great deal of expertise and are not without their risks. As a last resort bypass surgery is performed where grafts are used to bypass the blocked artery. These surgeries are highly invasive with long recovery periods but in many cases are the only option either due to arteries that are beyond repair or inaccessible by the other two treatment options.

As mentioned earlier the autologous graft is not always available or suitable, requires extra surgical time, more patient discomfort postoperatively and donor site morbidity. If a synthetic alternative to the autologous graft could be developed; not only will all patients benefit from not requiring a donor vein/artery but the unfortunate few who do not have an appropriate donor vessel will have, for a first time, a viable alternative.

The primary reasons for failure of small calibre synthetic grafts are thrombosis and intimal hyperplasia (which will be discussed in detail in Section 2.1.4). Essentially both failure modes can be attributed to a combination of compliance mismatch and lack of healthy endothelial cell lining the luminal surface of the graft [14]. The latter of which is believed to be caused by insufficient porosity, pore size and pore-interconnectivity for spontaneous transmural endothelialisation to occur [3, 15, 16].

Currently there is much work being done to solve the patency issues of small diameter vascular grafts. The two main streams of focus at present are tissue engineering and

regenerative medicine. Tissue engineering involves seeding cells *in vitro* onto a tubular scaffold and allowing them to grow into engineered blood vessels that are then implanted as grafts [17]. This method is very labour intensive, expensive, requires specially designed facilities and requires each graft to be matched to a patient by using autologous cells [18].

In contrast regenerative medicine techniques involve implanting an engineered scaffold into the patient and allowing the patient's body to populate the graft with cells. For example, the Wang group have developed grafts which rapidly degrade *in vivo* to make space for cells to grow in its place while still providing cells with chemical and mechanical signals to guide cell differentiation into appropriate tissue [19, 20]. This work, while promising, still requires much optimization before clinical application, part of which is improved porosity to allow for spontaneous transmural endothelialisation.

1.2 Aims of Current Study

In the current study, the regenerative medicine approach is proposed. Current research points to porosity, pore size and pore interconnectivity as being key success factors in creating grafts with long-term patency [2, 3]. Pennel et al (2013) demonstrated that transmural endothelialisation was possible with high-porosity (pore diameter $\approx 150\mu m$) grafts made of foamed polyurethane produced by a phase inversion/porogen extraction technique [16, 21].

This project was aimed at developing a method for creating electrospun (electrospinning is described in detail in Section 2.2) fibrous scaffolds of controllable porosity and mechanical properties and then subsequently modifying the surface chemistry of the polymer for more favourable regenerative outcomes. In order to achieve this goal a two-step fabrication process was designed: firstly dual electrospinning with sacrificial fibres, where a water soluble fibre was included and subsequently removed from the scaffold was employed; followed by surface immobilization with heparin, a known anti-coagulant and anti-thrombotic with growth factor binding properties.

The removal of the sacrificial fibres was expected to increase the void space between the remaining structural fibres making it possible to control porosity depending on the percentage volume of each fibre type incorporated into the scaffold, as has been shown previously by Baker *et al* (2008). However, this study differed from Baker's in that it utilized flow rate as a method of controlling fibre fraction rather than number of spinnerets or spinneret offset, and additionally investigated the effects of sacrificial fibre diameter on scaffold porosity (post sacrificial fibre removal).

It was hypothesized that high porosity scaffolds, with large interconnected pores would

exhibit improved cellular infiltration over low porosity scaffolds.

The results of this thesis would provide information on whether this method has promise for demonstrating spontaneous transmural endothelialisation in a circulatory model.

Objectives The objectives of this thesis were to (See Figure 1.1):

1. Modify and upgrade the existing electrospinning equipment to allow for dual-spinning.
2. Develop the dual electrospinning method to accommodate the fabrication of small diameter vascular grafts.
3. Optimise the spinning of PEO to produce either thin or thick fibres.
4. Show scaffold porosity and pore size increase with increasing PEO fibre weight percentage (fibre fraction).
5. Determine effects of sacrificial fibre diameter on porosity, pore size and mechanical properties.
6. Immobilize heparin on the surface of the scaffold structural fibres.
7. Determine effects of heparinization on porosity, pore size and mechanical properties.
8. Determine effects of porosity and pore size on cellular ingrowth and healing response *in vivo* (rat subcutaneous model).
9. Determine effects of heparinization on cellular ingrowth and healing response *in vivo*.

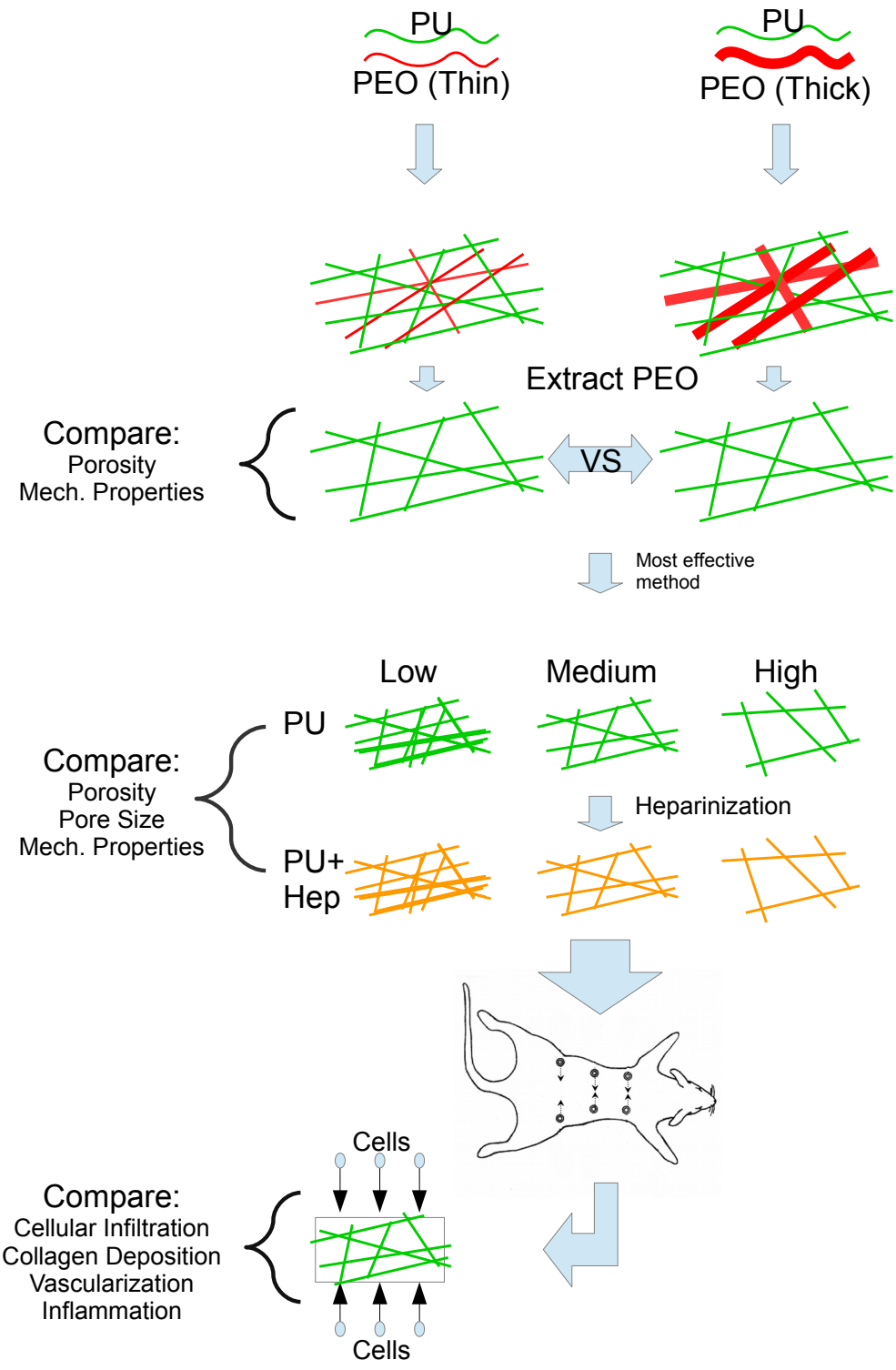

Figure 1.1: Graphical abstract of project objectives: Effectiveness of inclusion and subsequent removal of thin versus thick sacrificial fibres was assessed and compared. The most effective method was then used to create low, medium and high porosity scaffolds which were then heparinized and assessed for porosity, pore size and mechanical properties before being implanted *in vivo* in a rat subcutaneous model to assess healing response. (Rat cartoon adapted from [22])

Chapter 2

Literature Review

2.1 Vascular Grafts

2.1.1 Brief History of Vascular Grafts

The first recorded vascular surgery repair occurred in 1759 when Hallowell and Lambert repaired a brachial artery with a suture. More than a century later the first vascular anastomosis was successfully performed on a canine model by Nicholai Eck in Pavlov's laboratory. Robert Abbe documented the first prosthetic graft implant in 1894 by placing hour-glass shaped tubes in the proximal and distal lumens of a feline aorta. The glass tubes were then enclosed in silk and sutured to the vessels on either side of the tube. [23].The study of vascular repair then accelerated in the early 20th century resulting in numerous breakthroughs with arguably the most prevalent being the first autograft procedure by Goyannes in 1906 with the repair of a popliteal artery aneurysm by transplanting it with a harvested popliteal vein from the same patient. [2]

Almost half a century later, in 1952, Voorhees created prosthetic grafts from a material named Vinyon "N" cloth, first documenting the importance of porosity in vascular grafts [24]; he used this material as a bypass graft for the abdominal aorta in 15 canine models with a relatively high success rate [24] which led to the materials use 2 years later in the surgical treatment of aneurysms of the abdominal aorta in humans [25].

The next 60 years would see polyethylene terephtalate (PET, Dacron®) and expanded polytetrafluoroethylene (ePTFE) grafts forming the gold standard for large calibre vascular prosthesis, while the autograft remains the gold standard for small and medium calibre bypass grafts to this day [2, 26].

2.1.2 Types of Grafts

Principally there are two different graft types available: Biological or synthetic. The former referring to the use of veins or arteries harvested from autologous, homogeneous or xenogeneic sources. Both synthetic and biological grafts can be modified further, either chemically for *in vivo* regeneration of native tissue or tissue engineered with a patients' own cells *in vitro* to improve healing outcomes [5, 27]. The subsections to follow will go into more detail on each type.

2.1.2.1 Biological Grafts

Autografts are veins or arteries extracted from elsewhere in the patients own body. In vascular replacement surgery of small and medium sized grafts the autologous vessel remains the gold standard to this day.

In the case of a coronary artery bypass the vessels of choice are the internal mammary arteries (left and right), greater saphenous vein (SVG), radial artery and the gastroepiploic artery [5, 28]. However, the surgeons decision on which vessel to use as a graft is not as simple as going down a list, there are many factors that need to be taken into consideration such as diseased vessel position; graft length requirements; calibre and compliance matching between vessel and graft; age and mobility of the patient and consideration for donor site morbidity [26, 28, 29].

Peripheral or lower limb bypasses regularly utilise the SVG as a first choice which can either be removed completely and reconnected as a bypass by reversing the direction of the vein *(ex vivo)*, or by anastomosing the SVG to the required sites on the target artery while leaving the SVG in place *(in situ)*. *In situ* bypasses require that the internal valves be removed to allow reverse direction flow but the advantage is that the *vasa vasorum* remain intact [2, 5, 30].

The desirability of autografts lie in their inherent immuno-compatibility and preservation of at least a proportion of their endothelial lining (surgical procedures are known to cause damage to the endothelial lining, especially in the case of SVGs [31,32]). However, it has been noted that autologous grafts are also susceptible to occlusion despite their superior biological composition [33].

Even though the autograft remains the dominant clinical solution in small to medium sized vessels, they exhibit various disadvantages that are not easily addressed [2] [5]:

- The donor vessel is not always available or suited for transplant.
- The associated donor site morbidity.

- Venous substitutes are not always capable of handling the hemodynamic forces associated with arterial circulation.
- The increased surgical time required to extract the donor vessels.

Allografts (Homografts) refer to the use of donor vessels from the same species but from a different individual. These types of grafts have been largely abandoned due to the practicalities of storage and/or sourcing the donor vessels. Fresh vessels placed in cold storage or cryopreserved vessels extracted from cadavers were used before synthetic grafts were accepted as a more viable option for large type grafts.

The biocompatibility of allografts is not always preserved as in autografts and the healing response of the grafts resembles atherosclerosis which leads to low patency rates over the long term [5].

Xenografts (Heterologous grafts) are grafts made from similar vessels extracted from a different species. Similar to allografts, xenografts (in their cellularised state) have been widely abandoned after the development of viable synthetic alternatives due to infection, antigenicity and storage concerns as well as a high incidence of thrombosis [34–36].

However, decellularised xenogenic tissues are still researched as scaffolds for tissue engineered vessels either in their decellularised form or after *in vitro* tissue culture [37–40]. While these constructs have shown promising results in animal models for large and medium calibre vessels, occlusion, intimal hyperplasia and incomplete endothelial coverage are observed for small calibre vessel [39–43].

2.1.2.2 Synthetic Grafts

PET (polyethylene terephthalate of the polyster family) also known by the trade-name Dacron®, was first patented in 1950. It is formed into fibres which are bundled into yarns that are either woven or knitted to form grafts.

The biomechanical properties of Dacron grafts depend on how the yarns are assembled, they can either be woven in an over-under fashion in a criss-cross structure or knitted by looping the filament bundles around one-another (see Figure 2.1). Woven Dacron is stiffer, stronger, less porous and resists kinking more than its knitted counter part [3]. Knitted Dacron exhibits anisotropic behaviour and its bio-mechanical properties will change depending on whether the wound filaments (yarns) are knitted circumferentially (weft-knit) or longitudinally (warp-knit). Weft-knit grafts were reported to dilate and unravel and so research moved to focus on warp-knit type grafts [2]. Warp-knit type grafts

exhibit greater porosity and compliance than woven Dacron grafts while still retaining sufficient strength to resist bursting and facilitate suturing [5].

Dacron grafts are a surgeon's first choice for the replacement of large diameter blood vessels with proven clinical performance and data indicating patency rates as high as 93% after 10 years [44]. However, this performance has not been transferred to small diameter (<6mm) vascular grafts where occlusion is frequent, with patency rates as low as 50% after 5 years [3, 45, 46].

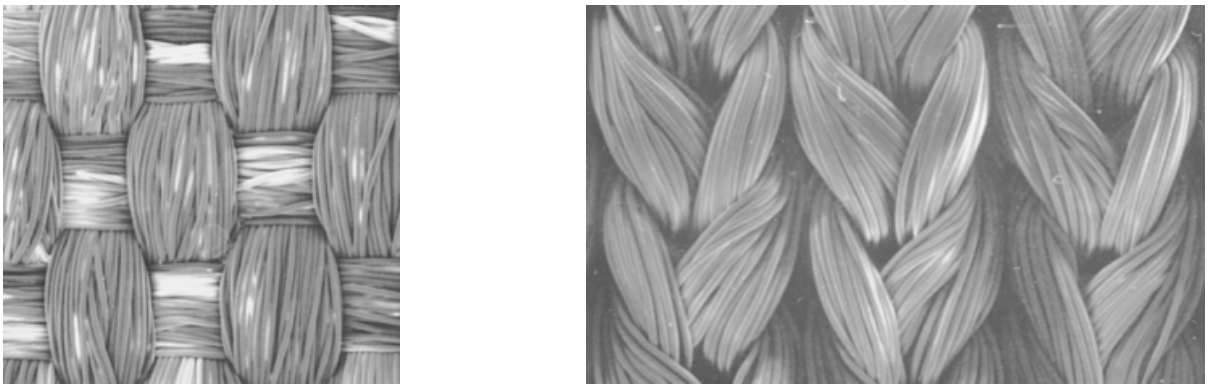

(a) Woven Dacron (b) Knitted Dacron

Figure 2.1: Scanning electron microscopy of (a) woven dacron and (b) knitted dacron. In general knitted dacron has greater porosity with larger pore sizes than woven dacron. [47]

ePTFE (expanded polytetrafluoroethylene) was patented by Wilbert L. Gore as Gore-Tex® in 1969 [2]. It is produced by a ram extrusion process to form a structure consisting of nodes and interconnecting fibrils. ePTFE became popular due to its inert biochemical properties and is the second choice for medium sized vascular replacements (when an autograft is unavailable). ePTFE grafts are preferred over Dacron grafts in peripheral bypass surgeries, and are the most frequently utilized synthetic grafts for the operation, however, evidence for this preferential treatment is unfounded as numerous studies have shown no statistical patency differences between the two graft types when used in this application in humans [45, 48–52].

ePTFE grafts exhibit poor patency rates when used in small calibres (±50% at 5 years [5,53]), where it is thought that the insufficient porosity (preventing transmural endothelialization [3,16]) and compliance lead to thrombosis and intimal hyperplasia, resulting in occlusion [43,48,54]. The porosity of ePTFE is conventionally defined by the inter-nodal distance (IND), however, the practical porosity is far less than the stated IND value due to the tightly packed fibrils between nodes, see Figure 2.2 [3].

Polyurethane (PU) grafts are generally made from segmented thermoplastic elastomers which have been specifically developed for medical applications to be tough,

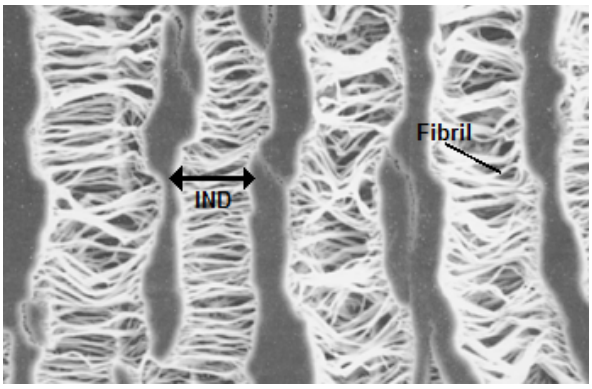

Figure 2.2: Scanning electron microscopy of ePTFE. The nodular structure with the associated internodal distance is depicted in this figure. It can be seen that the quoted IND is not a true representative of porosity due to the interference caused by the fibres crossing between the nodes. [47]

compliant, fatigue resistant and have good biocompatibility and manufacturability properties [5, 55, 56]. Thermoplastic PUs are block copolymers consisting of hard segments (providing stiffness and rigidity) and soft segments (providing flexibility) which can be varied to adjust the mechanical properties of the bulk material [55, 56]. PU can be synthesised to be either degradable (e.g. Degrapol®) or non-degradable (e.g. Pellethane®, Bionate®, Carbosil®) under physiological conditions depending on the polymer used in the soft domain [57]. The advantages of PU grafts, over traditional synthetics, are their elasticity, which better match the compliance of natural vessels than stiffer, crystalline ePTFE and Dacron grafts [58, 59].

Porous PU grafts are typically grouped into two morphological classes: foamed and fibrillar. The former can be produced by replamineform [60], thermal inversion [61], blowing/reticulation [62], gas expansion [63] and phase inversion techniques [15,21] which typically posses larger pore sizes than their fibrillar counter-parts [3, 5, 15]. The later can be manufactured by knitting [64] or weaving [65] (similar to Dacron), electrospinning [66–71] and winding [72, 73]; benefiting from high surface area per unit volume, anisotropic mechanical properties similar to native vessels [71] and good cellular adhesion properties (for small diameter fibrillar structures) [74–76]. However, the disadvantage of most fibrillar type grafts is their inherently tightly packed structure which is often impenetrable to transmural cellular infiltration [3].

Despite their success at producing *in situ* endothelialisation in pre-clinical research [16, 66, 77], PU grafts have not yet received wide acceptance in the clinical setting despite advantages in manufacturability and superior compliance properties to ePTFE and Dacron [78, 79]. This lack of acceptance is mainly due to *in vivo* degradation observed in clinical trials of first generation PUs caused by spontaneous degradation of their polyether

or polyester diol soft segments [2, 56, 80]. However, modern PUs are carbonate and/or siloxane based, containing no ester/ether soft segments and have been shown to be far more stable *in vivo* [56, 81, 82].

Some early commercial attempts at polyurethane peripheral bypass grafts include the Corvita® (Corvita Corp., Miami, FL), Thoratec® (Thoratec Lab Corp., Berkeley, CA) and Pulse-Tec® (Newtec Vascular Products Ltd., Clwyd, UK). The Corvita graft consisted of a helically wound poly(carbonate urethane) (PCU, specifically Corethane®) graft with an external PET mesh for reinforcement and showed improved patency after 6 months (100%, canine abdominal aorta model) when compared to ePTFE controls (50%) [83]; however, Georg *et al* (2014) reported severe biodegradation of the PCU liner after 13 years of implant in the abdominal aortic position in a 75 year old man [84]. The Thoratec vascular graft, originally designed as a vascular access graft (Vectra®), consisted of poly(ether urethane urea) and was produced by a multilayer casting technique following reinforcement by wrapping a polyester monofilament at varying pitches [79]; however a 6 month implantation in dogs showed extensive material degradation and a high degree of thrombus formation which aided in impeding transmural tissue ingrowth [85]. Pulse-Tec grafts are produced by a low-temperature phase separation technique out of poly(ether urethane) to produce large, irregular pores ($\approxeq 28\mu m$) within the bulk volume of the material but possessed a low porosity skin on both its luminal and abluminal surfaces [79]. These low porosity skins have been shown to deter tissue ingrowth and the poly(ether urethane) material exhibited significant degradation after 6 months of implantation in a canine model [85].

More modern PU grafts include Myolink®, a poly(carbonate-urea)urethane vascular graft which has been shown to be mechanically stable after 36 months of implantation (beagle dogs) [58], and UCL-NANO™, a nanocomposite polymer of polycarbonate urea-urethane incorporated with polyhedral oligomeric silsesquioxane (POSS) nanocages [86, 87].

Another issue needing to be addressed with non-degradable vascular grafts is mineralisation (calcification). The degree of calcification has been shown to be more strongly correlated with soluble calcium levels and device function (e.g. high rates of cyclic deformation associated with heart valves) than polymer chemical composition [88]. While synthetic vascular grafts have also been shown to be susceptible to calcification [88], where deformation is more moderate than in heart valve applications, ePTFE has been shown to be significantly more prone to calcification than PU *in vitro* [89]. Slow degradable materials such as PCL have also been shown to exhibit calcification in long term vascular graft (18 months, rat abdominal aorta) studies [90].

2.1.2.3 Preferences per Vessel Calibre

Each type of graft has met with varying degrees of success depending on the vascular region where it is applied, which are summarised in Table 2.1:

Table 2.1: Prefered Graft Types per Vascular Region (Adapted from [2])

Arterial Region	Size (mm)	Application	Prefered Graft Type	Secondary Graft Type
Large-calibre	≥8	Aorta, Illiac, Common Femoral	Synthetic	Allograft/ Autograft
Medium-calibre	6 - 8	Carotid, Subclavian, Common Femoral, Above-the-knee arteries	Autograft/ Synthetic	Autograft/ Synthetic
Small-calibre	≤6	Coronary, Below-the-knee arteries	Autograft	Allograft/ Synthetic
Venous Grafts	All	Vena Cava,Ilico-femoral, Portal, Visceral	Autograft	Allograft/ Synthetic

2.1.3 Requirements of a Prosthetic Graft

The task of a prosthetic graft is very simple, "form a vessel in which blood can be transported from one end to the other without leaks nor blockage". However, the environment in which it must accomplish this simple task makes it far more complex. The physiological environment is highly active with inter-dependencies between the cellular structure of the vessel wall and the biochemical environment of the lumen.

When all factors are considered a more exhaustive list of properties / characteristics that the ideal vascular graft should possess are [2, 34, 56, 91]:

1. Mechanical Strength
2. Matched compliance to native vessel
3. Non-toxicity
4. Non-Immunogenicity
5. Biocompatiblity
6. Off-the-shelf availability
7. Suture retention
8. Ease of surgical handling

9. Thrombosis resistance *in vivo*
10. Infection resistance
11. Haemostasis between graft and surrounding tissue
12. Ability to grow *in vivo* if required
13. Easy sterilization

2.1.4 Reasons for Failure of Small Diameter Vascular Grafts

With over 60 years of development in the field of vascular grafts, researchers have identified what is thought to be the root causes of the failure observed in small diameter synthetic grafts. The two major causes of failure being midgraft thrombosis and intimal hyperplasia are described below [92].

Midgraft Thrombosis: The endothelial cells lining the inner wall of blood vessels perform crucial functions in maintaining haemostasis. Synthetic grafts are typically without an endothelial lining at the time of implantation and as a result blood is exposed to foreign surfaces, often resulting in a thrombogenic reaction which is amplified in the low flow states associated with small calibre grafts [27, 91, 93]. Attempts have been made to replicate the antithrombotic properties of the endothelium through drug elution of antithrombotics, such as heparin, nitric oxide (NO), hirudin and aspirin [27], or by chemical modification of the grafts luminal surface with immobilized heparin [15, 94, 95] or carbon-coating to improve electronegativity of the surface [96,97]; however, for long term patency a healthy endothelium is second-to-none [2, 3, 93]. Endothelial cell seeding, with the patients own cells, onto the synthetic grafts surface prior to implantation has shown efficacy in numerous trials [98–100]; however this two-stage procedure is expensive, involves long waiting periods and has scalability issues due to the sophisticated clinical facilities and cellular culture techniques required for it to become a true contender to the autologous vessel [18, 42, 91, 93].

Currently it is understood that there are three different mechanisms of endothelial growth: transanastomotic from the neighbouring native vessel; transmural from surrounding tissue and fall-out from the blood stream. [3, 27]. In humans, transmural endothelialisation seems to be the only option where transanastomotic growth is limited to about 10-20mm from the anastomosis and fall-out leads to small "islands" of endothelialisation rather than a confluent surface. [3, 16, 27]. Thus it can be appreciated why promising animal studies with synthetic materials have met with disappointing results in clinical trials, where current synthetic grafts, ePTFE and PET, do not have sufficient porosity to allow for transmural endothelialisation [2, 3, 16].

Intimal Hyperplasia: Intimal hyperplasia is believed to be caused due to suboptimal haemodynamic and biomechanical properties over the anastomotic region. These properties include: [3, 92]

- **Compliance mismatch** between the stiff graft and the more elastic vessel.
- **Flow rate** variations due to sudden changes in diameter between the native vessel and prosthesis.
- **Shear rate** variations caused by the diameter change between the native vessel and prosthesis.

The difference in compliance between small diameter ePTFE ($C_d = 1.6 \pm 0.2\%$ /100mmHg) / Dacron ($C_d = 1.9 \pm 0.3\%$ /100mmHg) [5,78,97] grafts and native vessels (femoral artery = 7% to 14% /100mmHg, popliteal artery = 5% to 9% /100mmHg [21, 101, 102]), is believed to be linked to intimal hyperplasic response [5, 103]. Salacinski *et al* (2001) observed a highly significant (p=0.019) correlation (r^2=0.877) between compliance and graft patency, where more compliant grafts (5 %/100mmHg) exhibted higher patency rates than less complianct grafts (2 %/100mmHg) [92]. Trubel *et al* (1994) found that constriction of venous grafts (reversed deep femoral vein) with an outer Dacron mesh tube, resulted in significant (p=0.001) increases to intimal hyperplasia at the distal anastomosis when compared to unrestricted vein grafts (femoropopliteal bypass, sheep model, n=12) [104]. Ballyk *et al* (1997) suggested, in a numerical model study, that increased intimal hyperplasic response in graft materials with unmatched compliance to the native artery is due to increased suture line stresses at the site of anastomosis [105].

Tai *et al* (2000) found that PU grafts almost exactly matched the average compliance of muscular arteries, offering them a potential advantage over Dacron and ePTFE grafts [106]. However, the compliance of PU grafts is largely dependant on the chemical make-up and ratio of hard to soft segments of the material as well as the method of fabrication of the graft [55, 78, 79].

It has also been shown that the presence of an even and healthy layer of endothelial cells aids in preventing the proliferation of smooth muscle cells known to cause intimal hyperplasia, indicating the importance of having a confluent endothelial lining for graft patency [14].

2.2 Electrospinning

2.2.1 Overview of Electrospinning

Electrospinning utilises high voltage electric fields to create nano-to-micrometer diameter polymer fibres. In the case of solution electrospinning, the polymer is dissolved in a suitable solvent and dispensed at a constant flow rate with appropriate equipment (e.g. syringe and metered pump or reservoir air pressure through a spinneret (capillary with a controlled aperture size) [107]). A high voltage differential is then created between the spinneret and collector (10-40kV depending on application) with a suitable distance between them. The polymer solution becomes highly charged at the nozzle tip and eventually overcomes its own hydrostatic forces, forming the characteristic conical shape known as the Taylor cone [108], to eject in a thin fibrous jet which then deposits on the collector. The pattern of motion of the jet changes as it travels from the nozzle to the collector. Initially travelling in a straight line but after a short distance begins to spiral in a phenomenon known as bending/whipping instability [109, 110] (Figure 2.3).

Bending instability is, simply-put, a result of the repulsive forces between adjacent, like-charged particles in the jet acting to repel sections perpendicularly-and-outward to the motion of the jet, thereby resulting in a parabolic shape [110–114] (See Figure 2.4).

There are many variations of electrospinning techniques depending on the desired outcomes of the process, these modifications include but are not limited to: spinneret design (co-axial [115–122], tri-axial [123, 124] and needleless [125]), collector design (tubular [69, 126, 127], patterned [128] and temperature controlled [129]), electric field manipulation (jet polarity [130], AC electrospinning [131] and electrostatic guidance [126, 132]) and control of ambient conditions [133].

2.2.2 Brief History of Electrospinning

The relationship between electrostatic forces and the surface tension of a liquid droplet was first quantified in 1882 by Lord Rayleigh [135]. Three and a half decades later, Zeleny was able to photograph and describe the phenomenon of a liquid droplet overcoming its own surface tension due to electrostatic forces [136]. In 1964 Taylor expanded on Zeleny's work and determined the critical angle of the conical interface (49.3°) between two fluids in an electric field, which was thereafter named the Taylor cone [137].

It wasn't until 1934 that the first patent for electrospinning was filed by Anton Formhals as a commercially viable invention [138], and almost half a century later the first patent detailing electrospun vascular grafts was filed by G. Martin and I. Cockshott in 1977 [139]

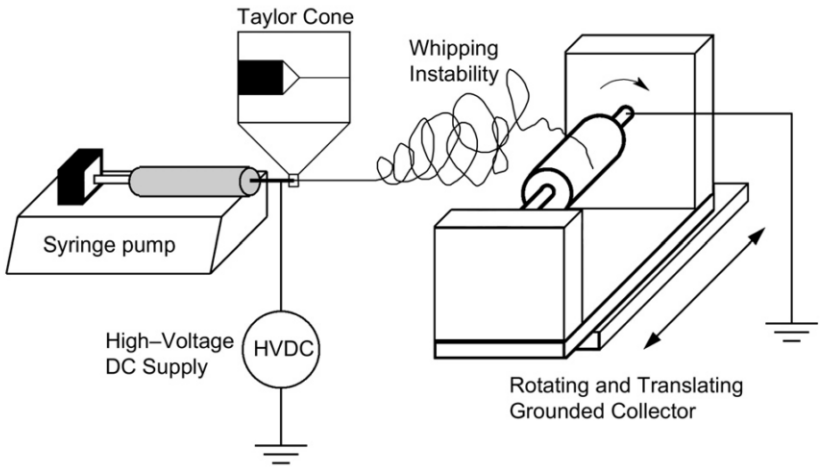

Figure 2.3: Diagrammatic overview of electrospinning equipment and process with a syringe pump and rotating collector. The syringe pump maintains a steady flow rate to replenish the polymer mass being converted into a jet. Electrostatic elongation forces overcome viscous and surface tension forces of the fluid, forming a Taylor cone and fibrous jet at the spinneret tip. The jet follows a linear path between the nozzle and collector initially but then whipping instability ensues. The jet eventually collides with and accumulates on the collector to form a fibrous tube. [134]

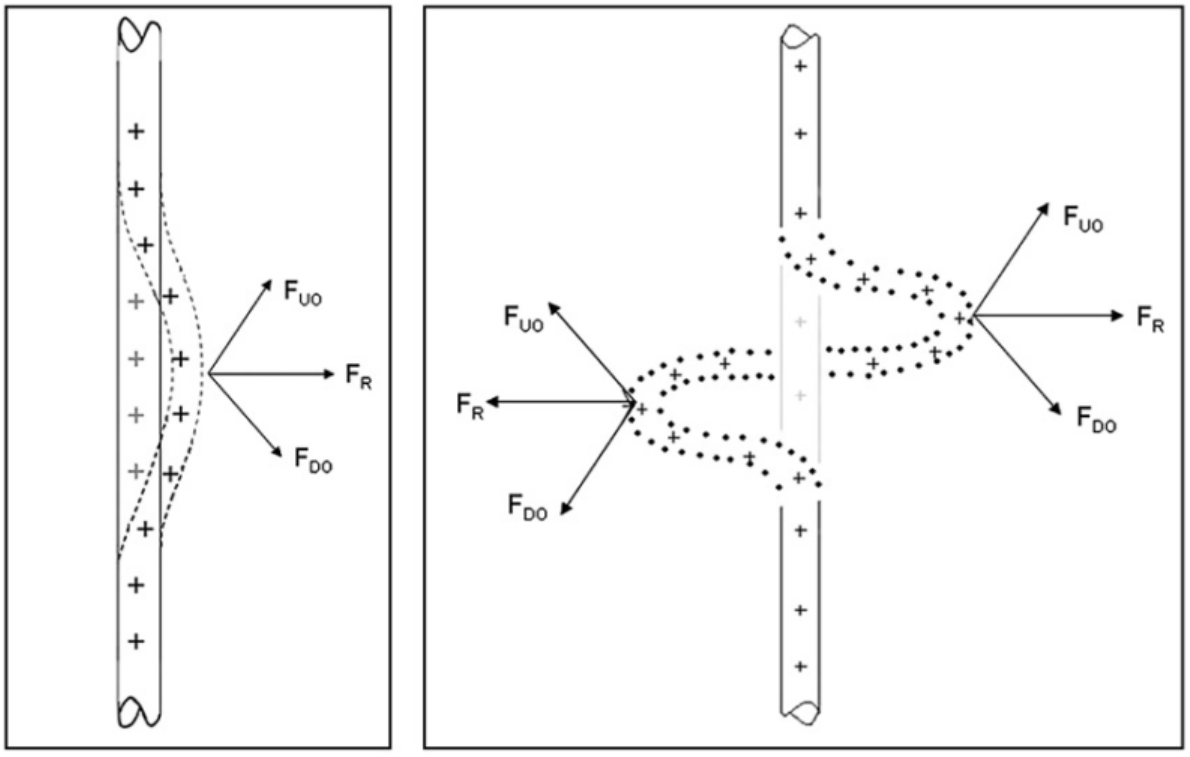

Figure 2.4: A cropped segment of an electrospun jet with uniformly spaced, positively charged particles. The adjacent particles exert a repulsive force on one-another causing the intermediate particles to be forced outwards forming a parabolic shape. [110]

and two more shortly after in 1979 and 1983 by A. Bornat and T. How, respectively [140, 141]. However, the adoption of electrospinning in research was slow until the mid 1990s when it became of interest in the field of nanotechnology to Reneker *et al* [142] and a few years later in vascular graft development to Chaikof *et al* [143] and Bowlin *et al* [144, 145].

Since then electrospinning research has accelerated, finding applications in multiple sectors of industry, ranging from textiles to astronautical and medical engineering [109].

2.2.3 Electrospun Vascular Grafts

This section, while not attempting to provide an exhaustive review of progress in electrospun vascular graft development, will outline some of the main streams of research in the field.

Electrospinning has the ability to create nano-to-micrometer diameter fibrous, non-woven, polymeric sheets [110], with advantages including ease of production, high throughput, minimal waste, high surface area per unit volume, fibrous morphologies similar to those of the extra cellular matrix (ECM) [146] and ability to incorporate drugs with diverse elution profiles as well as spin both natural and synthetic polymers [122, 134, 147, 148]. As a result electrospinning has been widely researched as a method of producing scaffolds for tissue engineering and regenerative medicine approaches for musculoskeletal, nervous, skin and cardiovascular applications [147–152]. Additionally, for the specific application of vascular prostheses, electrospinning allows for easy fabrication into tubular constructs (multi-layered with different polymers if required [153, 154]) where the fibre orientation can be controlled.

A prominent stream of electrospinning research aims at improving the healing outcomes of electrospun vascular grafts by spinning conduits from solutions of natural instead of synthetic polymers. Natural polymers, such as collagen, elastin, fibrinogen, silk and gelatin, are electrospun in the same fibre diameter scale as the native ECM and contain an abundance of binding domains for cellular attachment, which are critical for cellular-matrix interactions [149,150,155]. However, synthetic polymers, while lacking the binding moieties of their natural counterparts, are stronger, more cost effective and customizable and carry less risk of viral/disease transmission [155]. Strategies to improve the mechanical properties of natural polymers include cross-linking to improve strength and decrease water solubility [156], however, cross-linking often adversely effects binding site density/function and scaffold morphology [155, 157]. Synthetic polymers can be surface treated [158–164] to improve their cellular interaction properties, however the obtained surface characteristics are still thought to be inferior to natural polymers [155]. In an

attempt to obtain the attractive properties of both polymer types, hybrid scaffolds of the two have been produced where layers of each polymer are electrospun in layers, where the natural polymer provides for cellular interaction and the synthetic provides mechanical strength [153, 155, 165–167].

Another method aimed at improving patency of electrospun vascular grafts is by elution of anti-thrombotic/anti-coagulative drugs from the electrospun fibres. Wang *et al* (2013) used coaxial electrospinning to incorporate a heparin core inside a PCLA sheath which facilitated the controlled release of heparin *in vivo*, improving patency over non-heparin eluting PCLA scaffolds [168].

Table 2.2 summarises the *in vivo* circulatory studies found in literature where electrospinning was used to create vascular grafts. Note that while most studies exhibited high patency rates and obtained confluent endothelial layers, the combination of short graft lengths (<50mm) and poor cellular infiltration indicates that the mode of endothelialisation was likely transanastomotic and thus it is unlikely that these positive results will translate to human trials [3, 16]. It is also interesting to note that while the majority of studies report on fibre diameter, few report on graft porosity and pore size. Where higher porosity scaffolds were compared with those of lower porosity, an associated increase in transmural cellular infiltration was observed from the adventia [67, 169].

While transmural angiogenesis may prove a better predictor of transmural endothelialisation than cellular infiltration, only two of the in vivo circulatory studies (Hashi *et al*, 2010 and Pektok *et al*, 2008) reported on angiogenesis and even then their reporting was qualitative rather than quantitative [163, 170]. For the purposes of this review it was more effective to report on cellular infiltration because it is sensible that increased cellular infiltration will correlate with increased angiogenesis (in order to supply nutrients to the cells deeper into the scaffold wall. Thus cellular infiltration would provide an indirect method of predicting capillary infiltration. It can be appreciated that more studies on large-pore, high porosity electrospun vascular graft scaffolds are required to determine the effects of advential cellular ingrowth and vascularisation on graft patency.

Table 2.2: Published *In Vivo* Circulatory Studies of Electrospun Vascular Grafts (Adapted from [171])

ESVG Design	GID (mm)	GL (mm)	Animal Model	*In Vivo* Dur.	Patency*	End. (weeks)	Cell Inf.	FD (μm)	Porosity %	PS (μm)	Ref.
PCL											
As-spun PCL	2.0	13	Rat (AA)	12	9/9	12	NR	1.9	NR	NR	[172]
As-spun PCL	2.0	13	Rat (AA)	24	15/15	6	50%	1.9	NR	NR	[170]
As-spun PCL	2.0	10	Rat (AA)	78	3/3	13	40%	2.2	NR	NR	[90]
Bilayer PCL (HP^a/LP^b)	2.0	20	Rat (AA)	12	$5/5^{c\&d}$	12	$35\%^c/12\%^d$	$2.2^a/0.8^b$	$83\%^a/65\%^b$	$9^a/3^b$	[169]
PCL+Paclitaxel surface mod.	2.0	NR	Rat (AA)	24	3/3	24	55%	1.6	NR	NR	[158]
PCL+CAG surface mod.	0.7	7	Rat (CCA)	6	6/8	2	NR	NR	NR	NR	[159]
PCL+RGD surface mod.	2.2	15	Rabbit (CCA)	4	5/5	4	NR	0.5-3.0	NR	NR	[160]
PCL+Heparin surface mod.	2.0	40	Dog (FA)	4	4/4	4	NR	NR	83%	NR	[161]
PCL:Collagen blend (1:1)	4.75	40	Rabbit (AIB)	4	7/8	NR	None	0.52	NR	NR	[165]
PCL/chitozan/pNSR32 blend	1.2	15	Rat (AA)	8	NR	NR	Yes (NR)[e]	NR	NR	NR	[166]
PCL+Heparin surface mod. + PU layer	2.5	40	Dog (FA)	8	5/6	Yes	NR	0.15/0.2-1	49%	NR	[162]
ES elastin + ES PCL sheath	2.8	20	Rabbit (CCA)	4	3/3	NR	NR	1.67	NR	NR	[153]
PLLA											
Rolled MSC seeded PLLA sheet	0.7	NR	Rat (CCA)	7.5	NR	5	Yes	0.5	NR	NR	[173]
PLLA + hirudin surface mod.	1.0	7	Rat (CCA)	26	6/7	5	Min	2	NR	NR	[163]
PCLA											
PCLA + collagen coating	1.0	10	Rabbit (EGV)	7	3/3	No	None	0.47	NR	NR	[174]
Coaxial PCLA (Heparin core)	2.5-3.5	50	Dog (FA)	4.5	1/4	2	None	NR	NR	NR	[175]
EC seeded coaxial PCLA (Heparin core)	4.0	50	Dog (FA)	24	7/8	Yes	NR	<1	NR	NR	[168]
EC seeded coaxial PCLA (Heparin core)	4.0	50	Dog (FA)	24	3/4	Yes	NR	0.32	NR	NR	[176]
PU											
PEUU/PMBU blend (85:15)	1.3	10	Rat (AA)	8	6/9	Yes	None	0.5	NR	NR	[177]
PEUU s/ PMA surface mod.	1.3	10	Rat (AA)	8	11/12	8	None	1	NR	NR	[164]
Pellethane® as-spun	1.5	15	Rat (AA)	26	10/10	Yes	Min	0.88	NR	NR	[66]
PU HP^a/LP^b	1.5	15	Rat (AA)	26	$7/7^{a\&b}$	4	Mod^a/Min^b	$1.0^a/0.9^b$	$80\%^a/53\%^b$	$4^a/2^b$	[67]
TPU as-spun	1.6	20	Rat (AA)	52	14/14	4	Mod	1.4	75%	4.7	[178]

*= Patency of longest implant duration sample set, a= High Porosity, b= Low Porosity, c= Inside Barrier, d= Outside Barrier, e= No Quantitative Value, ESVG= Electrospun Vascular Graft, GID= Graft Inner Diameter, GL= Graft Length, Dur.= Duration, End.= Confluent Endothelium, Cell Inf.= Adventitial Transmural Ingrowth, FD= Fibre Diameter, PS= Pore Size, PCL= poly(ϵ-caprolactone), PLLA= poly(l-lactic acid), PCLA= poly(ϵ-caprolactone-co-L-lactic acid), PU= Polyurethane, PEUU= poly(ester urethane)urea, TPU= thermoplastic polyurethane, PMBU= poly(2-methacryloyloxyethyl phosphorylcholine-co-methacryloyloxyethyl butylurethane), PMA= phospholipid copolymer, CAG= cysteine-alanine-glysine trimer peptide, RGD= arginine-glycine-aspartic acid, mod.= modification, AA= Abdominal Aorta, CCA= Common Carotid Artery, FA= Femoral Artery, AIB= Aortoiliac Bypass, EGV= Inferior Epigastric Vein, MSC= Mesenchymal Stem Cells, EC= Endothelial Cells, MDSC= Muscle Derived Stem Cells

2.2.4 Control of Fibre Morphology

The variables affecting electrospun fibre morphology are numerous and, in an attempt to logically sort them, have been categorized into process and solution parameters as well as ambient conditions, as described in the sections to follow.

2.2.4.1 Process Parameters

Applied Voltage The applied voltage has the most prominent impact on fibre formation but is also the most ambiguous in its effects [134, 148]. The general rule of thumb is that fibre diameter decreases with an increase in applied voltage, up to a point [134, 179].

Deitzel *et al* studied the fibre formation of a Poly(ethylene oxide) (PEO) solution in water over a range of applied voltages. The authors noted the following: 1) jet formation only occurred over a certain threshold voltage; 2) a continuous fibrous jet was observed with increasing applied voltage until a "critical voltage", where the onset of beading abnormalities begins; 3) above the critical voltage bead density increases with applied voltage [180].

However, Reneker *et al* (2000) observed that large diameter jets, produced from highly viscous and concentrated solutions, displayed branching when spun at supra-critical voltages [110, 114]. Branching is the term given to the anomaly of secondary jets ejecting perpendicularly to the primary jet as it traverses towards the collector; caused by the repelling of diametral undulations in the primary jet by surrounding charges into smaller secondary jets [181].

To summarize, the relationship between the applied voltage and fibre morphology is not of a monotonic nature [134, 148]. There exists an optimal applied voltage setting (normally accompanied by the formation of a stable Taylor cone as seen in Figure 2.5) which is co-dependent on the solution system being spun as well as the other process parameters [180].

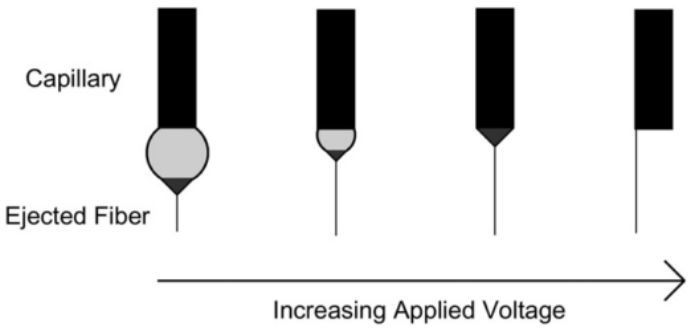

Figure 2.5: Effects of applied voltage on Taylor cone formation. Abnormalities occur at both too high and too low voltages with the "sweet spot" for fibre formation existing in-between. [134]

Solution Flow Rate After applied voltage, the solution flow rate is the next most influential parameter on fibre morphology [134]. The flow rate not only has an effect on fibre diameter but also on fibre porosity and shape [134].

As with applied voltage, there exists multiple critical values for solution flow rate where if exceeded, effects on fibre morphology differ drastically. At the one extreme, when flow rate is too low to replenish the volume of solution being converted into the fibrous jet, then beaded morphologies occur [108].

Exceeding this minimum flow rate the fibre diameter increases proportionally to the flow rate up to the upper critical value. In the cases where the solution vapour pressure favours pore development, the density of the nano-pores observed on the fibre surface also increased with increasing flow rate [182].

When the flow rate exceeds the high-level critical value, beaded abnormalities occur due to insufficient time for the solvent in the fibrous jet to evaporate before deposition on the collector ("wet" deposition). If a majority of the fibres deposited wet, then agglutination of the fibres occurs and in the most severe cases, a film-like morphology develops [116, 180, 183]. The density of both beaded and shape defects increases with increasing flow rates thereafter [182].

Working Distance The distance the fibrous jet needs to travel before colliding with the collector is known as the working distance (also known as the capillary to collector distance). This distance can affect the diameter of the formed fibres by 1 - 2 orders of magnitude [134].

Taylor first observed that the diameter of the jet decreased as the jet travelled further away from the capillary tip [108], with further studies coming to the same conclusion [142, 184]. It was also found that if the capillary to collector distance was too short then beaded and agglutination morphologies occurred; this was attributed to insufficient travel time for the jet to evaporate [182, 183].

To summarise, for increasing capillary to collector distance the fibre diameter decreases and the fibrous jet has more time to evaporate.

2.2.4.2 Solution Parameters

Polymer Molecular Weight Gupta *et al* (2005) observed that molecular weight plays a critical role in determining whether a polymer is electrospun into fibres or electrosprayed into beads [185]. They found that low molecular weight poly(methyl methacrylate) (PMMA) formed droplets (electrospraying) due to insufficient chain overlap for fibre

formation; as molecular weight increased so did fibre formation, with decreasing quantity of beaded abnormalities. They also noted that solutions with narrow molecular weight distributions produced more uniform fibre morphologies with fewer beads than those with wider molecular weight distributions.

Nezarati *et al* (2013) noted a similar trend when spinning two different batches of poly(carbonate urethane) (PCU) under the same conditions. They found that the inherent batch-to-batch variability was sufficient to make observable differences in fibre formation [133]. The first batch (Mw = 241kDa) produced uniform and dry fibres whereas the second batch (Mw = 217kDa) resulted in beaded fibres being formed. They hypothesize that the effects of molecular weight on fibre morphology are indirectly caused through a corresponding change in solution viscosity.

Polymer Concentration The polymer concentration directly influences both solution viscosity and surface tension, which in turn are fundamental in determining whether fibre or a droplet is formed during electrospinning [134, 180].

If the solution is too dilute then the force of surface tension will dominate, causing droplets to be formed instead of continuous fibres. On the other hand, if the solution is too concentrated then it will be difficult to control the polymer flow rate to the tip of the collector due to the increased viscosity [134, 180].

Between the two extremes exists an optimum range where continuous fibres can be produced. Within this optimum range it has been observed that fibre diameter increases with increasing polymer concentrations (Figure 2.6) [134, 180, 186].

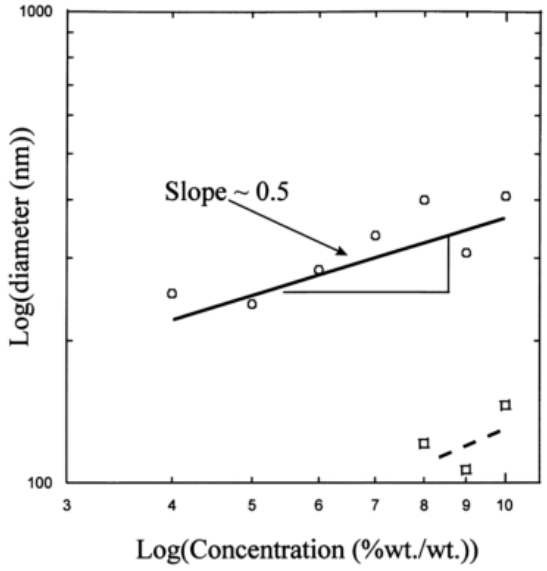

Figure 2.6: Average fibre diameters of electrospun Poly(ethylene oxide) (PEO) spun from DI water over various solution concentrations. Primary distribution is represented by circles and secondary by squares. It can be seen that within the optimal range of solution concentrations the fibre diameter increases with increasing concentration. [180]

Solution Conductivity The solution conductivity is directly related to the solutions charge carrying capacity. The greater the charge carried by the solution, the greater the tensile force applied on the jet by the electric field, resulting in longer, thinner fibres [122, 134, 187, 188].

Increasing the solution conductivity has also been shown to produce more uniform fibres with fewer beaded deformations [148, 188]. Increasing the solution conductivity can be accomplished by adding ionic salts to the solution, where the salts ionize and increase charge density. Zong *et al* (2002) tested the effects of three different salts (KH_2PO_4, NaH_2PO_4 and NaCl), in a solution of poly(D,L-lactic acid) PDLA in dimethylformamide (DMF), and found that in all cases there was a reduction in bead deformations and fibre diameter (Figure 2.7) [188].

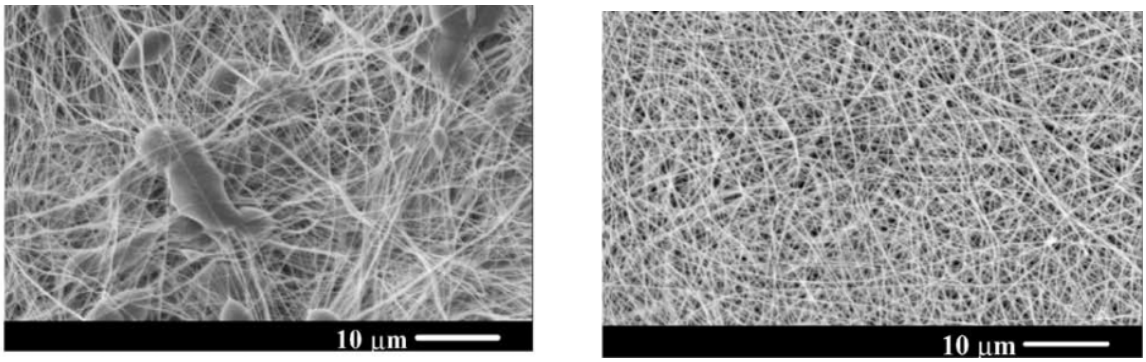

(a) Without NaCl Additive (b) With NaCl Additive

Figure 2.7: SEM images of fibres spun from 30 wt% solutions PDLA/DMF with all process parameters held constant bar solution conductivity. a) Resultant fibre morphology without NaCl additive; note the irregular fibre diameter and presence of beads. b) When NaCl is added to the solution the resultant increases in solution conductivity causes a reduction in bead formation as well as fibre diameter [188]

.

Solvent Dielectric Constant The dielectric constant is an indicator of a materials ability to hold charge in an electric field. It has been observed that solvents with high dielectric constants are able to produce fibres with smaller diameters and reduced beading defects [133, 189].

Wannatong *et al* (2004), when spinning polystyrene (PS) fibres, found that solvents with higher dielectric constants (m-Cresol and DMF) produced thinner fibre diameters with more uniform distributions at higher productivity rates (number of fibers produced per unit area, per unit time) than solvents with lower dielectric constants (Toluene and THF). They hypothesise that solvents with high dielectric constants have an increased susceptibility to the applied electric field, which in turn increases the drawing force on the jet, acting to simultaneously elongate the fibres and increasing mass throughput through the spinneret [183].

Solution Viscosity It is widely accepted that the change in solution viscosity is the key driving factor in the morphological effects observed when adjusting the solution concentration and molecular weight [133, 134, 142, 180].

As observed with solution concentration, there exists a minimum and maximum threshold for a given polymer where a continuous fibre will be formed. Under the minimum threshold, the force of surface tension will cause the fibre to break apart into beads due to Rayleigh Instability [133]. Above the maximum threshold, continuous fibres will be difficult to produce due to the flow rate fluctuations through the spinneret caused by the high viscosity [133, 134].

In-between the above stated minima and maxima values it has been observed that fibre diameter increases with increasing viscosity [133, 134, 180].

Solvent Volatility Solvent volatility has been shown to be related to the production of nano-pores on the fibre surface. Megelski *et al* (2002) spun PS in varying mixtures of tetrahydrofuran (THF) and dimethylformamide (DMF) and studied the morphological effects on the resultant fibre formation [182]. They found that solutions made in 100% THF (more volatile) exhibited greater pore density (number of pores per unit area) than mixtures of THF and DMF. Fibres spun in DMF (less volatile) showed no signs of nano-pores [182]. They concluded that nano-pore formation was dependant on the vapour pressure of the solvent, with increasing solvent vapour pressures leading to an increased number of nano-pores formed.

Wannatong *et al* (2004) found that (when spinning PS in m-Cresol, Toluene, THF or DMF) fibre diameter decreased exponentially with increases in solvent boiling point, they hypothesize that this is due to the jet's inability to reduce in diameter once it

had completely evaporated (dry), thus for high volatility solvents (THF and Toluene) the jet would dry much sooner along their flights and hence would not have had time to elongate and thin as much as their low volatility counterparts (DMF and m-Cresol) [183]. However, in a study by Luo *et al* (2010) it was argued that the difference in fibre diameters observed between solvents are dominated by their dielectric properties rather than volatilities; where they found that fibres spun from methanol and THF (with boiling points of 65°C and 66°C and dielectric constants of 32.6 and 7.6, respectively) had average fibre diameters of 0.4μm and 3.5μm, respectively.

2.2.4.3 Ambient Conditions

While it is known that environmental conditions such as ambient temperature, air velocity, atmospheric composition and pressure play a role in the outcome of the electrospinning process [122, 142], there has been limited work specifically describing their effects.

Environmental Humidity Nezarati *et al* (2013) studied the effects of both humidity (5% - 75%) and solution viscosity on the resultant fibre morphologies when electrospinning three different polymers; namely poly(carbonate urethane) (PCU), polycaprolactone (PCL) and poly(ethylene glycol) (PEG) [133]. It was observed that at low humidity values fibre breakage would occur; however, the effects of high humidity values depended on the properties of the polymer being spun. For instance PCL developed nano-pores on the fibre surface, while PEG showed signs of beading. Megelski *et al* (2002) also observed increased pore density when increasing relative humidity while spinning PS in a THF solution. [182]

Nezarati *et al* concluded that the effects of humidity on electrospinning of a particular polymer vary depending on the solvent volatility and miscibility as well as the polymer hydrophobicity. Their work also suggests that each polymer has its own optimal humidity value for the creation of smooth, regular fibres.

2.2.4.4 Summary

Table 2.3 summarises the effects of the different process and solution parameters on the morphology of the spun fibres.

Table 2.3: ffects of Electrospinning Parameters on Fibre Morphology

Parameter	Below Minima	**Increasing** within Optimal Range	Above Maxima	References
Applied Voltage	No jet formation	↓ Fiber diameter	↑ Bead density, ↑ Branching / Multi-jets,	[110, 114, 134, 148, 179–181]
Solution Flow Rate	Bead formation	↑ Fiber diameter	↑ Bead density, ↑ Shape defects	[108, 134, 182]
Capillary to Collector Distance	Bead formation	↑ Fiber dryness, ↓ Fiber diameter	No jet formation	[108, 134, 142, 182, 184]
Environmental Humidity	Fiber breakage	↑ Pore density, ↑ Bead density	Wet deposition	[133, 182]
Polymer Molecular Weight	Electrospraying	↑ Fiber diameter	↑ Bead density (difficult to control flow rate)	[133, 185]
Polymer Concentration	Electrospraying	↑ Fiber diameter	↑ Bead density (difficult to control flow rate)	[134, 180, 186]
Solution Conductivity	Bead Formation / Not Spinnable	↓ Fiber diameter, ↓ Bead density, ↑ Fibre uniformity	Not Applicable	[122, 134, 148, 188, 190]
Solvent Dielectric Constant	Not Spinnable	↑ Productivity, ↓ Fibre Diameter	Not Applicable	[133,183,189,191]
Solution Viscosity	Electrospraying	↑ Fiber diameter	↑ Bead density (difficult to control flow rate)	[133, 134, 180]
Solvent Volatility	Wet deposition	↑ Fiber dryness, ↑ Nano-pore formation, ↑ Fibre Diameter	No Data	[182,183,191,192]

2.2.5 Controlling Scaffold Properties

Since the sudden increase of electrospinning activity in the 1990s many fields of research have attempted to suit the process to their specific needs. As a result there has been a multitude of different techniques and set ups developed for controlling bulk scaffold properties (fibre alignment, porosity, pore-size etc.). Techniques of note in the development of vascular grafts are fibre alignment and porosity control which will discussed separately in the sections to follow.

2.2.5.1 Fibre Alignment

Fibre alignment is an important factor for both scaffold mechanical properties (strength, elasticity etc.) and cell adhesion, alignment and function [127, 193, 194]. Drilling *et al* (2009) argue that complete fibre alignment is not necessary or even favourable for the development of burst pressure competent electrospun grafts, and suggest that a degree of isotropy is favourable for producing grafts that can resist surgical handling, suture stress and sheer stresses associated with pulsatile flow; while still retaining sufficient strength to resist burst pressures greater than those of the native vessel [127]. On the contrary, it has been shown that cellular alignment, differentiation and function are influenced by synthetic fibre alignment, thus in order to reproduce the structure of the circumferentially aligned tunica media in native vessels, a degree of fibre alignment is required to help guide cell differentiation and function [193, 195, 196].

As a result of the diverse applications of electrospinning and fibre alignment requirements thereof, a variety of collector types are available to tailor fibre alignment, some of these will be discussed in this section.

Electrostatic Collectors The fibre alignment can be manipulated by tailoring the electrostatic properties of the collector. Xie *et al* (2010) utilised a double U-shaped collector to produce aligned fibres between two sets of randomly orientated fibres [197]. The electric field created by the uniquely shaped collector caused the fibres to collect on the flat sections of the collector but stretch across in-between. They hypothesized that this fibre morphology would be well suited for assisting in tendon repair by seeding fibroblasts into the fibrous mesh.

Magnetic Alignment Yang *et al* utilised magnetic fields created by two permanent magnets to align fibres spun onto a flat collecting plate [198]. They doped poly(vinyl alcohol) (PVA) with Fe_3O_4 nano-particles to allow the fibrous jet to be influenced by the magnetic field. The method, coined magnetic electrospinning (MES), was able to produce mats where up to 75% of the fibres were parallel to each other (0 - 5deg). However, the effects of the presence of Fe_3O_4 nano-particles in the deposited fibres on biological response and mechanical properties requires further testing.

Rotating Mandrel Fennessey *et al* (2004) found that by increasing the surface velocity of a rotating mandrel collector they could produce a narrower alignment distribution of electrospun fibres (Figure 2.8) [199]. By varying either the diameter or the rotational speed of the mandrel, the surface velocity where the fibre collides with the collector can be manipulated, thus rotational speed is a useful parameter for controlling fibre

alignment. Additionally, this method collects fibres in a tubular form, which is useful in the application of vascular grafts, where diameter can be varied by changing the diameter of the mandrel. See Figure 2.3 for a diagrammatic representation of a rotating mandrel system.

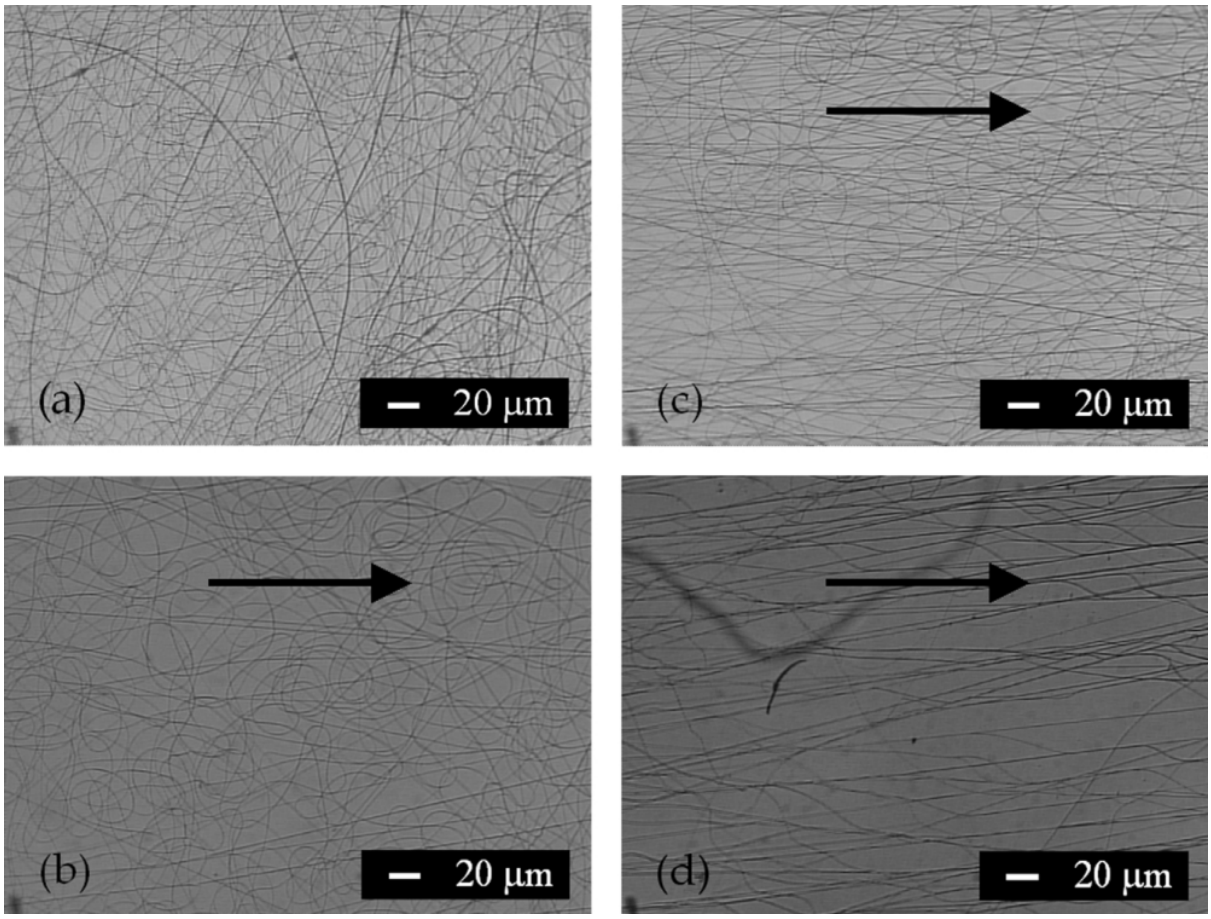

Figure 2.8: Optical micrograph of electrospun polyacrylonitrile (PAN) fibres spun from DMF. Fibres were collected at surface velocities of a) 0 m/s b) 3.5 m/s c) 6.1 m/s and d) 12.3 m/s. The arrow indicates the direction of motion. [199]

2.2.5.2 Porosity Control

Porosity, pore size and pore-interconnectivity are critical factors influencing cellular infiltration, viability and growth in 3-dimensional scaffold structures [3, 150]. A major challenge of electrospinning has been to create large, interconnected pores, due to the tightly packed fibrous meshes that are created under normal conditions. As a result there has been much research and a variety of methods investigated for improving and controlling these critical porosity factors. See Table 2.4 for a summary of the methods used to increase porosity and pore size in literature.

Fibre Diameter and Packing Density It has been shown that porosity and pore size can be increased by increasing the diameters of the fibres within the scaffold [75, 132, 200–204] and are related to the packing density of the fibres [67, 132]. However, smaller fibre diameters are desired for cell adhesion [74–76, 203] and packing density was increased in these studies rather than decreased through the manipulation of electric fields (by guiding deposition with electrostatic rings surrounding the path of the jet), thus offering no way to further improve porosity from standard means. Additionally, Milleret *et al* (2012) observed that the blood coagulation reaction to electrospun vascular grafts produced from Degrapol and PLGA favoured smaller diameter fibres [202]. Where larger fibre diameters correlated with higher thrombin formation and platelet adherence, indicating that increasing pore size by means of increasing fibre diameter may lead to undesirable increases in thrombogenicity when used in vascular graft applications.

Custom Collector Designs Modified collectors which have been specifically designed for increasing porosity and pore size, ranging from patterns in the collector surface to refrigerated drums for freezing fibres and local moisture on collection, are found throughout literature and will be discussed below.

Patterned collectors are able to create local electric field gradients which alter local fibre deposition morphology. Zhu *et al* (2008) used a rotating frame (Figure 2.9a) to alternate the alignment of the fibres spanning adjacent struts, which for different rotational speeds altered fibre packing density [205]. Similarly, Vaquette *et al* (2011) utilized flat plate collectors with a myriad different patterned holes to improve local pore size (Figure 2.9c).

McClure *et al* (2012) used an internally pressurised collector mandrel which was patterned with small holes connected to a compressed air supply, allowing for air flow through the small holes in the mandrel to reduce local fibre packing density. They tested the effects of various internal pressures (0-200 kPa) and found that 100 kPa produced the largest pore sizes (7.6±3.1 μm) between fibres collected within the patterned regions and showed improved cellular penetration in these regions when compared to scaffolds spun on standard collectors [206].

Perhaps the most creative of these electric field modifying patterns is that aptly, albeit forcibly, named Focused, Low density, Uncompressed nanoFiber (FLUF) which consists of a hollowed-out half-sphere shaped collector with an array of pins extruding out of the inner surface, causing fibres to discharge at different depths into the bowl resulting in a low density, "fluff-ball" (Figure 2.9e) [207]. Also along the lines of custom collector designs, Simonet *et al* (2007) utilized a collector drum loaded with dry ice and a humid environment to decrease packing density by separating fibres with ice crystals which were

subsequently dried, creating large pores in their wake. This method has been named Low Temperature Electrospinning (LTE, Figure 2.9g) [129, 208].

While these techniques have shown efficacy in reducing fibre packing density, each have their own shortfalls with regard to application in small diameter vascular grafts; whether it be scalability (4-6mm diameter collectors) in terms of the rotating strut frame and LTE or difficulty in removing cylindrical constructs such as in patterned or FLUF collectors.

Dual Electrospinning Dual-spinneret, co-spinneret or side-by-side spinning set ups were initially devised to create constructs which combined attractive properties of two different materials [209–211]. It was not until later that Baker *et al* (2008) utilized this approach for improving the porous characteristics of electrospun meshes [212]. The two primary approaches utilising dual-spinnerets are dual electrospinning and electrospinning/electrospraying. Each method will be discussed in detail below.

Dual electrospinning was first utilised as a method to improve porosity characteristics by Baker *et al* (2008) where poly(ethylene oxide) (PEO) and poly(σ-caprolactone) (PCL) were spun simultaneously and the PEO fibre was subsequently washed out, leaving only the PCL fibres remaining with void spaces in the wake of the PEO fibres (Figure 2.10). This process was coined porosity control via 'sacrificial fibres' [212]. This method allowed for improved porosity while still maintaining structural anisotropy. When various scaffolds were seeded with mesenchymal stem cells (MSCs), they found that with increasing percentages of PEO content cellular infiltration was improved. However, this was at the cost of mechanical strength and at PEO contents above 60% the scaffold structure would deform on removal of the sacrificial fibres. Since then the method has been shown to increase porosity and pore size in numerous studies [71, 213–215].

A slight modification of electrospinning with sacrificial fibres is to incorporate electrosprayed porogens into the scaffold architecture, this is precisely what Ekaputra *et al* (2008) first explored when they spun PCL/Collegen blends with electrosprayed Heprasil (hyaluronic acid/heparin hydrogel) [216]. This study reported that the hydrogel produced significantly larger pore sizes which resulted in improved cellular infiltration. However, the process of electrospraying a hydrogel adds more complexity to the electrospinning process and required that the solution be spun within 30 minutes of preparing the Heprasil solution, which adds limits to spinning time and hence scaffold thickness. A similar, somewhat simpler, process was explored by Nam *et al* (2007) where NaCl crystals were deposited onto the collector mandrel while electrospinning and subsequently removed by immersion in water, producing large pores; however, the pores were found to be in the form of delaminations rather than homogeneous interconnected pores [217].

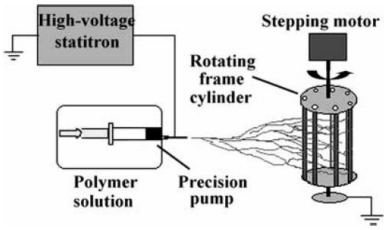

(a) Zhu *et al*: Strutted frame [205]

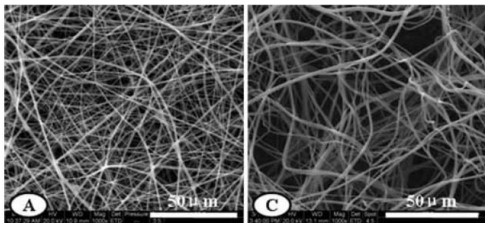

(b) Zhu *et al*: Resultant fibre morphology [205]

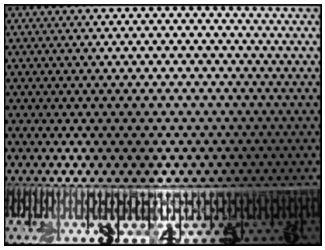

(c) Vaquette *et al*: Patterned collector [128]

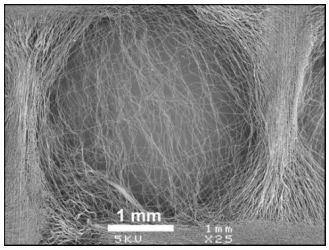

(d) Vaquette *et al*: Resultant fibre morphology [128]

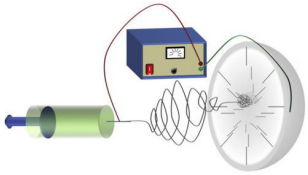

(e) Blakeney *et al*: FLUF collector [207]

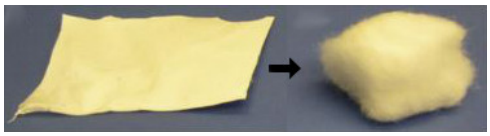

(f) Blakeney *et al*: Comparison of standard vs FLUF scaffold [207]

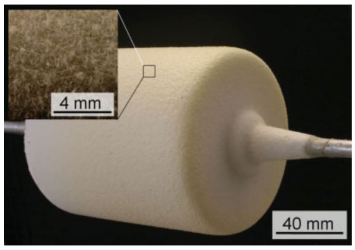

(g) Simonet *et al*: LTE collector [129]

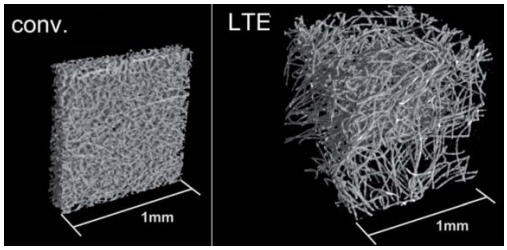

(h) Simonet *et al*: Comparison of standard vs LTE scaffold [208]

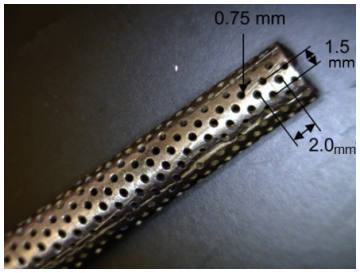

(i) McClure *et al*: Air-Impedance [206]

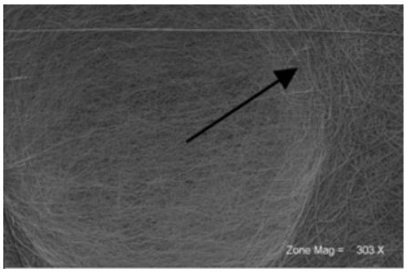

(j) McClure *et al*: Fibrous morphology over "blow-hole" [206]

Figure 2.9: Custom collector designs utilized to decrease fibre packing density and thereby increase pore-size and porosity.

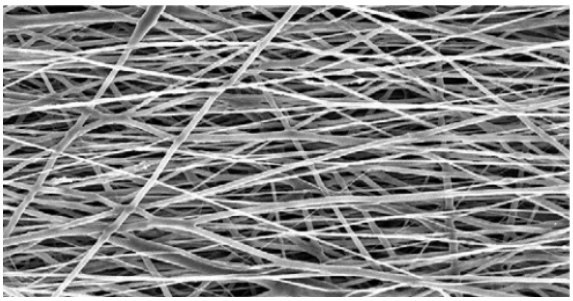

(a) SEM image of scaffold before PEO removal (2008)

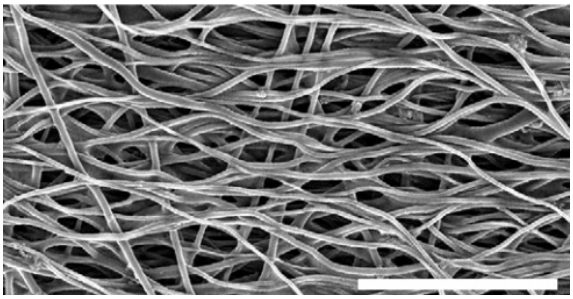

(b) SEM image of scaffold after PEO remvoval by water immersion

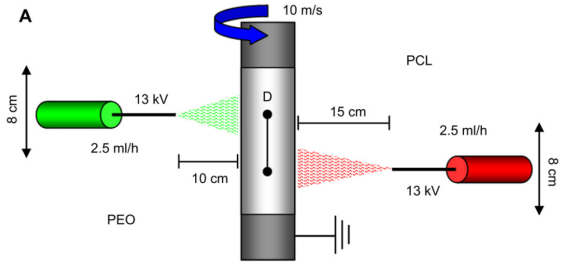

(c) Schematic diagram of dual-electrospinning set up

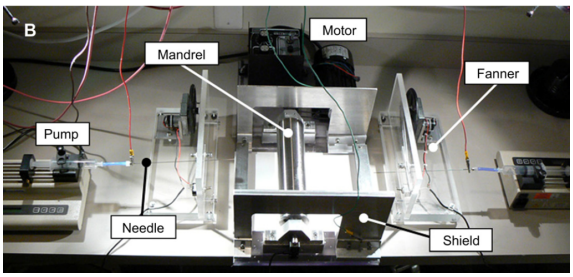

(d) Photograph of dual-electrospinning aparatus

Figure 2.10: Baker *et al* (2008): SEM images of scaffold architecture a) before removal of PEO and b) after removal through submersion in water. Note the improvement in pore-size. c) Schematic of electrospinning set up for dual electrospinning d) The electrospinning set up utilized two spinnerets charged with like-polarity on either of a grounded mandrel. The spinnerets were guided by custom built 'fanners' to evenly distribute fibres over the length of the mandrel. In order to prevent the like charged fibrous jets from repelling each other to opposite ends of the collector they utilized charged electrostatic shields on either side of the mandrel [212].

Other Methods Some notable methods recently used to increase porosity and create larger pores cannot be grouped into any of the classifications above and thus will be discussed separately.

Cai *et al* (2013) doped Zein and PEG solutions with sodium dodecyl sulfate (SDS) which they showed to increase surface conductivity of the resultant electrospun fibres. They hypothesize that when these fibres came in contact with the oppositely charged collector they inherited the charge of the collectors, thereby creating a net repulsion force between the collector and the fibres, acting to reduce fibre packing density [218]. This method, however, requires that SDS be soluble in the polymer solution and also may leave traces of SDS in the fibre structure.

Lee *et al* (2011) utilized high power ultrasonication to decrease the packing density of poly(L-lactic acid) (PLLA) fibrous scaffolds after spinning as a post-processing step. They found that pore sizes could be increased from 2.1±0.6μm to 13.5±6.8μm by varying the sonication energy the scaffolds were exposed to [219]. However, this technique has yet to

be shown with elastic materials such as polyurethanes and it may be that the stiffness of PLLA is critical for the efficacy of this technique [220, 221].

Another study which used a post-processing step to produce large pores was performed by Lee *et al* (2012) where a femptosecond laser was used to create circular holes with controllable depth and diameter by varying laser energy and number of pulses, respectively [222]. This technique, while simple and effective, requires specialized equipment and creates radial holes rather than three dimensional pores [3].

Table 2.4 provides a summary of the techniques found in literature to improve porosity and pore size of electrospun scaffolds.

Table 2.4: Porosity Enhancement Methods for Electrospun Constructs

Structural Polymer	**Sacrificial Polymer / Porogen / Method**	**Ave. Pore-size (μm)**	**Porosity**	**Appl.**	**Biological Testing**	**Ref**
Fibre Diameter						
PCL	N/A	40-60 [a]	>90%	TE	*in Vitro* (HUVEC)	[132]
PLCL & PLL & PCL	N/A	50	75%	TE	*in Vitro* (HUVEC)	[75]
DP & PLGA	N/A	35-45	ND	CV	*in Vitro* (PHhWB)	[202]
PCL & Collagen	N/A	1.5-40	ND	CV	*in Vitro* (hAEC & hSMC)	[203]
PCL	N/A	18-36	76-87%	TE	*in Vitro* (hDF)	[201]
Custom Collector Designs						
PLGA	Strutted Frame	130	>90%	Skin TE	*in Vitro* (hDF)	[205]
PCL	Patterned Collector	10 - 20	>94%	TE	*in Vitro* (FB)	[128]
PCL	Honeycomb Collector	80 - 360[f]	>90%	TE	None	[223]
PCL	FLUF	2 - 5	ND	TE	*in Vitro* (INS-1)	[207]
PLGA & DP	LTE	ND	>90%	TE	None	[129]
PCL & PLA	LTE	120 - 150[b]	>98%	TE	*in Vitro* (HVSC)	[208]
PCL	Air-flow Impedance	8	ND	CV	*in Vitro* (hDF)	[206]
P(LLA-CL)/SF	Air-flow Impedance	7	ND	CV	*in Vitro* (hSMC)	[224]
Dual Electrospinning with Sacrificial Fibres						
PCL	PEO	ND	ND	MS	*in Vitro* (hMSC)	[212]
PCL	PEO	ND	ND	MS	*in Vivo* (Rat SC)	[215]
Acr-PGS	PEO	ND	ND	CV[c] / MS	*in Vitro* (NNC) & in Vivo (Rat SC)	[213]
TRI	PEO	50	ND	Bone	*in Vitro* (hMSC)	[214]
DP & PLGA	PEG	ND	>85%	TE	*in Vitro* (FB)	[71]

Continued on next page

Structural Polymer	Sacrificial Polymer / Porogen / Method	Ave. Pore-size (μm)	Porosity	Appl.	Biological Testing	Ref
Electrospinning / Electrospraying						
PCL/Col	PEO & Gelatin & Heprasil	ND	ND	TE	*in Vitro* (hFOB)	[216]
PLA	PEG	ND	>85%	TE	None	[225]
SF	PEO	30	>95%	TE	*in Vitro* (FB)	[226]
PCL	PEO	32	>95%	CV	*in Vitro* (FB)	[227]
PCL	NaCl[d]	100-200[e]	>85%	TE	*in Vitro* (CFK2)	[217]
Other Methods						
Zein & PEG	Surface Conductivity	ND	>99%	TE	*in Vitro* (FB)	[218]
PLLA	Ultrasonication	14	>98%	TE	*in Vitro* (FB)	[219]
PCL	Femptosecond Laser	50-200	ND	TE	*in Vitro* (hMSC)	[222]

a= Statistically calculated, b= Spacial Fibre Distance, c= Heart Patch (Not Vascular), d= Spinkled not electrosprayed, e= Size of delaminations, f= size of pockets measured in side section SEM, TE= Tissue Engineering, N/A= Not Applicable, ND= Not Determined, MS= Musculoskeletal, CV= Cardiovascular, PLCL= poly(L-lactide-co-ϵ-caprolactone), PLL= poly(L-lactide), PCL= poly(ϵ-caprolactone), P(LLA-CL)/SF = poly (l-lactic acid-co-ϵ-caprolactone)/Silk Fibroin, PLGA= poly(DL-lactide-glycolide), PLA= poly(lactic acid), PEO= poly(ethylene oxide), Acr-PGS= Acrylated poly(glycerol sebacate), TRI= PCL/collagen I/hydroxyapatite, PEG= Poly(ethylene glycol), DP= Degrapol®, Col= Collagen, SF= Silk Fibroin, PLLA= poly(l-lactic acid), Zein= A natural maize derived protein, HUVEC= Human Umbilical Endothelial Cell, hAEC= Human Aortic Endothelial Cell, FB=Fibroblast, hDF= Human Dermal Fibroblast, HVSC= Human Vena Saphena Cell, hMSC= Human Mesenchymal Stem Cell, NNC= Neonatal Cardiomyocyte, hFOB= Human Fetal Osteoblast, hSMC = Human Smooth Muscle Cell, PHhWB = Partially Heparinized Human Whole Blood, SC= Subcutaneous

Chapter 3

Materials and Methods

This chapter describes the materials and methods used in this study. Firstly the materials used in the fabrication of the scaffolds will be discussed, Section 3.1, followed by descriptions of the electrospinning methods utilised, Section 3.2. In Section 3.3 the heparin surface modification process is described and in Section 3.4 the various methods of characterising and assessing the scaffolds *in vitro* will be outlined. Section 3.6 provides details on the protocol for the *in vivo* tissue response study and finally the statistical methods used will be given in Section 3.7.

3.1 Materials

The polyurethane (PU) chosen as the scaffold material for this study, Pellethane® 2363-80AE (Lubrizol, Wickliffe, OH, USA), is a well-known medical grade polyurethane with a glass transition temperature of -47°C. PEO (Poly(ethylene oxide), 200kDa, Aldrich, St-Louis, MO) was selected as a sacrificial material due to its rapid water-solubility and widespread use in electrospinning literature. The solvents Tetrahydrofuran (THF), Dichloromethane (DCM), Dimethylformamide (DMF), Methanol (MeOH), Ethanol (EtOH) as well as Rhodamine and Fluoroscein Free Acid (FFA) were purchased from Sigma Aldrich.

3.2 Electrospinning

3.2.1 Electrospinning Solution Preparation

All solution concentrations in this study are expressed as weight-per-volume percentages, i.e. a 10% solution will contain 10g of solute in 100ml of solvent.

3.2.1.1 Polyurethane

After literature reviews and own initial experiments a PU concentration of 15% was decided upon for use in subsequent experiments. Two different solvent systems were used: THF and a THF:DMF mixture (1:1), as will be described in more detail below.

THF is a commonly used solvent for electrospinning polyurethanes and is beneficial for its low cost and low boiling point (66°C), but suffers from a low dielectric constant (7.6). DMF, with a dielectric constant of 36.7, was mixed in a 1:1 ratio with THF in an attempt to improve the dielectric properties of the electrospinning solution. Pure DMF was not investigated as a solvent due to its high vapour pressure which, in initial experiments, resulted in fibres depositing on the collector before sufficient evaporation could occur, leading to fibre agglutination. All samples were analysed for resultant fibre diameter, fibre alignment and fibre deposition, Table 3.1 below summarises the experiment.

Table 3.1: PU Solvent System Comparison Parameters*

Solvent System	Flow Rate (ml/hr)	Sample Size
THF	0,75	2
THF:DMF (1:1)	2**	2

*All other electrospinning parameters were held constant: Spin Voltage = 20kV, Working Distance = 20cm, Mandrel Diameter = 25mm, Rotational Speed = 5000rpm, Environmental Temperature ≈ 20°C, Relative Humidity ≈ 30%. **Flow rate was adjusted to achieve a stable Taylor-cone. A small sample size was chosen due to the exploratory nature of the experiment and the large differences in fibre morphology anticipated between the groups (which has been shown in literature [190, 228]).

For both solvent systems, homogeneous solutions were obtained by mixing all parts of the solution in a sealed Pyrex® 250ml bottle and placing in a roller oven for 24 hours at 40°C.

3.2.1.2 Polyethylene oxide

For PEO, two different solvents were tested, DCM and 90%/10% EtOH/H_2O. DCM was used in an attempt to spin large diameter fibres due to its low boiling point (40°C) and low dielectric constant (8.9). Conversely EtOH, possessing a moderately higher boiling point (78°C) and a much higher dielectric constant (24.5), was utilized in the production of small diameter fibres.

Solution concentration was set to 20% as it proved the highest value within the usable viscosity range. Preliminary tests compared the resultant fibre diameters for DCM and

EtOH solvents at a range of solution flow rates. Table 3.2 below summarises the experimental parameters.

Table 3.2: PEO Solvent System Comparison Parameters*

Group	Solvent	Flow Rate (ml/hr)	Distance (cm)**	Sample Size
Thick	DCM	2	10	2
		4	10	2
		6	10	2
Thin	EtOH	2	20	2
		4	20	2
		6	20	2

*All other electrospinning process parameters held constant: Spin Voltage = 20kV, Mandrel Diameter = 25mm, Rotational Speed = 5000rpm, Environmental Temperature ≈ 21°C, Relative Humidity ≈ 25%. **Working Distance adjusted between solvents as Taylor cone would not form for DCM groups further than 10cm and for EtOH groups the jet would not completely evaporate before deposition at distances closer than 20cm.

The solutions were made-up in 250ml Pyrex bottles and placed in a roller oven for 24 hours at 35°C to ensure homogeneity and complete dissolution.

3.2.2 Electrospinning Equipment and Design

The electrospinning equipment used at the initiation of the project included two syringe pumps (SE400B, Fresenius, Bad Homburg, Germany), an adjustable high voltage power supply (custom made), a rotating and bi-directionally translating collector mechanism with 24 volt power supply for rotation speed control and a separate custom made controller for translation control. Two different collector mandrels, with large (25mm) and small (5mm) diameters made of 316 Stainless Steel were used. The collector mechanism was housed inside a specially designed box with a ventilation system fitted to safely remove any evaporated solvent created during the electrospinning process. Humidity and temperature were measured using a thermo-hygrometer (Lasec, South Africa).

In order to accommodate the dual spinning process two additional high voltage power supplies were obtained, one positive in polarity and the other negative (ES30P-5W/ES30N-5W, respectively, Gamma High Voltage Research, FL, USA). Purpose built electrostatic guides (1mm thick aluminium plate, 20mm x 100mm), for countering the repulsion force between like-charged fibrous jets, were designed and manufactured in-house and erected on either side of the rotating mandrel in parallel. Two blunted 16G hypodermic needles were used as spinnerets. See Figure 3.1 for 3D CAD renders of the final equipment utilized.

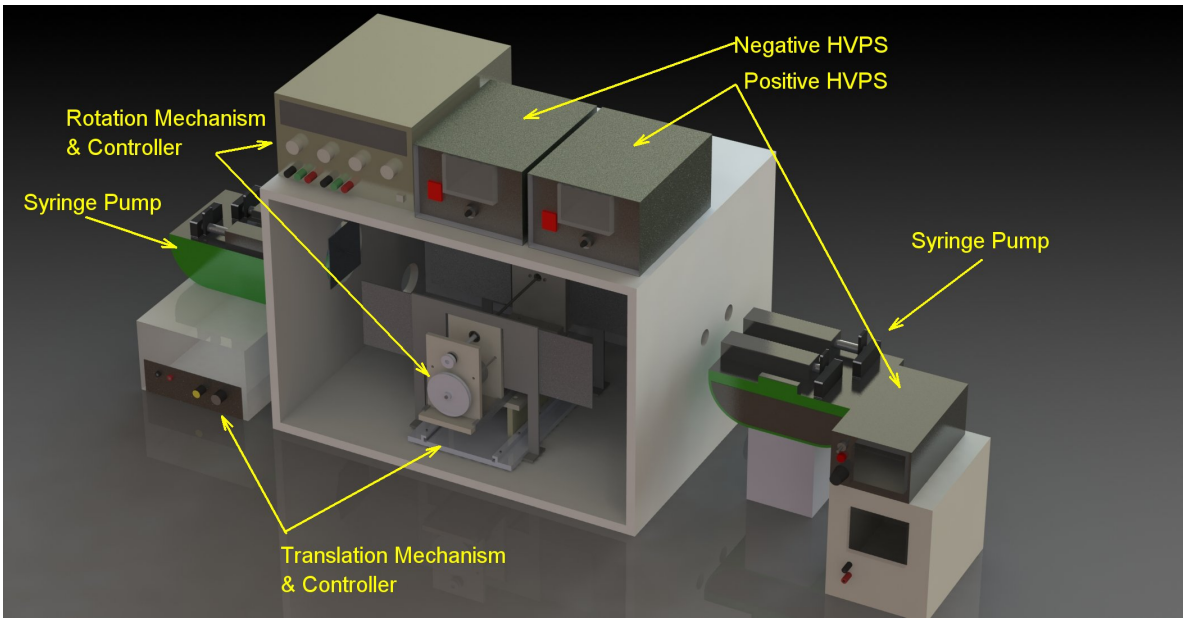

(a) Trimetric View

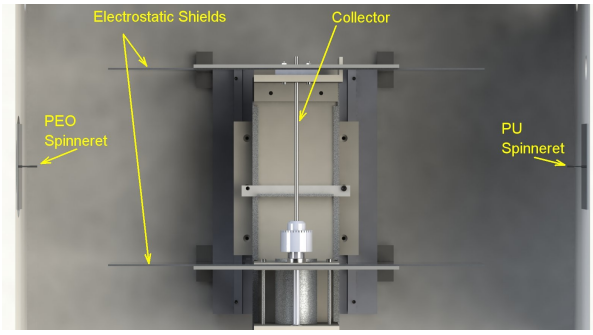

(b) Top view

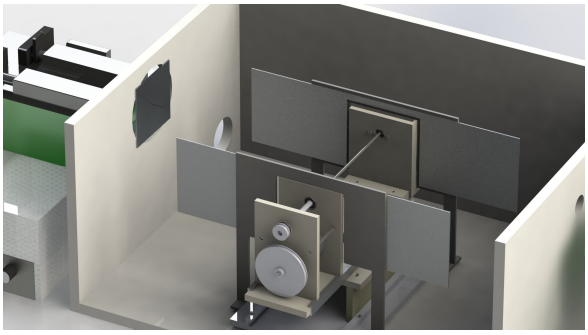

(c) Trimetric View (Inside Box)

Figure 3.1: 3D renders of modified electrospinning equipment for dual electrospinning. Note the spinnerets positioned on opposite sides of the collector mandrel with electrostatic shields erected parallel and offset to the jet direction. HVPS = High Voltage Power Supply.

3.2.2.1 Tailoring the Electric Field for Dual Electrospinning

In an attempt to direct the deposition of the two polymer jets a variety of electric field configurations were theoretically and experimentally assessed. Fundamentally there were only three different electric field configurations that could be used: spinnerets charged with the same polarity, spinnerets charged with opposing polarities and configurations using alternating current (AC) electrospinning. This study investigated the effectiveness of both like and opposing polarity configurations as well as modifications of each to further improve the control over the electrospun jets; AC electrospinning was not investigated due to the safety concerns associated with high voltage AC electric fields.

3.2.3 Composite Scaffold Fabrication

The electrospinning parameters used for this study were chosen after an iterative process of optimization.

PU was spun from a 15% solution in THF:DMF (1:1) at a constant feed flow rate of 3ml/hr and an applied voltage of +20kV at 200mm working distance.

Two different classes of PEO fibre were investigated, one comprising large diameter fibres (*thick*) and the other small diameter fibres (*thin*, See Table 3.3). The large and small diameter PEO fibres were spun from 20% solutions of DCM and 90%EtOH, respectively and at distances of 100mm and 200mm, respectively. For both, the applied voltage was set to +20kV. PEO solution flow rate was adjusted depending on the PU fibre fraction required and ranged from 0ml/hr to 6ml/hr.

Aluminium shields were charged to +7kV and erected parallel to the jet trajectory on either side of the rotating collector (5000rpm), at a distance of 90mm from the centre of its midpoint, to better direct the deposition of the like charged polymer jets.

For the production of small diameter grafts a mandrel size of 5mm was used while in the case where large samples were required for mechanical testing or *in vivo* studies a larger 25mm mandrel was used. In either case the collector was charged to -1kV to promote deposition on the mandrel. The collector was rotated at 5000rpm and translated 2.6mm/min over a distance of 30mm.

For all samples the recorded relative humidity and temperature were in the region of 20% - 28% and 20°C - 24°C, respectively.

Description	**Graphic**
Thick sacrificial fibres: PU/(THF:DMF) & PEO/DCM - Large diameter, aligned sacrificial fibres. *Thick* groups (n=49)	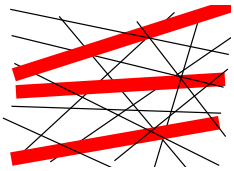
Thin sacrificial fibres: PU/(THF:DMF) & PEO/EtOH - Small diameter, dispersed sacrificial fibres. *Thin* groups (n=101)	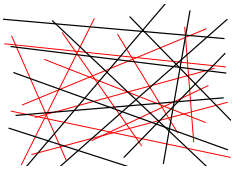

Table 3.3: Thin and thick sacrificial fibres were experimentally assessed for differences in porosity achieved after removal of their respective sacrificial fibres. Fibre fraction was varied by controlling PEO flow rates (2ml/hr - 6ml/hr) for each group.

3.2.4 Sample Preparation

Samples were prepared differently depending on the mandrel size used and the desired use of the sample (Figure 3.2). Grafts spun on 5mm mandrels were cut to size while on the mandrel and initiated into the PEO extraction process while still on the mandrel. The grafts were then removed and dried.

Scaffolds required for *in vivo* studies were spun on a 25mm mandrel where only the centre 10mm was used (thickest part of the sample), the samples were cut to size (10mm by 10mm by approximately 1mm thick) and measured for exact size(as per section 3.4.5). Samples were then processed for PEO extraction and drying.

Samples required for mechanical testing were spun on a 25mm mandrel and cut in the circumferential direction 30mm long by 5mm wide. Samples required for testing in the transverse direction were cut 30mm long in the transverse direction by 5mm wide. Samples were then processed for PEO extraction and drying.

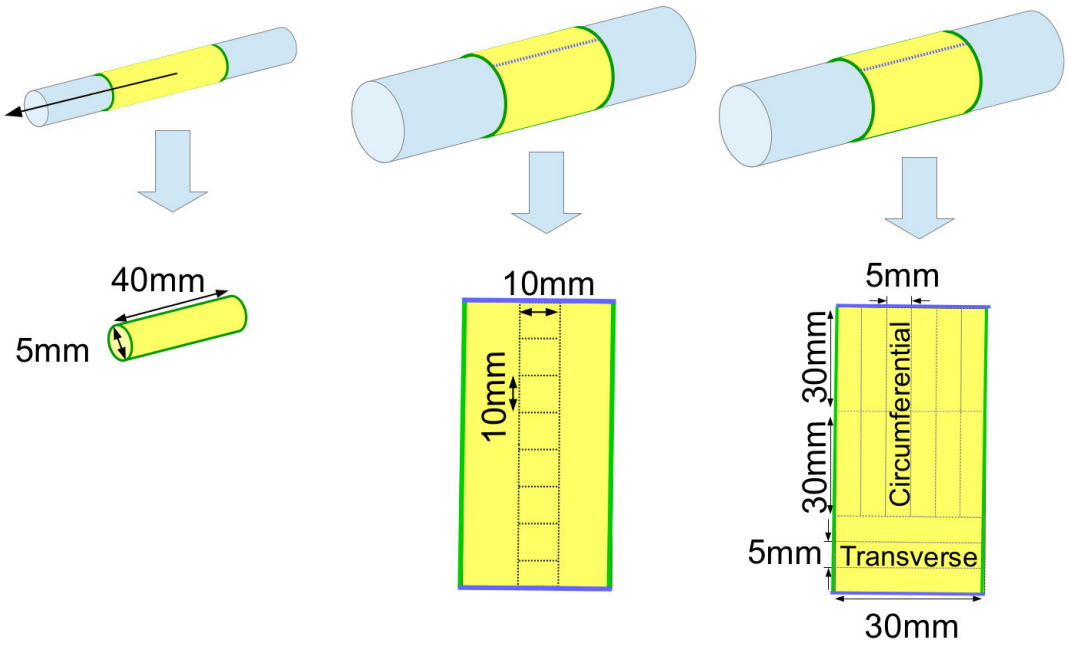

(a) Grafts (b) *In vivo* Studies (c) Mechanical Testing

Figure 3.2: Graphical depiction of sample preparation process for each application. c) Note both circumferential and transverse direction samples taken from one electrospun sheet with paired samples in the circumferential direction. Blue and green lines indicate transverse and circumferentially cut lines, respectively.

3.2.5 PEO Extraction

PEO was extracted after spinning by immersion in gradually decreasing mixtures of alcohol and deionised (DI) water, starting at 50% EtOH for 1 hour and then decreasing by 10% per hour until only DI water remained.

Two different drying processes, lyophilization (freeze-drying) and vacuum drying, were evaluated for their effects on scaffold shrinkage. The length of 100%, 70% and 40% fibre fraction grafts were measured and recorded before undergoing the PEO removal process and after drying (n=2). The final shrinkage values ($\frac{length\ before\ PEO\ removal}{length\ after\ drying}$) were calculated and compared between drying methods for each fibre fraction. For lyophilization, samples were frozen in liquid nitrogen (while immersed in water) prior to vacuum exposure.

3.3 Heparin Surface Modification

Heparin was covalently bound to the surface of the PU fibres in a process which has been previously described [15]. Briefly, the heparinization process involved rinsing scaffolds (post PEO-extraction and lyophilization) in deionised (DI) water and immersion in a solution containing: acrylic acid (4M, Aldrich, USA), acrylamide (1M, Aldrich), $Cu(NO_3)_2$ (0.1M, Saarchem Holpro, RSA) and, after removal of oxygen, cerium ammonium nitrate (0.006M, Saarchem). Scaffolds were sonicated (Waterbath, 100W, UMC5, Integral Systems) in the solution for 40 minutes at RT, after which they were rinsed in DI water at RT, exchanging water 3 times (once every 10 minute) and left overnight on a shaker.

The scaffolds were then aminated through reaction (2hr, sonication, RT) with ethylene diamine (EDA, 0.5M, Fluka) in 2-(N-morpholino)ethanesulfonic acid buffer (MES, 0.5M, pH=5, Fluka) containing 0.05M 1-ethyl-3(3-dimethyl-aminopropyl)carbodiimide (EDC, Sigma) and rinsed in DI water.

Finally, heparin was covalently attached through reductive amination by treating (2hr, 50°C, sonication) the aminated scaffolds with a solution of nitrous acid de-aminated (NAD) heparin (2mg/ml, Celsus, USA) in an acetate buffer (0.4M, pH=4.6) sodium cyanoborohydride ($NaCNBH_3$, 0.016M, Sigma). The heparinized scaffolds were then rinsed in DI water (3x10 minutes and overnight on shaker) and dried by lyophilization.

3.3.1 Qualitative Verification of Heparinization

Verification of each step in the heparinization process was achieved by using the same staining technique as developed as described previously [15]. Toluidine Blue, a cationic

dye, was used to stain the negatively charged carboxyl groups (blue) and heparin (purple) in the AAc grafting and final heparinization steps, respectively. Conversely, Ponceau S, an anionic dye, was used to stain the positive aminated structures of the second step (red). Thus each stage of the process was monitored for efficacy before the next is initiated.

3.3.2 Quantitative Testing of Heparinization

Quantitative values for describing the degree of heparinization achieved were obtained by means of a 3-methyl-2-benzothiazolinehydrazone-hydrochloride (MBTH) assay which has previously been adapted by this group [15] from Riesenfeld and Rodèn [229] . Heparinized and non-heparinized (controls) scaffolds were immersed in 250µl DI water before 500µl nitrous acid solution (0.025M HNO_2, 0.9M HCl) was added and sonicated at RT, to selectively cleave glucosamine-(1,4)-uronic acid glycosidic bonds of the heparin molecule to form di/tetrasaccharides. The degradation reaction was stopped after 30 minutes by the addition of 250µl of ammonium sulfate solution (1M) and vigorously mixed. This degradation solution was transferred into a clean test tube and the remaining scaffold was rinsed with 500 µl NaCl solution (1M) which was then added to the degradation solution. 500µl of MBTH solution (0.011M) was added and reacted with the degraded heparin at 50°C for 15 minutes . Subsequently the MBTH molecule was complexed by the addition of 500µl $FeCl_3$ (9.031 M) solution (50°C, 20 minutes) and the resultant solution was allowed to cool before its absorbance was determined by UV spectroscopy (660 nm, Shimadzu UV-1601PC).

A standard curve was generated in a similar fashion which differed only in the absence of a scaffold and the replacement of the 250µl DI water with the same volume of control solutions of heparin (0 - 2.4mg/ml, 14 points). Scaffold heparin content was determined using the standard curve and expressed as milligram heparin per gram of scaffold matrix.

3.4 Scaffold Characterisation

3.4.1 Scanning Electron Microscopy (SEM)

Samples were gold sputter coated (Polaron SC7640, Quorum Technologies, East Grinstead, England) prior to imaging by SEM. Two different scanning electron microscopes were used depending on the application: for visualisation of fibre morphology a secondary scatter mode SEM (Nova NanoSEM 230, FEI, Oregon, USA) was used at an operating voltage of 20keV; whereas for quantification of fibre morphology and pore-size distribution a backscatter mode desktop SEM (Phenom ProX, Phenom-World, Eindhoven,

Netherlands) was used at an operating voltage of 10keV. Samples were scanned on both their luminal and abluminal surfaces.

3.4.2 Fibre Diameter, Alignment & Pore-Size Measurement

Fibre diameter and pore size were automatically quantified with the FiberMetric and PoroMetric software, respectively (Phenom-World). Image contrast and brightness were adjusted until only the top-most fibre layer was visible to prevent measurement errors associated with focal length (see Figure 3.3).

Fibre alignment was characterised using the OrientationJ-Measure plug-in (19.11.2012, BIG, EPFL, Switzerland [230, 231]) for ImageJ/Fiji (1.49c, NIH, USA [232]) which produces a "coherency" value from an image and can be interpreted as the degree of anisotropy in the scaffold (see Figure 3.4).

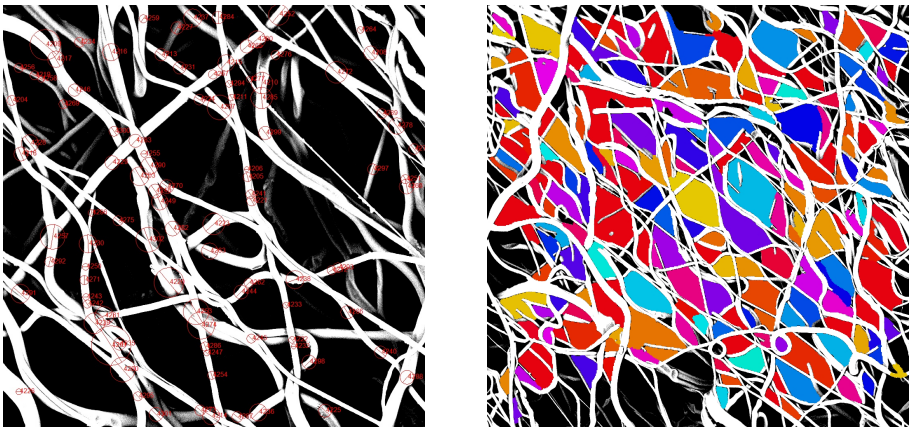

(a) Fibre Diameter Measurement (b) Pore Size Measurement

Figure 3.3: Depiction of typical fibre diameter and pore-size measurements using the Phenom FiberMetric and PoroMetric software in a) and b), respectively. Note a) and b) are taken at different magnifications to improve the accuracy of the automated measurements .

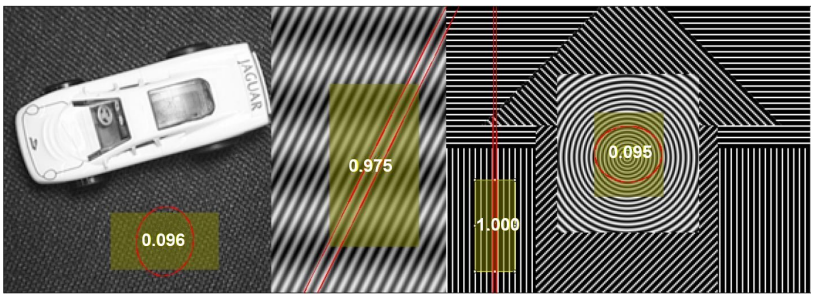

Figure 3.4: Example of anisotropy determination, the calculated "coherency" values for each region are displayed inside the regions boundaries and represent the degree of visual anisotropy present in the region. The coherency values range from 0 to 1 representing complete isotropy and anisotropy, respectively. Image adapted from [233]

3.4.3 Confocal Microscopy

PU and PEO solutions were dyed prior to electrospinning with Fluoroscein Free Acid (0.2%) and Rhodamine (0.1%), respectively, allowing for visual verification of fibre type and inter-dispersion. Samples were imaged under confocal laser scanning microscopy (Zeiss LSM 510 Meta NLO, ZEN 2009 Software, Carl Zeiss Microscopy, Jena, Germany).

3.4.4 Fibre Fraction Determination

Fibre fraction was defined as the percentage PU mass in the scaffold and was determined as the ratio of the mass of the scaffold post PEO extraction to the mass prior to PEO extraction.

$$FF_{PU} = \frac{m_{PU}}{m_{PU} + m_{PEO}} = \frac{m_{after}}{m_{before}} \qquad [\%] \tag{3.1}$$

Where FF_{PU} is the PU fibre fraction, m_{PU}, m_{PEO} are the mass of PU and PEO present in the scaffold, respectively and m_{before} and m_{after} are the mass of the scaffold before and after PEO extraction, respectively.

Mass was determined with a 5 decimal balance (XS105, Mettler-Toledo AG, Greifensee, Switzerland).

3.4.5 Porosity Determination

Porosity was estimated by gravimetric means using the following equation:

$$P = 1 - \frac{V_f}{V_b} \qquad [\%] \tag{3.2}$$

where P is the calculated porosity, V_b is the bulk volume of the scaffold and V_f is the volume of the scaffold fibres. The bulk volume (V_b) was calculated by estimating the scaffold's boundaries as a rectangular cuboid, where the length and width were measured with a Vernier Calliper and the thickness was determined with a Leica DFC280 stereo microscope (Leica Microsystems GmbH, Wetzlar, Germany). The fibre volume was estimated by dividing the mass of the sample post PEO removal (m_{after}) by the manufacturer stated density of Pellethane (ρ_{PU}, 1.12 g/ml); where the mass of the sample was measured on a 5 decimal balance.

Similarly, the porosity of a scaffold before PEO extraction was estimated after its PU fibre fraction had been calculated (FF_{PU}, Equation 3.1). First, the fibre volume of the composite scaffold was determined using Equation 3.3, the recorded mass of the sample

(m_{before}) and the manufacturer stated density of PEO (ρ_{PEO}, 1.21 g/ml). The calculated value of V_{fb} was then used in place of V_f in Equation 3.2 to determine the porosity of the scaffold before PEO removal.

$$V_{fb} = m_{before}\left(\frac{FF_{PU}}{\rho_{PU}} - \frac{1 - FF_{PU}}{\rho_{PEO}}\right) \qquad [mm^3] \tag{3.3}$$

In order to verify the assumption that the density of the electrospun PU fibres were equivalent to the density of the bulk material, an initial study compared measured porosity values of 20 samples with various fibre fractions by both gravimetric and densitometric means. Equivalence was determined with a paired, two-tailed students t-test and setting the confidence interval (CI) to 90% with a significant mean difference interpreted as a value greater than 1%.

The densitometric method is similar to the gravimetric method except that the fibre volume is estimated by Archimedes principle. The scaffold is weighed both in air and while immersed in liquid (EtOH, ρ = 0,789 g/ml) and the fibre volume calculated according to equation 3.4 below.

$$V_f = V_{EtOH} = \frac{m_{EtOH}}{\rho_{EtOH}} \qquad [mm^3] \tag{3.4}$$

3.4.6 NanoCT 3D Rendering of Scaffold Micro-Architecture

1mm^3 cubes of low and high porosity samples (defined in Section 3.6.1.1) were scanned with a Nanotom S (General Electric, PA, USA) at 500nm voxel resolution and analysed with VGstudioMax 2.2 (Volume Graphics, Heidelberg, Germany) for determination of porosity and morphology.

3.5 Mechanical Testing

All mechanical testing consisted of uni-axially tensile testing specimens until failure on an Instron 5544 (Instron, Norwood, USA), equipped with a 500N load cell. Samples were prepared as described in section 3.2.4. Three different groups of mechanical tests were performed as summarised in Table 3.4.

Table 3.4: Summary of Mechanical Tests Performed on Specimens

		Dry @ RT		PBS @ 37C	
Sac. Fibre Class.	**Direction**	**Before**	**After**	**After**	**Hep**
Thick	Circ.	72	52	-	-
	Trans.	12	8	-	-
Thin	Circ.	84	69	45	43
	Trans.	23	10	10	13
None	Circ.	-	4	4	-
	Trans.	-	4	4	-
			a	b	c

a) Comparative testing between scaffolds incorporated with thin vs thick sacrificial fibres - values indicate sample sizes of whole range of fibre fractions (20%-70%) tested per group, including PEO only (0%, n_{DCM}=4 and n_{EtOH}=4) and PU only (100%, n=4); b) Assessment of influence of hydration in PBS at 37°C (100% PU scaffolds only, n=4); c) Effect of heparinization - range of fibre fractions tested = 20% to 100%.

The effects of PEO incorporation and extraction on scaffold strength were tested dry at room temperature due to PEO's rapid dissolution in water. Conversely heparin modified samples needed to be tested wet due to their hydrogel nature, thus the second set was tested while immersed in PBS (7.4 pH) at 37°C, to simulate physiological conditions.

Continuous data sets were analysed by comparing the linear regressions fitted (least squares) to each group, where the x-axis was set as scaffold fibre fraction or porosity and the y-axis was the mechanical measurable under observation (UTS, Young's modulus and maximum elongation).

Dry samples were tested using standard Instron grips modified with diamond pattern rubber grip surfaces; while for submerged samples custom made 304 stainless steel grips were used, also attached with diamond pattern rubber surfaces, see Figure 3.5.

Samples were tested both in the circumferential and transverse direction relative to the

scaffolds deposition on the collector mandrel in order to quantify the mechanical effects of fibre alignment (see Figure 3.2c).

Ultimate tensile strength (UTS) and maximum elongation (strain) were obtained from stress/strain curves and were defined as the stress and strain, respectively at the point of global maximum stress. Young's modulus was defined as the slope of the line fitting the stress/strain data between strains of 0% and 10% (depicted in Figure 3.6).

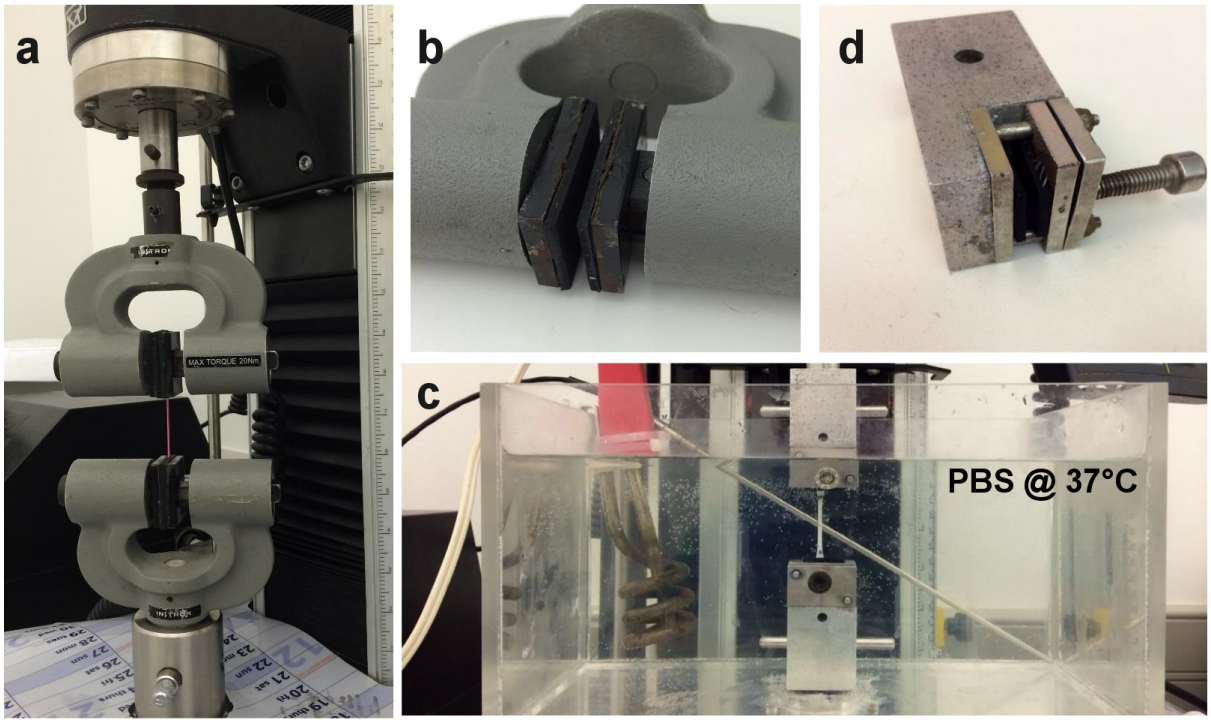

Figure 3.5: a) Tensile testing in dry conditions, b) Close-up of Instron grips used for dry testing, c) Tensile testing in PBS-filled water-bath temperature controlled at 37°C, d) Custom-made grips for testing under physiological conditions.

3.5.0.1 Compliance and Burst Pressure Estimation

Theoretical compliance and burst pressure values were calculated for tubular constructs by transforming tensile testing data using thick walled cylinder theory. Briefly, burst pressure was calculated by assuming the tensile stress in uni-axially extended scaffold sheets to be equivalent to the hoop stress in cylindrical constructs according to the simplified version of Lame's equations (Equation 3.5) which assumes negligible external pressure, maximum hoop-stress at the inner diameter of the cylinder and negligible radial and axial stresses and strains. Thick cylinder theory was used because for small diameter grafts $r/t > 10$ in most cases, thus large errors are associated with thin walled theory.

$$\sigma_h = P_i \frac{r_o^2 + r_i^2}{r_o^2 - r_i^2} \qquad [MPa] \tag{3.5}$$

Where σ_h, P_i, r_i and r_o are the hoop stress (tensile stress, MPa), internal pressure (MPa), inner radius (mm) and outer radius (mm) of the theoretical cylinder, respectively. The UTS of the material (MPa) was then used to determine the maximum internal pressure responsible for failure which was then converted to mmHg.

In order to calculate diametral compliance, the standard equation was first modified slightly to replace diameter as in input with strain, this process is described below:

Diametral compliance:

$$C_d = \frac{D_s - D_d}{(P_s - P_d)(D_d)} \times 10^4 \qquad [\%/100mmHg] \tag{3.6}$$

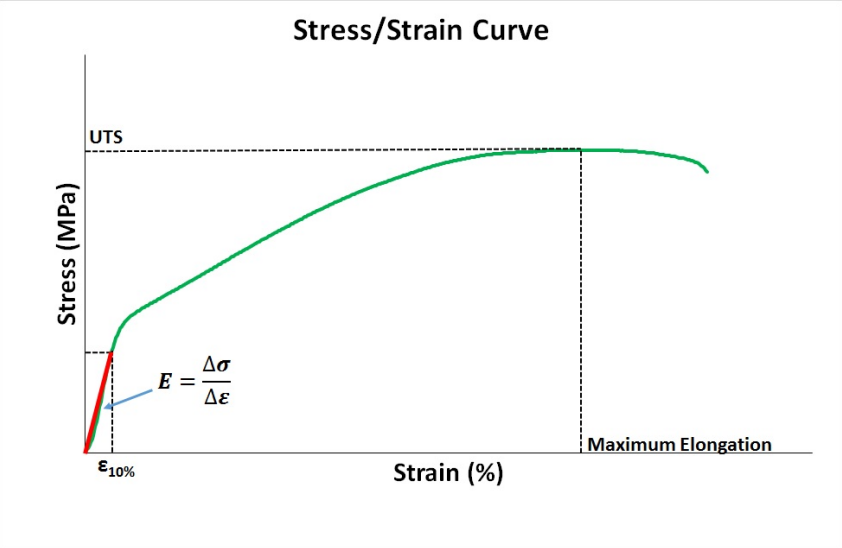

Figure 3.6: Typical stress/strain curve showing values definitions for UTS, maximum elongation and Young's Modulus.

Using the definition of strain and converting length (circumference) to equivalent diameter:

$$D_x = D_0(\epsilon_x + 1) \qquad [mm] \tag{3.7}$$

Substituting 3.7 into 3.6:

$$C_d = \frac{\epsilon_s - \epsilon_d}{(P_s - P_d)(\epsilon_d + 1)} \times 10^4 \qquad [\%/100mmHg] \tag{3.8}$$

Where C_d, D_s and D_d are diametral compliance, diameter of the imaginary graft at systole and diastole. Additionally, D_x is the equivalent diameter of the conduit at a given strain (ϵ_x). σ_s, σ_d and ϵ_s, ϵ_d are the equivalent hoop stresses and strains at systolic and diastolic pressures, respectively.

Now, by determining the equivalent hoop stress (Equation 3.5) at 80mmHg (P_d, 1.07×10^{-2} MPa) and 120mmHg (P_s, 1.60×10^{-2} MPa) internal pressures, the corresponding strain values were read off of the stress/strain curve, which was previously obtained from uni-axial testing (see Figure 3.7). Utilizing these strain values in Equation 3.8 a theoretical diametral compliance could be calculated for each sample that had been uni-axially tested.

Compliance was calculated for theoretical grafts 0.5mm thick with internal diameters of 6mm for PU and PU+Hep at physiological conditions (PBS at 37°C).

3.5.1 Strain Rate Calculations

In order to simulate the physiological conditions that the material would undergo as a vascular graft an ideal strain rate was calculated using healthy blood vessels as a reference: The average compliance of a healthy blood vessel was estimated by Tai *et al* [106] to be 8%/100mmHg, equating to 3.2%/40mmHg for a healthy 120/80mmHg blood pressure. The 40mmHg pulsatile pressure is experienced over the systolic ejection period of the cardiac cycle, which is dependant on heart rate (HR) and, according to Weissler *et al* [234], can be calculated using the following equation:

$$t_{systole} = 0.413 - 0.0017 \times HR \qquad [s] \tag{3.9}$$

Assuming a healthy average HR of 72bpm [235] the systolic period is approximately 290ms.

Thus an ideal blood vessel would experience a compliance of 3.2% over a duration of

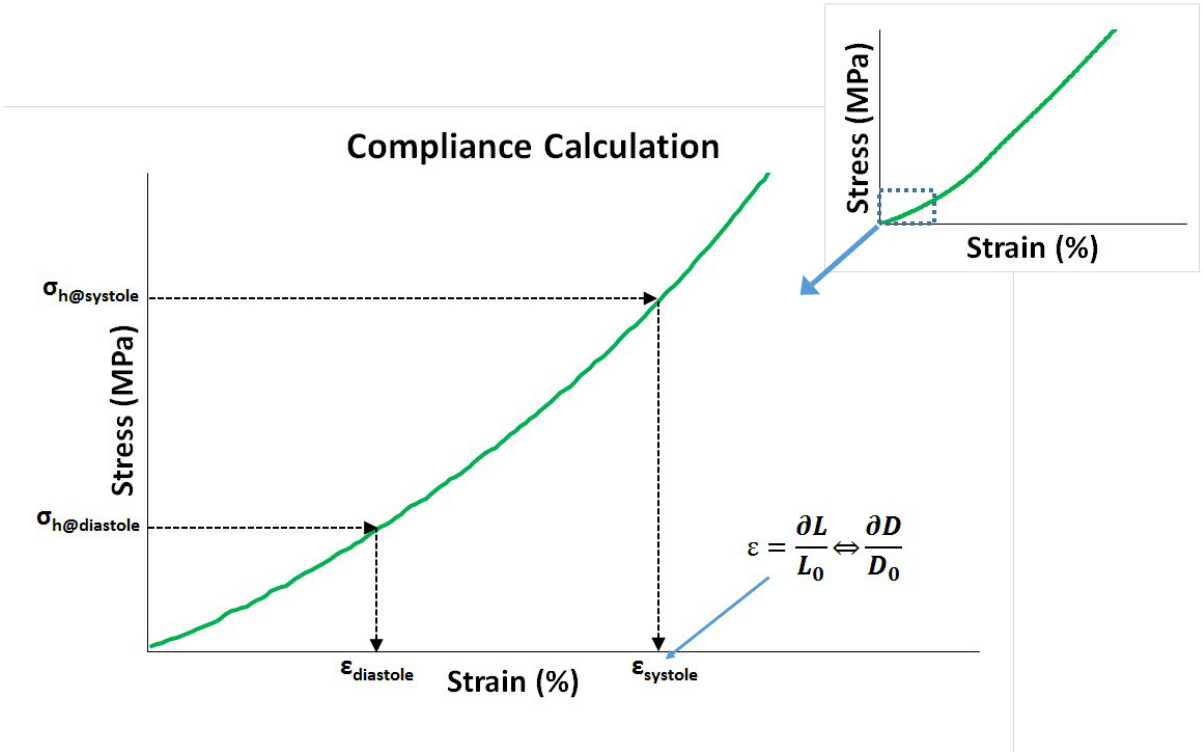

Figure 3.7: Calculation of compliance, first equivalent hoop stresses calculated for internal systolic and diastolic pressures, this is assumed to be equivalent to the tensile stress observed in uni-axially extended samples. The strain at the resultant stresses from systolic and diastolic pressures are then obtained from the stress/strain curve which can then be used to calculate compliance with Equation 3.8.

290ms, this equates to a strain rate of:

$$\frac{3.2\%}{0.29s} = 11\%/s \tag{3.10}$$

Thus, for the chosen gauge length of 10mm, the strain rate was set to 1.1mm/sec.

3.6 *In Vivo* Subcutaneous Study

All animal experiments performed in this thesis were in compliance with the Animal Protection Act (Act 71 of 1962), the Veterinary and Paraveterinary Professions Act (Act 19 of 1982) and the South African National Standard for the Care and Use of Animals for Scientific Purpose (SANS 10386:2008), and were approved by the Departmental Research Committee and Animal Ethics Committee of the University of Cape Town before commencement.

3.6.1 Experimental Design

Scaffolds of three different porosity classes (low, medium and high) and their heparinized versions were assessed for tissue ingrowth, inflammation and angiogenesis through dorsal subcutaneous implantation in male Wistar rats (250g - 300g).

In order to detect a mean difference of 10% between groups with a standard deviation of 5% within each group a sample size of 6 was calculated ($\alpha = 0.05$ (one-tailed); $\beta = 0,9$) with StatsMate (StatsMate 2.00, GraphPad,CA,USA). In order to determine differences in the rate of tissue ingrowth, vascularization and inflammation between samples, three different time points were investigated: 7, 14 and 28 days. Figure 3.8 below summarises the experiment graphically.

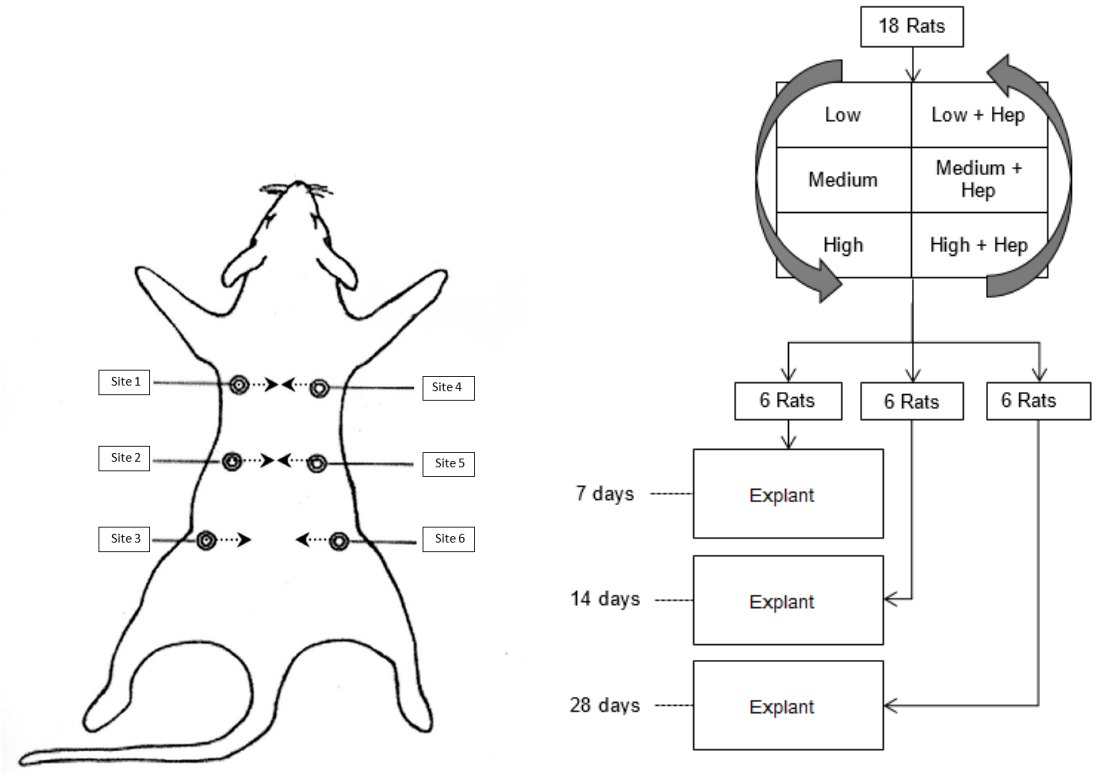

(a) Dorsal View (Adapted from [22]) (b) Experiment Flow Chart

Figure 3.8: Scaffolds of different porosity classes (High/Medium/Low) and heperanised versions (High-Hep/Medium-Hep/Low-Hep) of each (6 total), prepared as described in section 3.2.4, were subcutaneously implanted into dorsal pockets of male Wistar rats (250g - 300g) for three different durations (7, 14 and 28 days) with a sample size of 6 per time point (totalling 18 rats). Sample locations were rotated between rats to compensate for anatomical variation.

3.6.1.1 Scaffold Fabrication

Low, medium and high porosity scaffolds were defined as those with porosities of 70%, 80% and 90%, equating to PU fibre fractions of 100%, 70% and 30%, respectively (when estimated from Figure 4.11 in Section 4.2.5).

Fibre fraction was controlled by varying the PEO solution flow rate according to values calculated by Equation 3.12 below; where η, ρ, C and Q represent the electrospinning efficiency constant, density, concentration and flow rate, respectively of each solution. η can be estimated empirically with Equation 3.11, where t is the spinning duration and m_{loss} is the mass of polymer that was spun but did not deposit in the scaffold region. η will vary for different electrospinning set-ups, solutions and parameters.

$$\eta = \frac{mass\ spun - mass\ loss}{mass\ spun} = \frac{\rho QCt - -m_{loss}}{\rho QCt} \qquad [\%] \tag{3.11}$$

$$FF_{PU} = \frac{m_{PU}}{m_{PEO}} = \frac{(\eta\rho CQ)_{PU}}{(\eta\rho CQ)_{PEO}} \qquad [\%] \tag{3.12}$$

For low porosity scaffolds, a second PU solution was spun in place of the PEO solution at 3ml/hr to simulate the inter-fibre forces present with the medium and high porosity scaffolds. Scaffolds were then prepared as described in section 3.2.4, dried by lyophilization and their fibre fractions and porosities determined as described in sections 3.4.4 and 3.4.5, respectively. Heparinized versions were then prepared as described in section 3.3.

3.6.2 Surgical Procedures

Animals were allowed to acclimatize in their groups (6 per cage) and surroundings for 2 days pre-operatively and were fed *ad libitum* throughout the experiment. Prior to surgery rats were weighed, placed under general anaesthesia through inhalation of 5% isoflurane in an enclosed perspex box (equipped with disposable absorbent pads), dorsally shaved and the surgical area disinfected with consecutive swabbing of F10 Skin Prep, 70% Alcohol and finally Iodine solution. At this point buprenorphine (0.05mg/kg) was administered subcutaneously for post surgical analgesia. The animals were then placed on a temperature controlled (37°C) operating board where general anaesthesia was maintained through nose-cone inhalation of 1.5% isoflurane at an oxygen output of 1.5l/min (1 Bar, 21°C). Surgery was performed under sterile conditions, inside a laminar flow hood.

Prior to incision, appropriate depth of anaesthesia was verified by lack of limb reflex on stimulation. Following sterile draping 1 cm incisions were made bi-laterally with respect

to the dorsal mid-line and pockets opened laterally using blunt dissection, while paying close attention to prevent communication with adjacent pockets. Scaffolds, which had previously been sterilized with Ethylene Oxide (EO) and stored in sterile PBS (7.4pH), were then placed in the pockets in a rotationally varied order and resealed with 2/0 Monofilament Nylon sutures (Ethilon, Ethicon, New Brunswick, NJ). After all 6 pockets had been resealed, rats were marked for identification with an ear punch (while still under general anaesthesia).

Rats were then placed under a warming lamp and monitored until fully conscious. Following surgery, animals were housed individually for 4 days, weighed every second day and monitored daily during that time, on the first day post surgery rats were administered with a second dose of 0.05mg/kg buprenorphine subcutaneously. After 4 days the rats were reintroduced to their original groups of 6 per cage and were monitored daily and weighed weekly thereafter.

Scaffolds were explanted with surrounding skin and fibrous capsule at 7,14 and 28 days after euthanasia by inhalation of 5% halothane in air. Death was confirmed by cardiac injection of 1 ml saturated KCl solution. Samples were cut in half using a sharp blade where one half was placed in Zinc fixative solution [236] and the other half in 10% Formalin.

3.6.3 Histological Analysis

After 4 days of fixation samples were dehydrated by immersion in ascending grades of alcohol, embedded in wax, cut into 5µm sections, mounted onto slides and de-waxed using 2,2,4-trimethylpentane followed by hydration in descending grades of alcohol. Sections were then stained with Haematoxylin and Eosin (HE) to characterise tissue colonization; Picroserius Red (PSR) to quantify collagen deposition; anti-CD31 (Fitzgerald International, North Acton, MA) to label endothelial cells for visualisation of angiogenesis; and anti-ED1 (Serotec Ltd, Oxford, UK) (Cy3 secondary antibody) counter stained with 4',6-diamidino-2-phenylindole (DAPI) for identification of tissue macrophages. Histological preparation of samples was performed in-house by the histology group of the Cardiovascular Research Unit.

Sections were imaged in cross-section (Nikon Eclipse 90i, Nikon, Tokyo, Japan) and stitched at appropriate magnifications (H&E = 2X, PSR = 4X, CD31 = 10X and ED1 = 20X) to include the visible graft area. All slides were imaged under bright-field microscopy except for ED1 slides (fluorescent microscopy). Captured images were processed for quantitative analysis using Visiopharm Integrated Systems (Visiopharm A/S, Hørsholm, Denmark).

Ingrowth index was defined as the average distance perpendicular to the graft edge where gross infiltration had occurred divided by half the scaffold width and was calculated, assuming a rectangular cross section, according to $Ingrowth\ Index = 2d_t/w_s$ where d_t and w_s represent the average tissue infiltration depth and scaffold width, respectively. Isolated cells, populating deeper regions of the scaffold away from the majority of the population, are excluded (n=6).

Ingrowth rate ($\dot{d}_t$) was calculated as the average change in ingrowth per week, defined by Equation 3.13:

$$\dot{d}_t = \frac{\Delta d_t}{\Delta t} \times \frac{1}{7} \qquad [\mu m/week] \tag{3.13}$$

where Δd is the change in infiltration depth (μm) over the difference in implant period Δt (days).

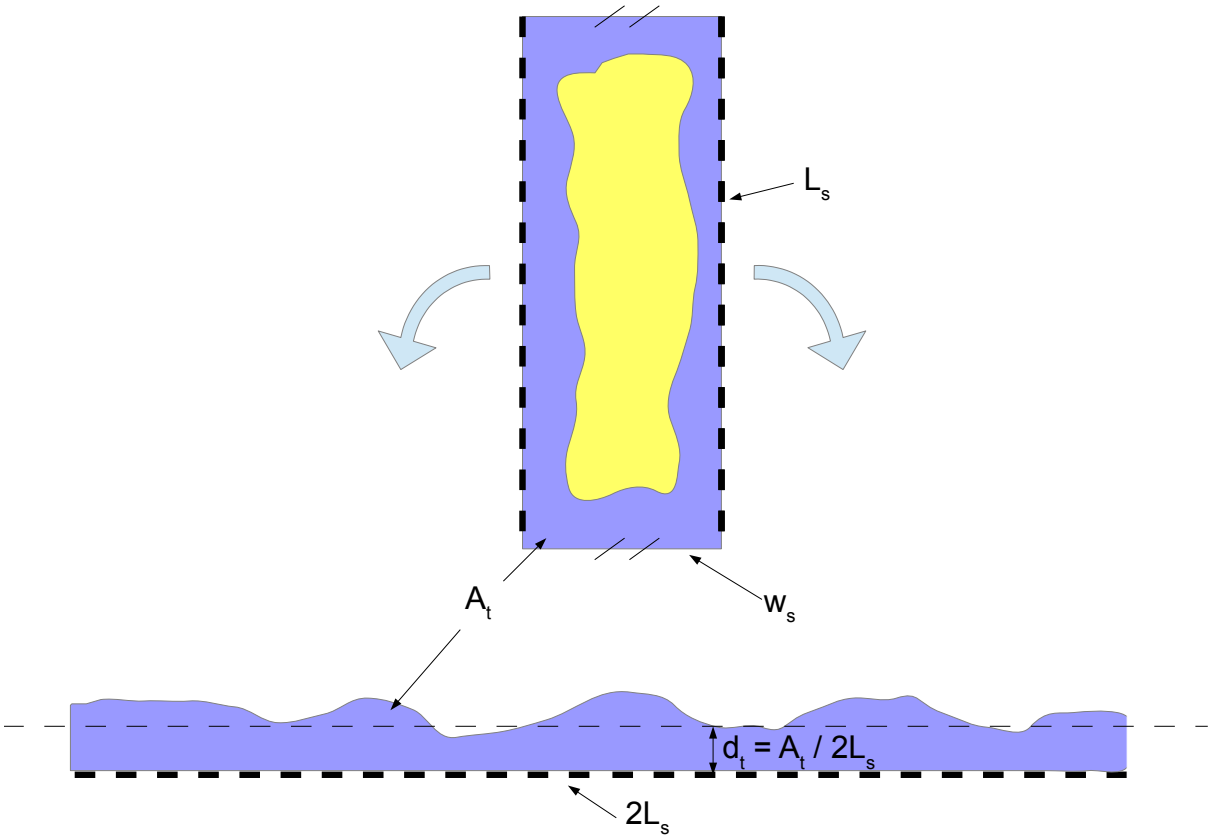

Figure 3.9: Graphical depiction of average ingrowth determination: image segmented, isolated cells excluded and average infiltration depth determined from the territory gained by the bulk of the tissue ingrowth.

Collagen fraction was defined as the area of collagen detected within the scaffold boundaries divided by the total scaffold area. An ingrowth adjusted index value was calculated as the absolute collagen value divided by the calculated ingrowth area from H&E stained slides (n=6).

Vascularisation was assessed by normalising the count of vessels by the total scaffold area and then scaling to density per mm^2 (Vessel density/mm^2). Half of each scaffold was imaged to reduce computational processing requirements (n=6).

Inflammatory response was assessed by dividing the total area of ED1 positive structures by the total scaffold area visible in the image (ED1 Positive Index). Nine fields (3x3) of one of the corners (to reduce computational strain when segmenting the image) of each scaffold was imaged at a magnification of 20X for each sample (7 & 14 days $\rightarrow$ n=2, 28 days $\rightarrow$ n=6).

3.7 Statistical Analysis

Statistical tests were performed with GraphPad Prism 6.05 (GraphPad Software, San Diego, CA) and differences were considered statistically significant for p-values of 0.05 or less. All data are expressed as means $\pm$ standard deviation of the mean unless otherwise stated. For multiple comparisons a two-way ANOVA test was performed and when significance was detected, multiple comparisons were executed with Tukey's test for P-value correction (unless otherwise stated). For single comparisons a two-tailed students t-test was performed (paired/unpaired depending on the application).

Chapter 4

Results

This chapter will proceed to state the results observed during this thesis which will then be discussed in Chapter 5. The results of the single spinneret electrospinning experiments, which formed a foundation for the rest of the thesis, will be described first in Section 4.1; followed by the results of the dual electrospinning experiments in Section 4.2. Qualitative and quantitative results obtained from the heparin surface modification will then be discussed in Section 4.3 and finally the *in vivo* subcutaneous rat study results will be discussed in Section 4.4.

4.1 Single Spinneret Electrospinning

Firstly, the PU solvent system comparison will be presented followed by a PEO fibre diameter analysis, which links with the sacrifical fibre analysis section described later (Section 4.2).

4.1.1 Polyurethane Fibre Optimization

No differences in fibre diameter or alignment were observed between luminal and abluminal surfaces for both PU/THF and PU/THF:DMF ($p>0.5$). However the PU/THF:DMF group resulted in smaller fibre diameters ($p<0.01$) and more isotropic fibre deposition ($p<0.0001$) than PU/THF. Besides morphological characteristics, it was observed that deposition occurred over larger area (along the transverse axis) of the collector mandrel for PU/THF:DMF ($\pm$ 120mm vs $\pm$ 60mm) than PU/THF. The stable region of the fibrous jet was distinctly shorter for the THF:DMF group and its whipping radius much larger than for THF group. Figure 4.1 and Figure 4.2 depict SEM micrographs and an analysis of the two groups respectively.

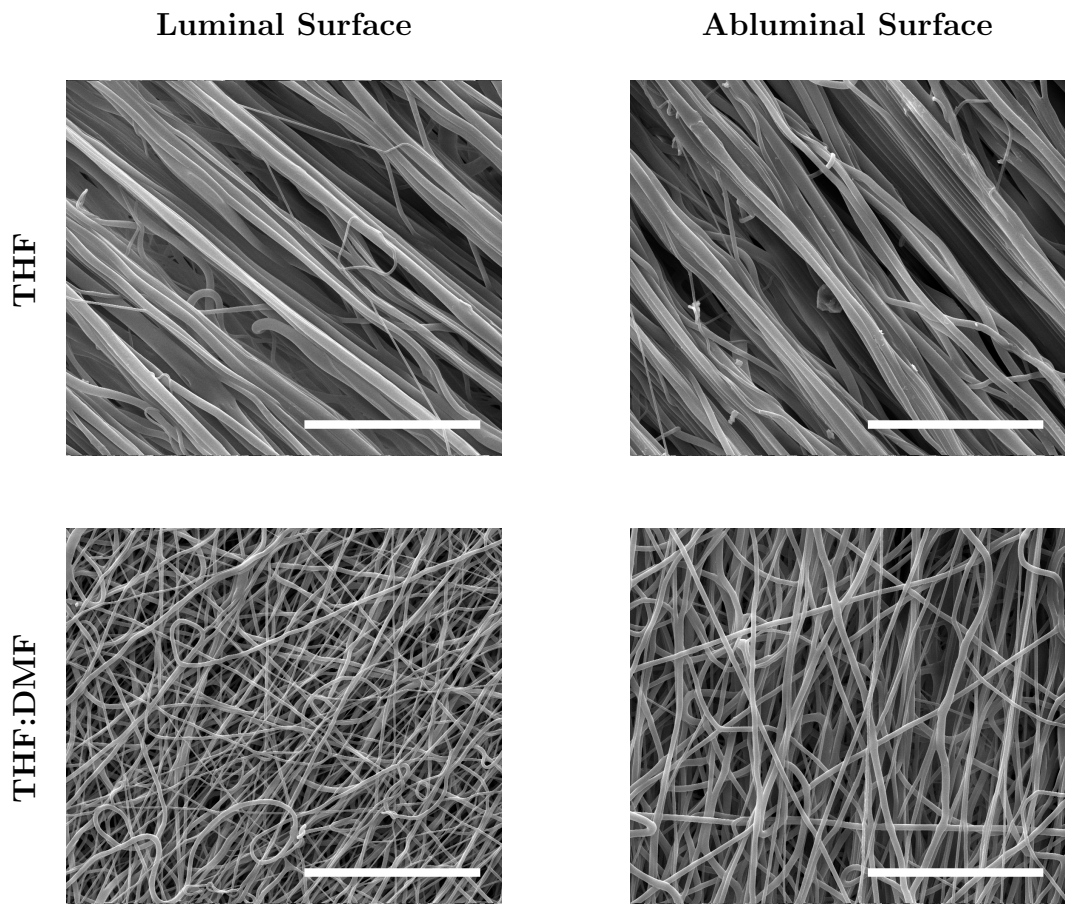

Figure 4.1: SEM images of the resultant fibrous structures of each solvent system. All images have been acquired at the same maginification and scale bars represent 50µm

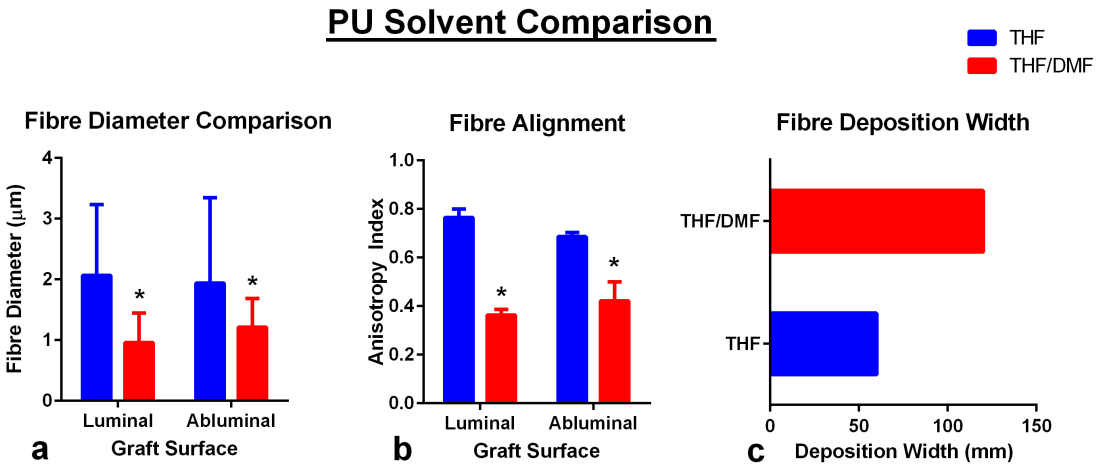

Figure 4.2: Comparison of morphological characteristics resulting from different PU solvent systems: a) Fibre diameter and b) Fibre alignment. c) THF:DMF resulted in a wider deposition band on the mandrel. *Denotes statistical significance between groups, $p<0.05$ (n=2)

4.1.2 PEO Fibre Diameter Analysis

PEO/DCM and PEO/EtOH were spun individually at 2 ml/hr, 4 ml/hr and 6 ml/hr and the resultant fibre diameters of each group compared. PEO/DCM required constant monitoring as excessive evaporation of the solvent at the capillary tip would result in blockage, requiring manual intervention to remove the blockages. This was not the case for PEO/EtOH, which additionally deposited over a much wider area (transverse direction) of the mandrel than PEO/DCM (±120mm vs ±40mm) and had a larger whipping radius. When PEO/DCM was spun at 6ml/hr the solvent did not evaporate sufficiently before deposition, resulting in a solid film structure on the luminal surface of the graft. When the capillary to collector distance was increased (>10cm) then the Taylor cone would erratically cease to form and interrupt jet formation.

On average, for all flow rates, PEO/DCM resulted in significantly larger fibre diameters than PEO/EtOH (mean difference = 6.2µm, $p<0.0001$). The effect of flow rate on fibre diameter differed between the two solvents where fibre diameter increased with increasing flow rates for PEO/DCM ($p<0.001$) but almost no differences were observed in fibre diameter across flow rates for PEO/EtOH (See Figure 4.3). PEO/DCM fibres were also observed to be non-uniform with many smaller diameter fibres ejecting perpendicularly from the primary, large diameter fibres. The small sample size (n=2) used in this preliminary study imposes limits on the conclusions that can be drawn about the effect of solution flow rate on fibre diameter. However, on average for all flow rates, it can be seen that fibres spun from PEO/DCM produced larger fibres on average than when spun from PEO/EtOH.

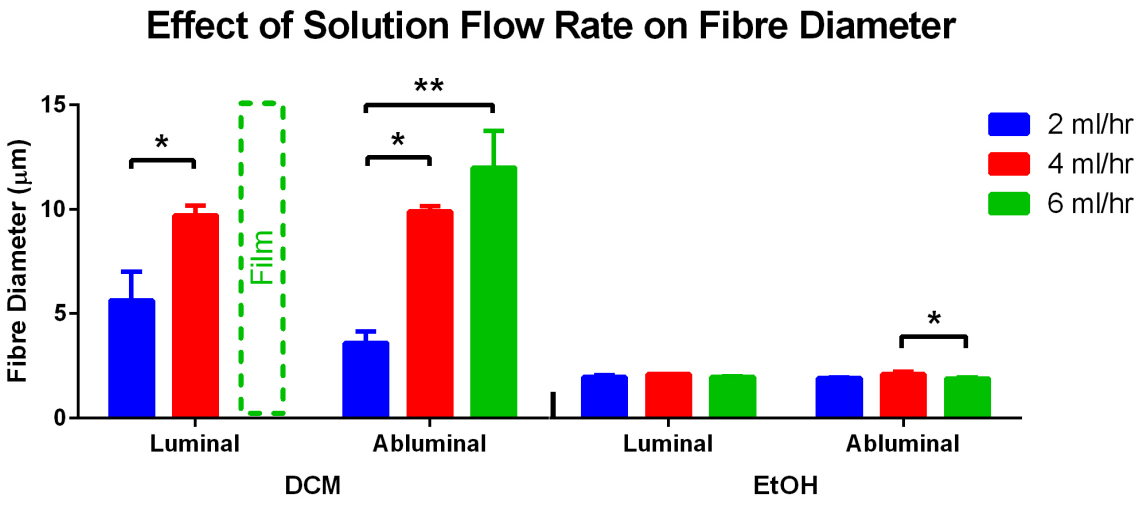

Figure 4.3: Effect of flow rate on fibre diameter for DCM (note: Luminal surface at 6ml/hr formed a film) and EtOH. *$p<0.05$; **$p<0.001$. (n=2)

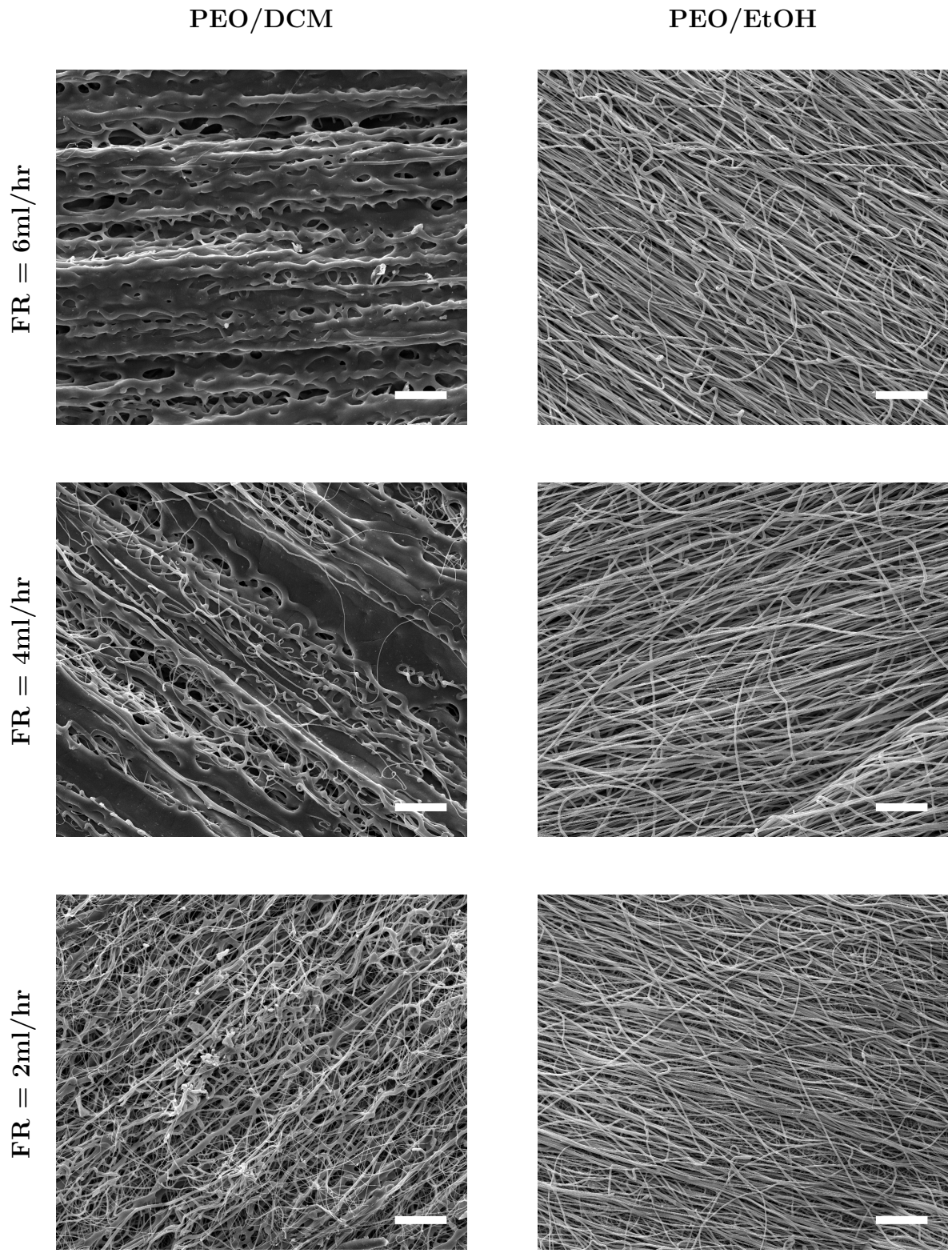

Figure 4.4: SEM images of the resultant fibrous structures (abluminal surface) for each solvent system and flow rate (FR). Scale bars represent 50μm

4.1.2.1 Effect of Flow Rate on PEO Mechanical Properties

Increases in PEO solution flow rate were found to cause increases in UTS ($p<0.0001$) and Young's modulus ($p<0.0001$) but decreases in the maximum elongation ($p<0.0001$) of 100% PEO scaffolds, for either DCM or EtOH solvents (Figure 4.5). However, for PEO/EtOH (thin), significant differences in mechanical properties were only observed between flow rates of 2 ml/hr and 4 ml/hr ($p<0.001$) but not 4 ml/hr and 6 ml/hr ($p>0.74$). PEO/DCM (thick) samples spun at solution flow rates of 6 ml/hr became brittle after removal from the mandrel and snapped during the sample preparation process. PEO/DCM produced scaffolds which were stronger ($p<0.01$), stiffer ($p<0.0001$) but endured less strain before failure ($p<0.0001$) than PEO/EtOH on average across solution flow rates.

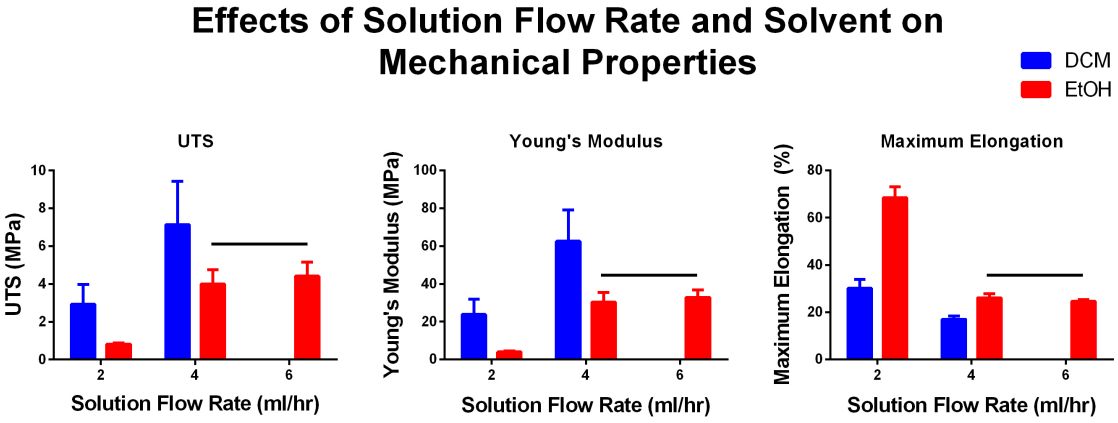

Figure 4.5: Effect of flow rate and solvent system on scaffold mechanical properties. Note: DCM at 6 ml/hr samples snapped during preparation process. All groups significantly different from one another ($p<0.05$, $n=4$) except for groups joined with a solid line.

4.2 Dual Electrospinning with Sacrificial Fibres

This section describes the results of dual-spinning PU with PEO as a sacrificial fibre. First the results of the electric field design experiments will be presented in Section 4.2.1 followed an assessment of the PEO extraction and drying process (Section 4.2.2) as well as verification of the porosity determination method (Section 4.2.3). Visualisation of the sacrificial fibre inclusion and removal will then be presented followed by an analysis of the relationship between scaffold fibre fraction, sacrificial fibre size and porosity. Note, the analysis of PEO fibre diameter was provided previously in Section 4.1.2.

4.2.1 Tailoring the Electric Field

Table 4.1 provides a summary of the results of different electrospinning configurations tested. Briefly, opposite polarity spinnerets created oppositely charged fibrous jets which resulted in a net attractive force between the two jets. For large collector mandrels (Figure 4.1.A.1) the jets deposited uniformly in an inter-dispersed manner in the middle (transverse direction) of the collector; however, for small collector mandrels (Figure 4.1.A.2) the jets collided in mid-air and little-to-no deposition occurred on the collector.

Conversely, like charged spinnerets resulted in a net repulsive force between the two jets. Both jets deposited efficiently on both the small and large collector mandrel however two distinct populations were apparent over the length of the mandrel (transverse direction, Figure 4.1.B.1). When charged electro-static shields (same polarity as spinnerets) were placed on either side of the collector (Figure 4.1.B.2) the inter-dispersion between the two fibre types was improved. By slightly charging the collector (|<2kV|, high voltages resulted in arcing to the electric motor circuit) in the opposite polarity to the spinnerets the inter-dispersion of the two fibre types was further improved (Figure 4.1.B.3).

Table 4.1: Electric Field Configurations Tested

	Description	Diagram	Electric Field
	Spinnerets charged with opposing polarities		
A.1	Oppositely charged spinneret polarities with large diameter grounded collector (25,4mm)	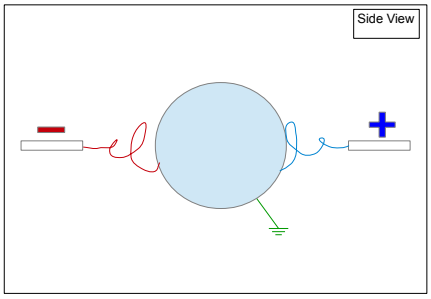	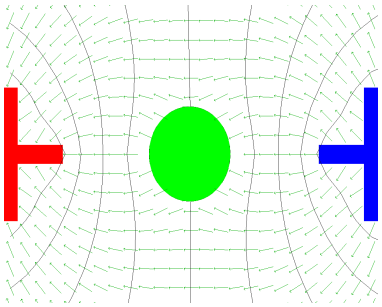
A.2	Oppositely charged spinneret polarities with small diameter grounded collector (<5mm)	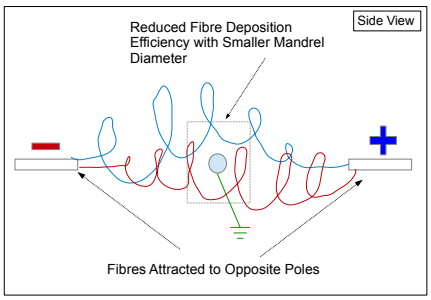	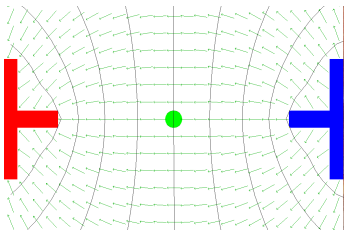

Continued on next page

	Description	Diagram	Electric Field
	Spinnerets charged with the same polarity		
B.1	Like charged spinnerets with grounded collector (all diameters)	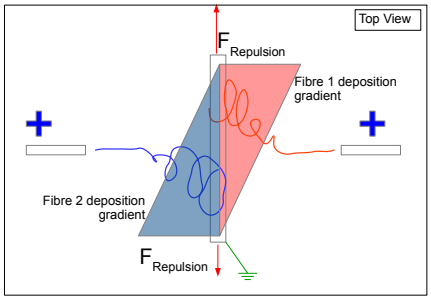	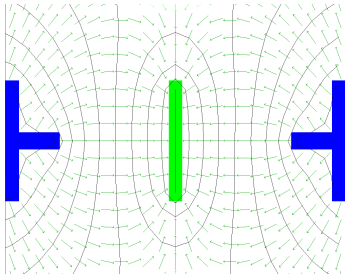
B.2	Modified version of B.1 with addition of electro-static guides	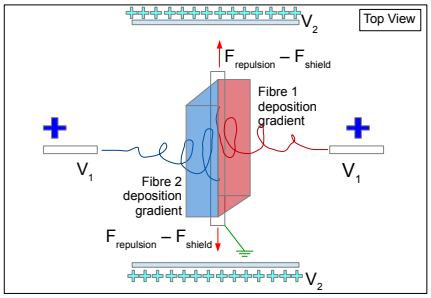	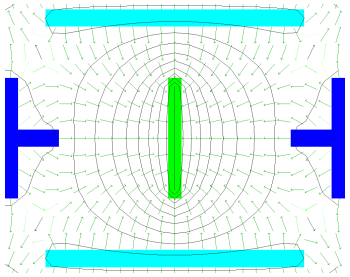
B.3	Modified version of B.2 with grounded collector replaced by a oppositely charged collector	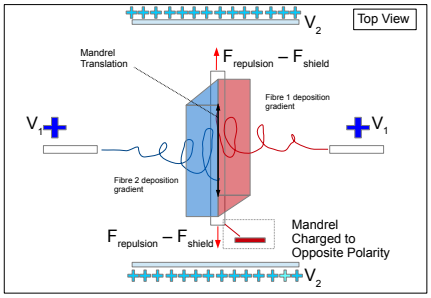	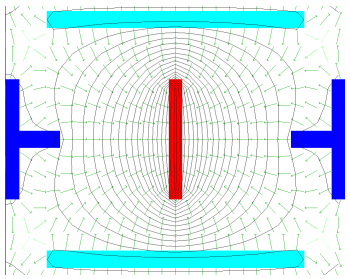

Electric Field column: blue, red, green represent positively charged, negatively charged and grounded objects, respectively, while cyan represent positively charged objects with potentials independant of blue objects. Note, type B.1 & B.2 configurations were tested with reverse polarities as well. Electric field simulations generated from [237].

4.2.2 PEO Extraction & Drying Process

Vacuum drying and freeze-drying were both tested as suitable methods of drying the grafts post PEO extraction. While no significant difference in shrinkage between methods was observed for 100% fibre fraction grafts (p=0.5); vacuum drying resulted in more

shrinkage for 70% (54% vs 40% shrinkage, p<0.05) and 30% (62% vs 34% shrinkage, p<0.01) fibre fraction grafts than freeze drying. Figure 4.6 summarises the results of the study graphically.

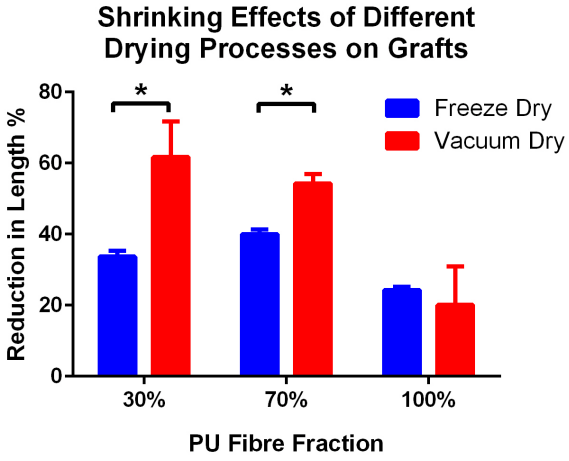

Figure 4.6: The effect of the drying process used is dependant on the fibre fraction of the graft, where high and low fibre fraction grafts are least and most affected by drying process, respectively (interaction: p <0.05, Two-way ANOVA). *Denotes statistically significant from other groups, p<0.05 (n=2). No adjustment for multiple comparisons.

4.2.3 Porosity Determination

No difference was observed between porosity measurements calculated by gravimetric and densitometric means (mean difference = 0.05%, p> 0.9). Figure 4.7 illustrates the calculated values from each method graphically.

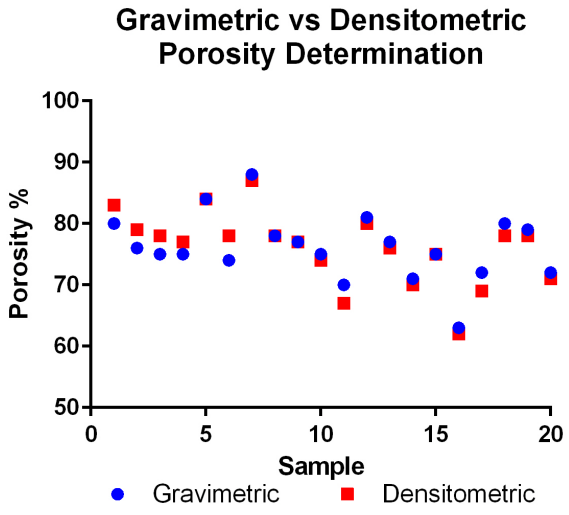

Figure 4.7: Plot of individual samples showing measured value for gravimetric and densitometric techniques. No statistical significance found between means, mean difference = 0.05%, CI = 90%, p>0.9

4.2.4 Visualisation of PEO Fibre Inclusion and Removal

The inclusion of distinct sacrificial fibre diameters was verified by incorporation of fluorescent dyes into the polymer solutions before electrospinning and imaging under fluorescent microscopy after. Figure 4.8 depicts the inclusion of both thick (a) and thin (b) PEO fibres. Both the PEO and PU fibres exhibited autofluorescence in the same bandwidth as Rhodamine (∼627nm, red) and Fluoroscein (∼515nm, green) but at lower intensities than fluorescently dyed fibres (thick PEO fibres are still observed to autofluorescence in the green channel). Scaffolds imaged post-PEO removal detected only autofluorescence in either the green or red channel indicating the removal of the dyes during the PEO removal process (image not shown).

SEM images taken before and after PEO-removal (Figure 4.9) show the resultant differences in packing density and pore-size achieved for 30% fibre fraction scaffolds using thin and thick sacrificial fibres. A 100% fibre fraction PU control was imaged before and after undergoing the the same process as used for PEO extraction, exhibiting no difference in morphology or fibre density (full pore-size and porosity quantification is provided in section 4.2.5).

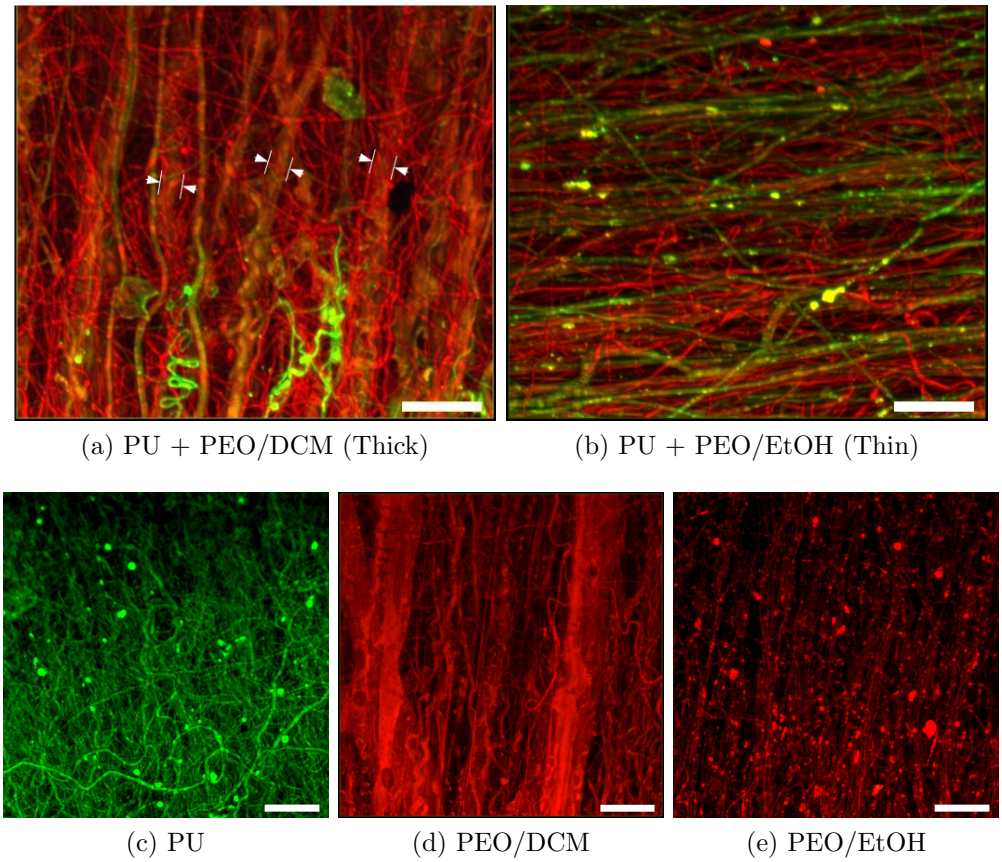

(a) PU + PEO/DCM (Thick) (b) PU + PEO/EtOH (Thin)

(c) PU (d) PEO/DCM (e) PEO/EtOH

Figure 4.8: Confocal images of scaffolds with the inclusion of thick (**a**) and thin (**b**) sacrificial fibres. **c-e**: Control stains of PEO (Rhodamine, red) or PU (Fluoroscein, green). Scale bars = 50µm

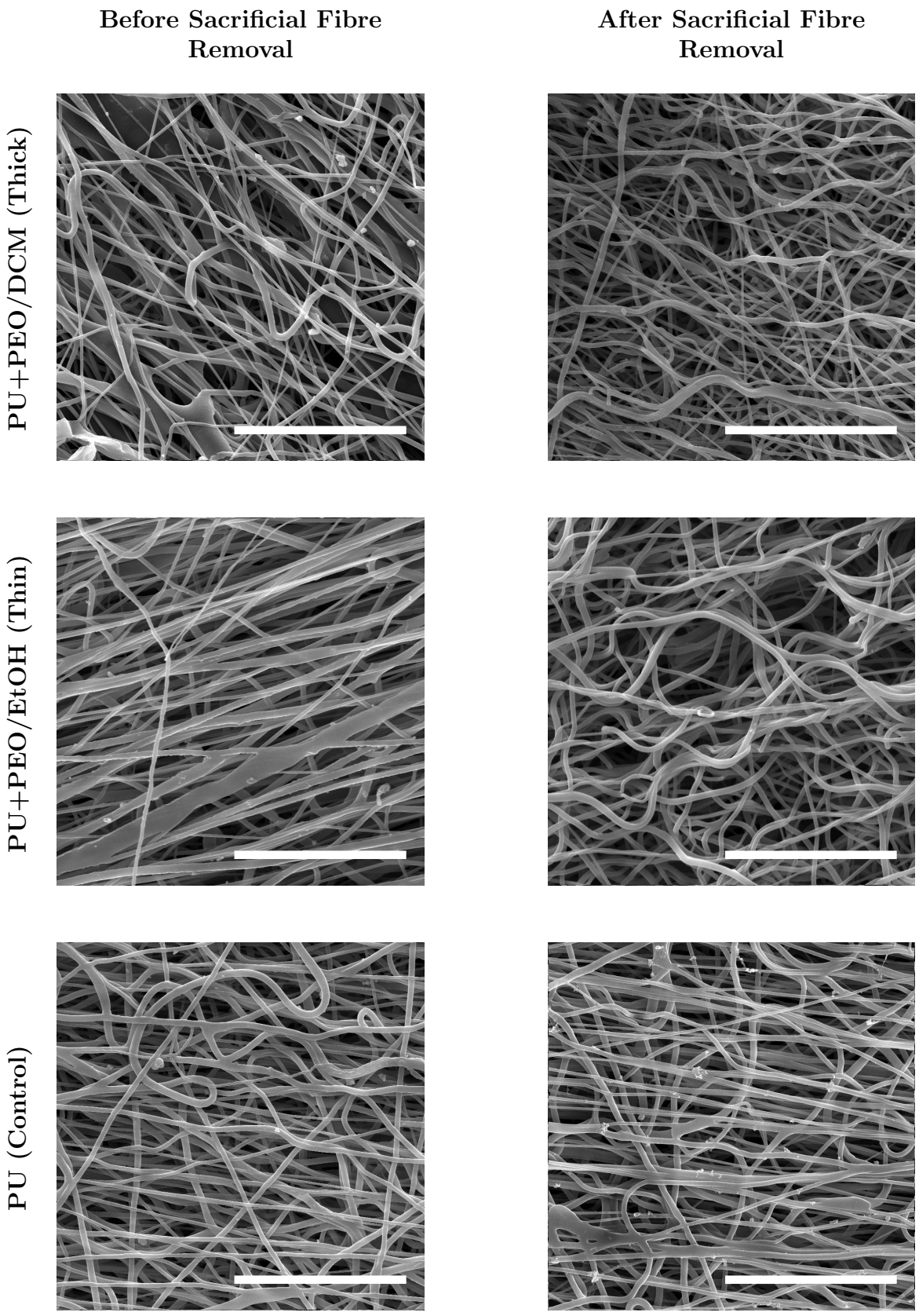

Figure 4.9: SEM images before and after removal of thick (PEO/DCM) and thin (PEO/EtOH) sacrificial fibres, observe the increase in pore-size between groups where sacrificial fibres had been included. 100% PU scaffolds subjected to the same extraction process show no discernible difference. Scale bars represent 50µm

Side section SEM images detail the morphological differences between scaffolds produced with thick, thin and no sacrificial fibres post PEO removal, where thick type scaffolds produced evidence of laminated rather than inter-dispersed fibre deposition. Laminated fibre deposition, where each material is sequentially spun onto an area rather than simultaneously, exhibits large flattened void spaces between dense PU sheets (Figure 4.10a & 4.10d) instead of increasing fibre-to-fibre distance uniformly between individual PU fibres (Figure 4.10b).

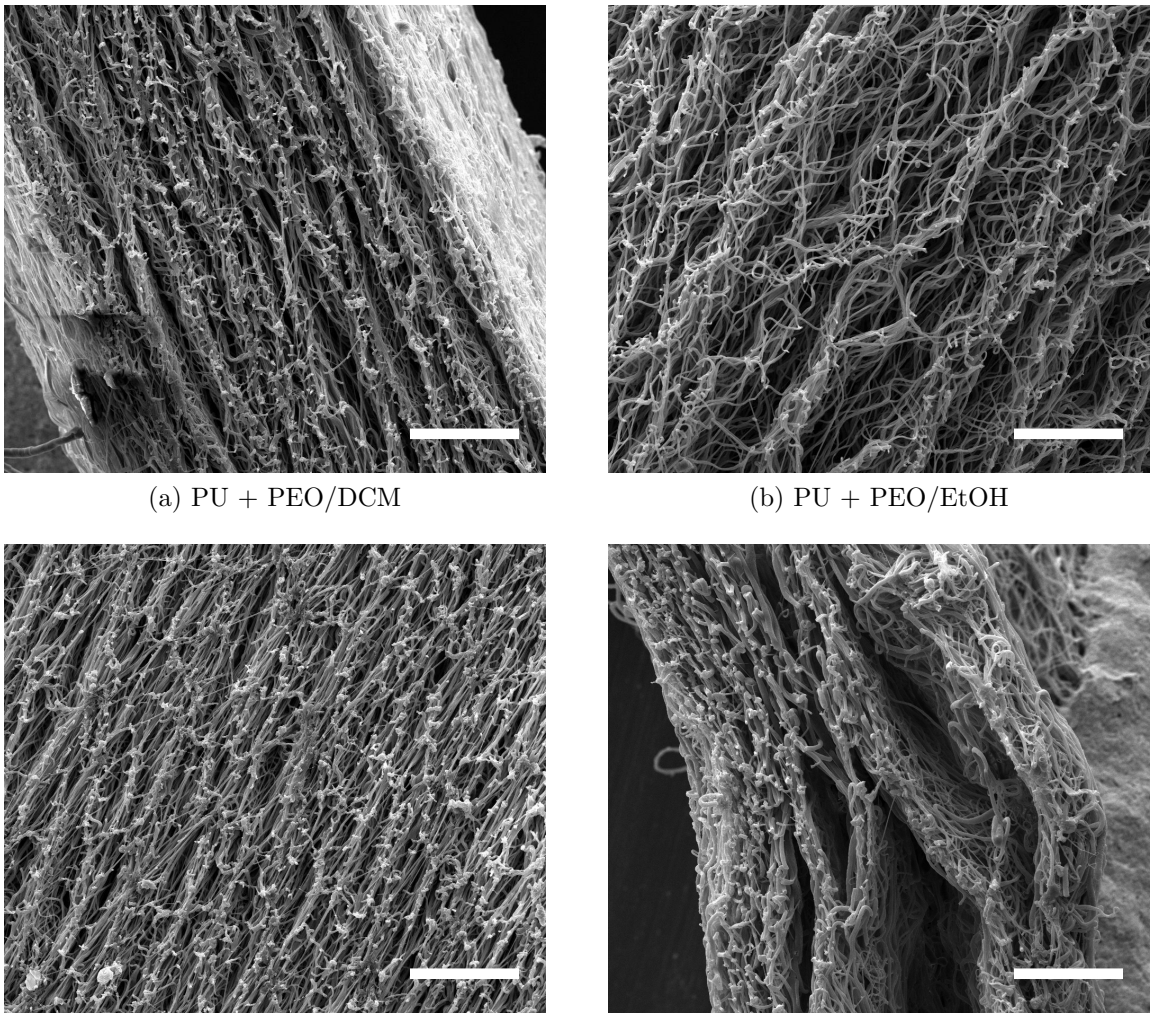

(a) PU + PEO/DCM

(b) PU + PEO/EtOH

(c) PU - Control

(d) Severe Lamination

Figure 4.10: Side-section SEM images of scaffolds post-PEO removal process with **a**) thick sacrificial, **b**) thin sacrificial and **c**) no sacrificial (control) fibres depicting effects of inter-dispersion of sacrificial and structural fibres on resultant scaffold morphology. **d**) Pronounced example of laminate instead of inter-dispersed fibre deposition showing gaps where PEO has been removed between dense layers of PU. Scale bars represent 100µm

4.2.5 Effect on Porosity

Porosity increased linearly with decreasing PU fibre fractions for scaffolds spun with thick ($P = -0.18FF + 89.1$, r^2=0.84) and thin ($P = -0.18FF + 93.5$, r^2=0.91) sacrificial fibres, where both lines shared a common ($m = 0.18$, p=0.85), non-zero (p<0.0001) slope but differed in their y-intercepts with thin sacrificial fibre type scaffolds being more porous by 4.4% (p<0.0001).

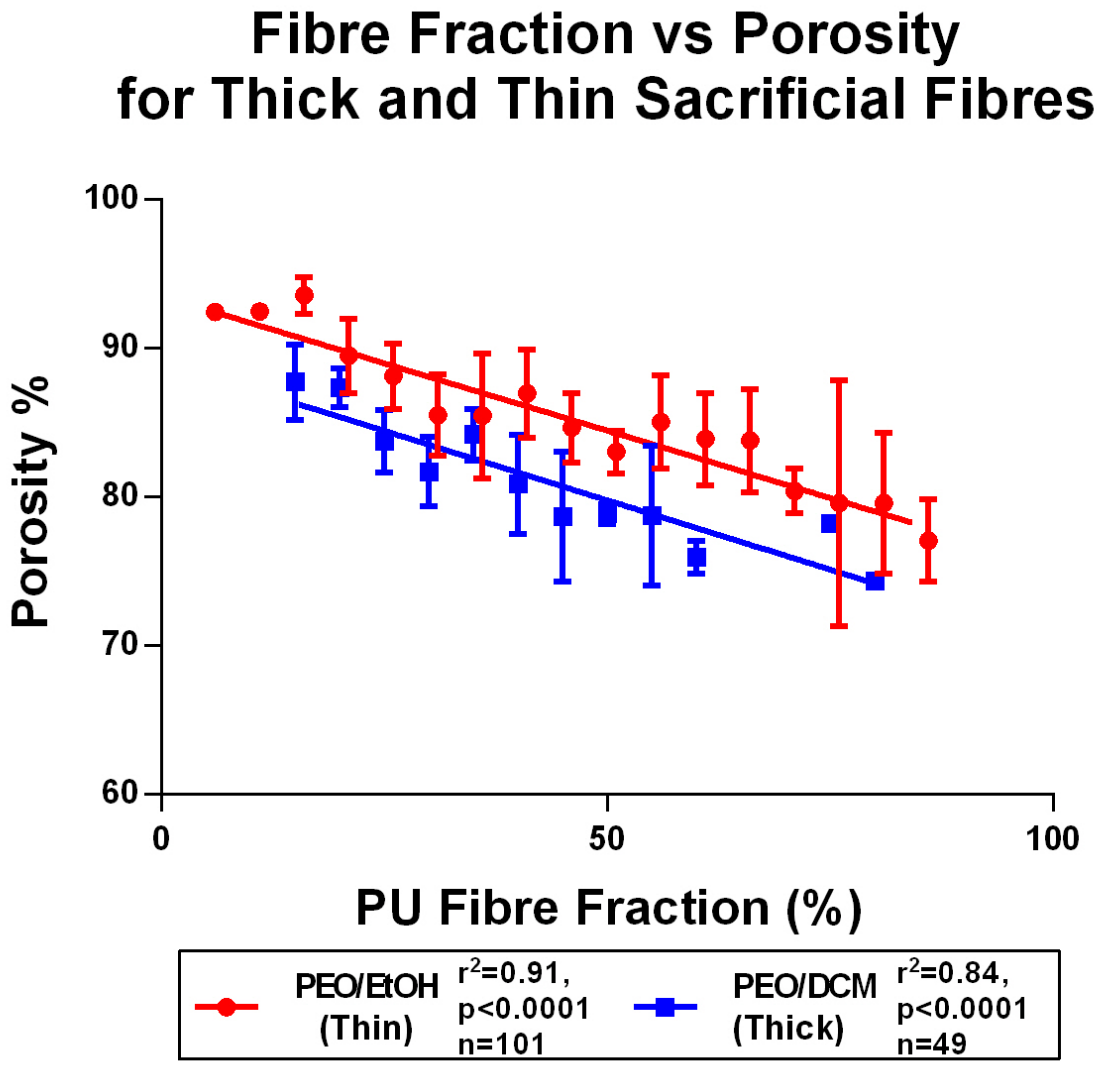

Figure 4.11: Linear regression of fibre fraction and porosity for PEO/DCM and PEO/EtOH. Common slopes (p=0.85) significantly non-zero (p<0.0001) but differ in their y-intercepts (p<0.0001)

Porosity was calculated before and after PEO removal for thin, thick and no sacrificial fibre groups and compared by means of a repeated measures two-way ANOVA. No differences in porosity were observed between groups before PEO removal ($p>0.38$); however, after removal thick and thin groups increased in porosity by 19% and 21% ($p<0.0001$), respectively, whereas the control group was unaffected by the PEO removal process ($p>0.9999$). Thick and thin groups, post PEO removal, were more porous than the control group by 15% and 19%, respectively ($p<0.0001$). See Figure 4.12.

Using the recorded bulk volume values before and after PEO removal for each sample an index for bulk volume reduction (shrinkage) could be obtained. It was observed that thick sacrificial fibre groups suffered greater shrinkage than thin (mean difference = 21%, $p<0.0001$) and control groups (mean difference = 31%, $p<0.01$). See Figure 4.12b below.

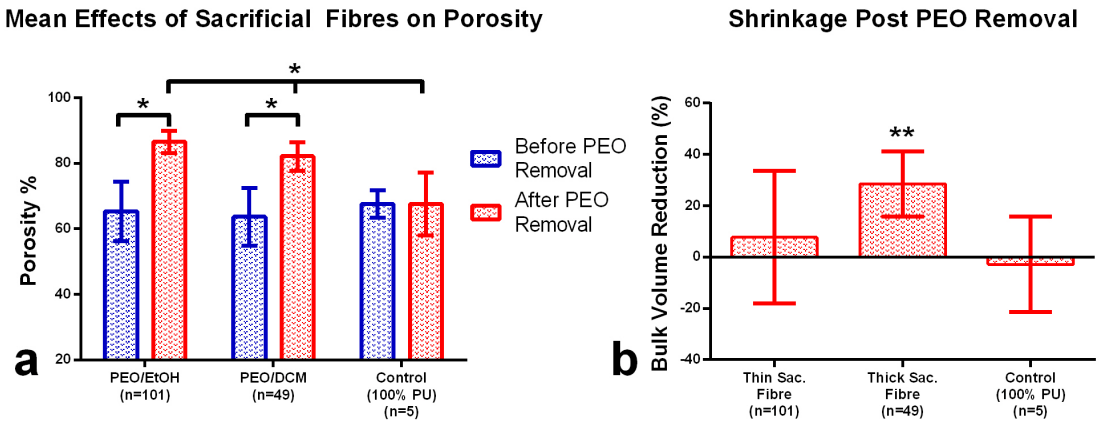

Figure 4.12: **a**) Mean effects of sacrificial fibre diameter on scaffold porosity both before and after removal, * $p<0.001$. **b**) PEO/DCM scaffolds experienced severe reductions in bulk volume loss, ** $p<0.01$.

4.2.6 Effect on PU Morphology

Post PEO removal, scaffolds fabricated with the inclusion of thin sacrificial fibres appeared slightly less aligned than 100% PU scaffolds (anisotropy index = 0.20±0.09 vs 0.38±0.06, $p=0.002$). However, no significant differences were observed in alignment between thick and thin ($p=0.13$) or thick and 100%PU groups ($p=0.07$, Figure 4.13a).

The addition and subsequent removal of thick and thin sacrificial fibres did not result in significant changes to fibre diameter when compared to 100% PU scaffolds ($p=0.42$, One-way ANOVA, Figure 4.13b)

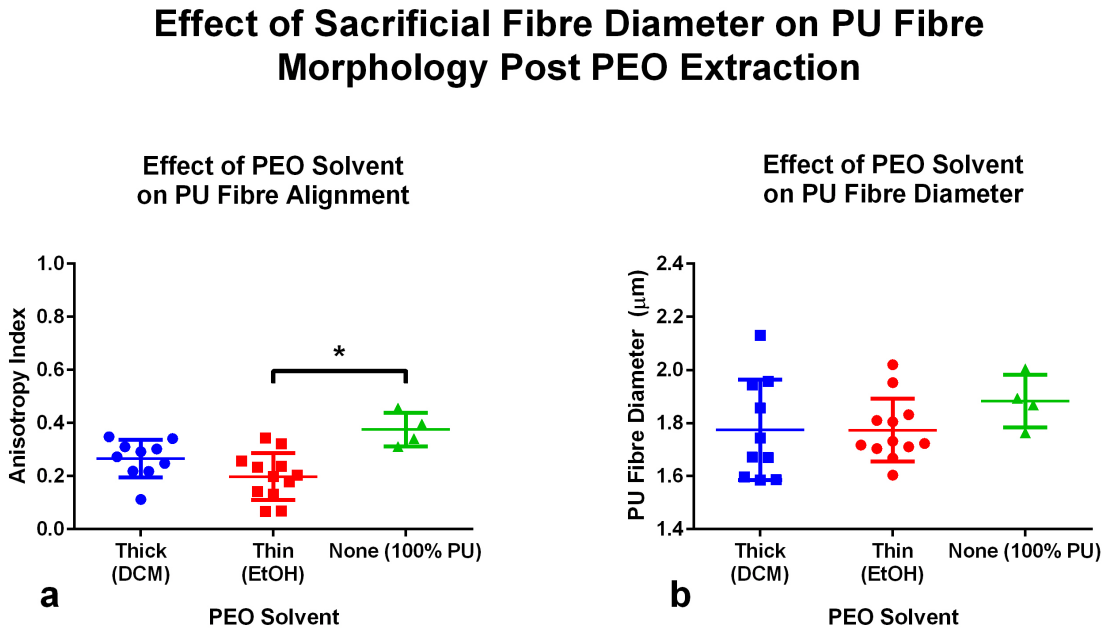

Figure 4.13: Effects of sacrificial fibre diameter on the **a**) alignment and **b**) diameter of the remaining PU fibres post PEO removal, * $p<0.05$.

4.2.7 Mechanical Properties

In an effort to improve the readability of this section, analysis of the mechanical testing data will be split into three parts: firstly, the mechanical effects of the inclusion and subsequent removal of sacrificial fibres will be detailed for thin (PEO/EtOH) sacrificial fibres only (Section 4.2.7.1); next, a comparison of thin and thick (PEO/DCM) sacrificial fibre type scaffolds will be provided (Section 4.2.7.2) and finally the effects of environmental conditions on the mechanical properties 100% PU constructs will be investigated (Section 4.2.7.3).

4.2.7.1 Effect of Sacrificial Fibre Inclusion and Removal

Figure 4.15 summarises the difference in mechanical properties between scaffolds comprising 100% PEO, 100% PU and a 30%/70% (PU/PEO) composite both before and after PEO removal. Note that all tests were conducted dry at room temperature to facilitate the testing of 100% PEO scaffolds which could not be tested in simulated physiological conditions due to PEO's rapid dissolution in aqueous solutions.

Circumferentially oriented (CD) samples possessed greater ultimate tensile stresses (UTS) than transversely oriented (TD) samples across all groups ($p<0.01$); however, TD samples were able to undergo greater elongations before failure for all groups ($p<0.005$). The effects of orientation on Young's modulus were not consistent across all groups where

PEO and PU/PEO (before PEO removal) groups were more rigid in the circumferential than in the transverse direction ($p<0.0001$) but no significant differences were noted between orientations for PU and PU/PEO (after PEO removal) groups ($p>0.9$).

Pure PU scaffolds which had undergone the PEO removal process differed, versus PU scaffolds that had not, only in their maximum elongation before failure where the mean differences in the circumferential and transverse direction were 85% ($p<0.001$) and 132% ($p<0.0001$), respectively. The UTS and Young's modulus of the pure PU scaffolds were unaffected by the PEO removal process ($p>0.05$).

Before PEO removal (CD), PU/PEO samples exhibited intermediary properties between pure scaffolds of each polymer. Post PEO removal the composite scaffolds were found have lower UTS values ($p<0.0001$), failed at lesser strains ($p<0.0001$) and had non-significantly lower Young's moduli ($p=0.4$) than pure PU scaffolds which had undergone the same PEO removal process.

PEO groups were more rigid (22.4 MPa vs 3.2 MPa, $p<0.0001$) but endured lesser maximum elongations (40% vs 533%, $p<0.0001$) than PU groups. PU samples were far stronger than PEO samples with UTS values approximately 4 times greater ($p<0.0001$).

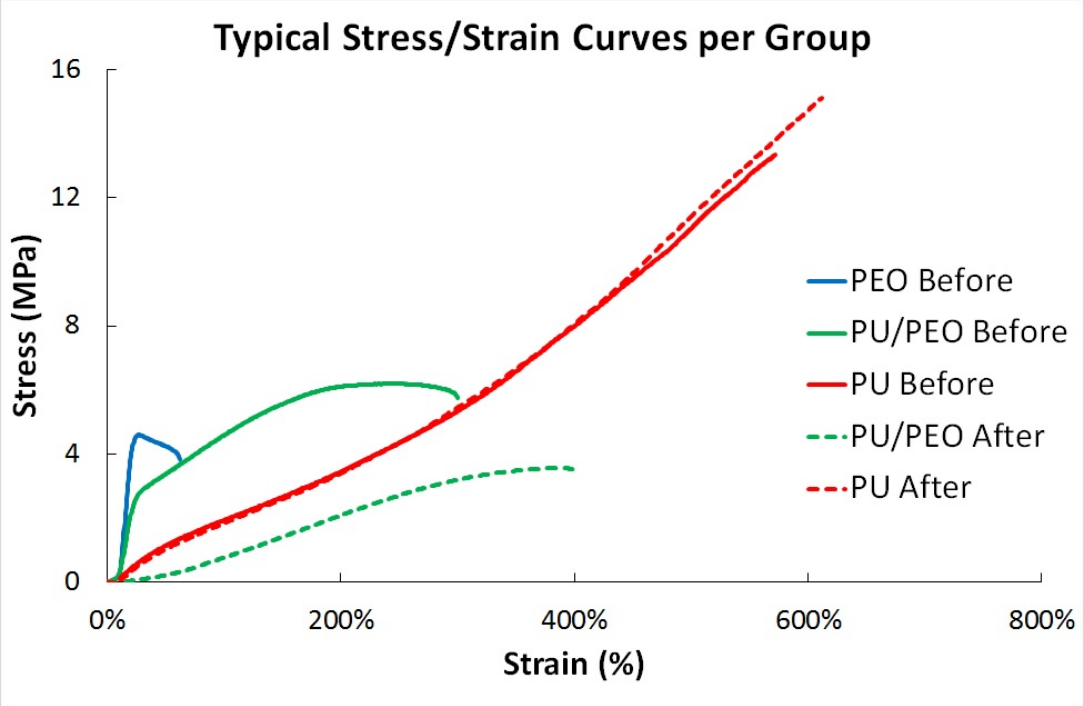

Figure 4.14: Typical stress/strain curves per group, note the steep elastic region on PEO and PU/PEO samples before PEO removal. Curves depict circumferentially oriented samples only.

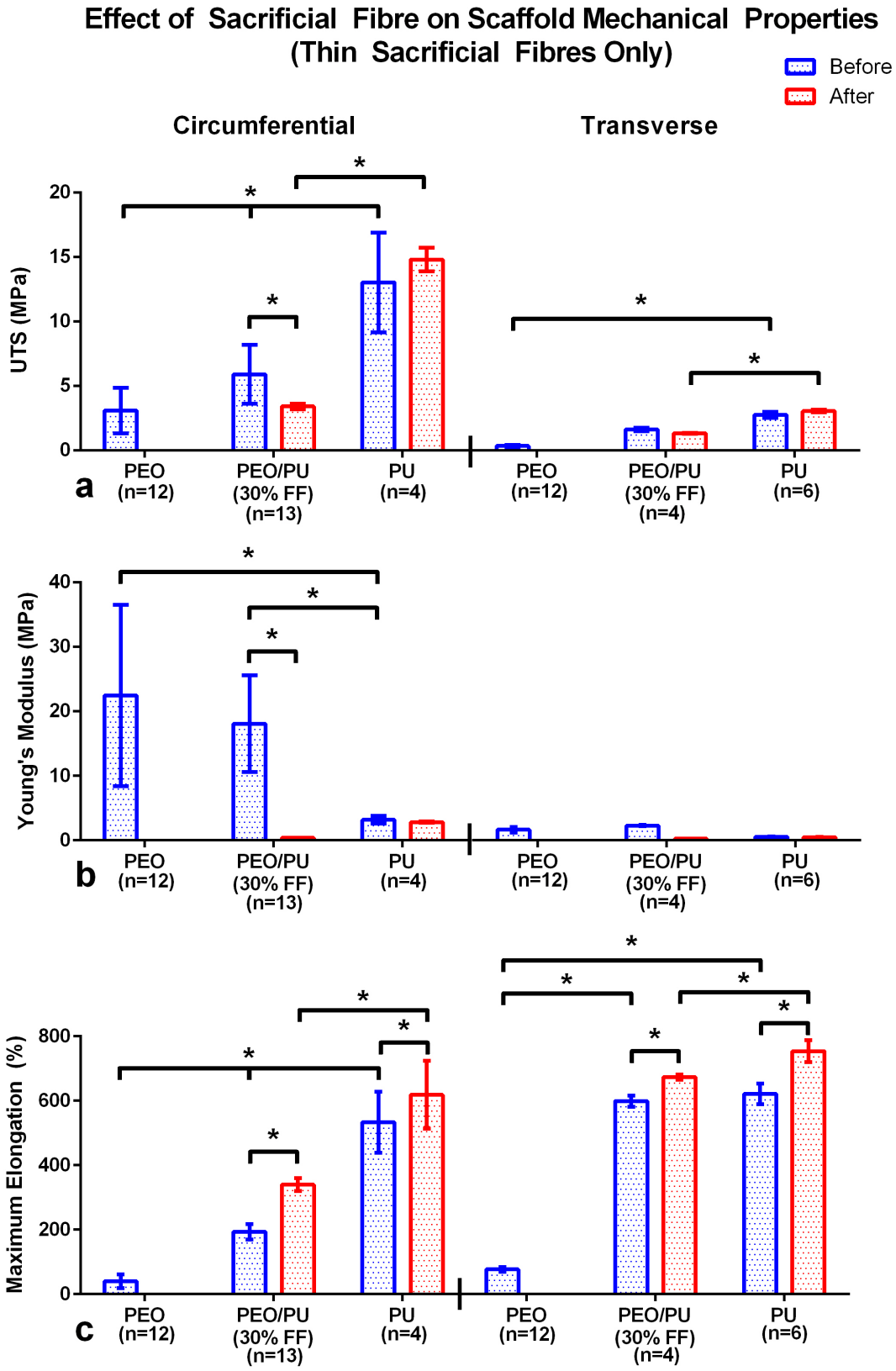

Figure 4.15: Mechanical properties of 100% PEO, 30%PU+PEO/EtOH and 100% PU constructs showing influence of sacrificial fibre before and after its removal on: **a**) ultimate tensile strength (UTS), **b**) Young's modulus and **c**) maximum elongation before failure. *Denotes significance between groups with $p<0.05$, Two-way ANOVA followed by uncorrected multiple comparisons.

4.2.7.2 Comparison of Thin vs Thick Sacrificial Fibres

Scaffolds of a range of fibre fractions (15% - 70%) were spun with either thick or thin sacrificial fibres and compared by means of linear regression both before and after PEO extraction. Figure 4.16 summarises the information obtained from the experiment but a detailed analysis is provided below.

Before PEO extraction the UTS of thin groups increased linearly (84±16 kPa/%PU, r^2 = 0.77, p<0.001) with increasing PU fibre fractions while an opposite effect was noted for thick groups, where slight decreases, and a weaker correlation, were noted in UTS for increasing fibre fractions (-42±16 kPa/%PU, r^2 = 0.46, p<0.05). No significant difference (p=0.06, common line: $E = 31.4 - 0.38FF$ MPa) was observed between groups for Young's modulus where scaffold stiffness decreased linearly, with increasing fibre fractions, for both thin (r^2 = 0.90, p<0.0001) and thick (r^2 = 0.72, p<0.001) groups. Little-to-no correlation was observed between fibre fraction and maximum elongation for thin (r^2 = 0.52, p=0.01) and thick (r^2 = 0.004, p=0.9), however thick groups endured significantly more strain before failure than thin groups (214% ± 21%, p<0.0001).

After PEO extraction similar slopes, but different elevations were observed between groups in all measures with thick groups consistently exhibiting greater values (p<0.0001) for all. A linear relationship was observed between fibre fraction and UTS (thin: 69±12 kPa/%PU, r^2 = 0.78, p<0.001; thick: 86±20 kPa/%PU, r^2 = 0.71, p<0.01) and Young's modulus (thin: 17±2 kPa/%PU, r^2 = 0.91, p<0.0001; thick: 22±4 kPa/%PU, r^2 = 0.80, p<0.001) but correlation was weak between fibre fraction and maximum elongation (thin: r^2 = 0.61, p<0.01; thick: r^2 = 0.06, p = 0.5).

When all measures, post PEO removal, were plotted with porosity as the x-axis, in place of fibre fraction, improved r^2 values were obtained for all line fits (excluding the thin group for Young's Modulus). Additionally, when compared with porosity on the x-axis it was found that thin and thick groups shared a common line for UTS (p=0.1, $UTS = -0.32P + 32$ MPa) and Young's modulus (p=0.5, $E = -0.08P + 7.9$ MPa). The fits for maximum elongation, while improved over fibre fraction as an x-axis, were still weak with r^2 values of 0.48 and 0.62 for thick and thin groups, respectively; however, thick groups were observed to stretch more before failure than their thin counterparts (mean difference = 156%±19%, p<0.001)

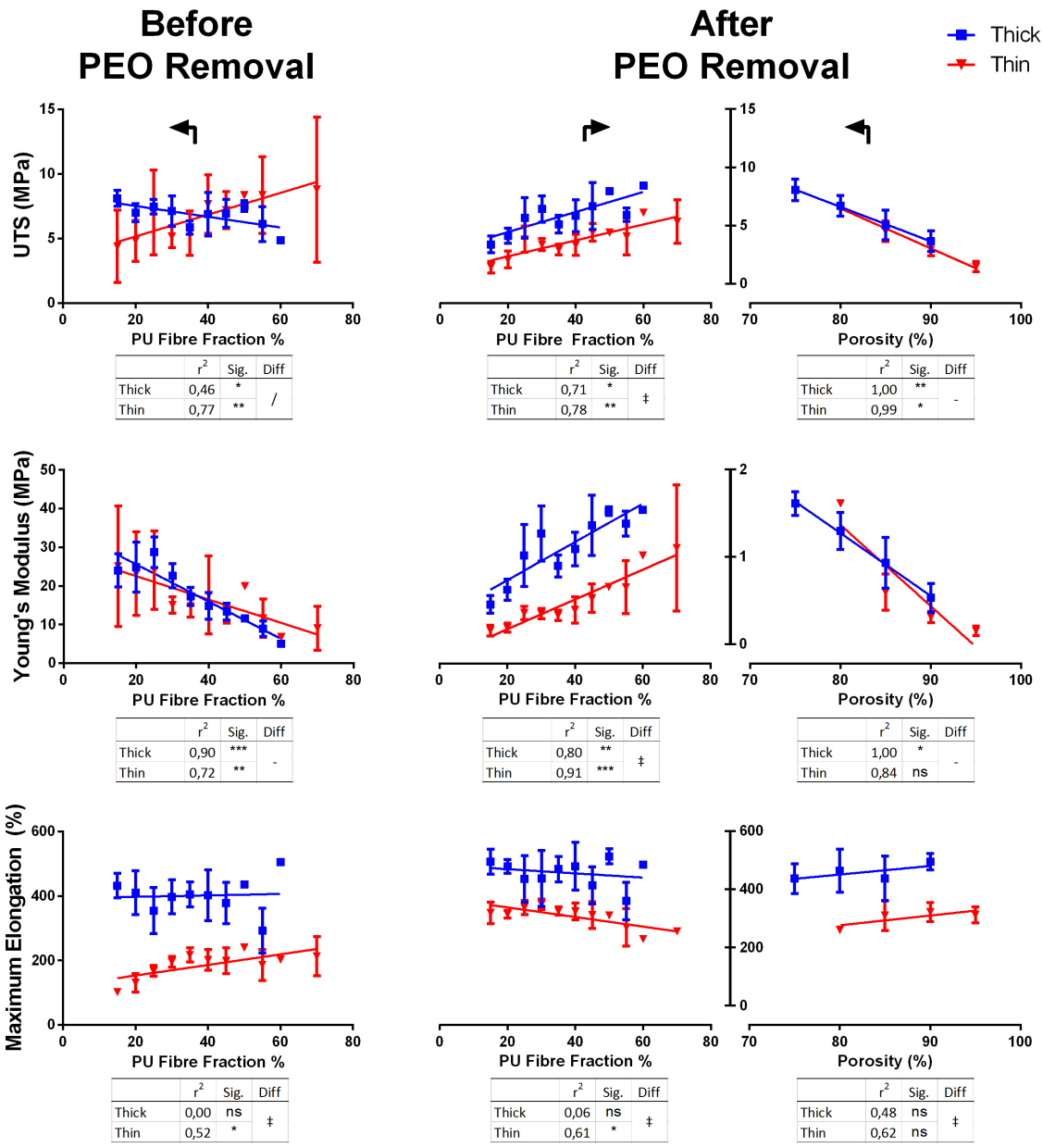

Figure 4.16: Comparison of constructs fabricated with thin (n=44) and thick (n=43) sacrificial fibres both before and after PEO removal. Thick groups compared on the fibre fraction axis consistently exhibit superior mechanical properties than their thin counterparts; however when compared on the porosity axis, both are equivalent in their mechanical properties except for maximum elongation. Note that y-axis scales for Young's Modulus are different between "Before" and "After" graphs. "Sig." denotes non-zero significance of fitted slopes. "Diff." expresses the difference between fitted slopes.

4.2.7.3 Effect of Testing Conditions on Scaffold Strength

No significant differences in UTS, Young's modulus and maximum elongation were found between "wet" and "dry" groups in the circumferential orientation ($p>0.06$). However, in transversely oriented groups small but significant increases in Young's modulus (0.65 ± 0.03 vs 0.24 ± 0.06 MPa, $p<0.0001$) and maximum elongation ($497\pm35\%$ vs $426\pm13\%$, $p<0.01$) were observed when tested in physiological conditions compared to dry at room temperature. Figure 4.17

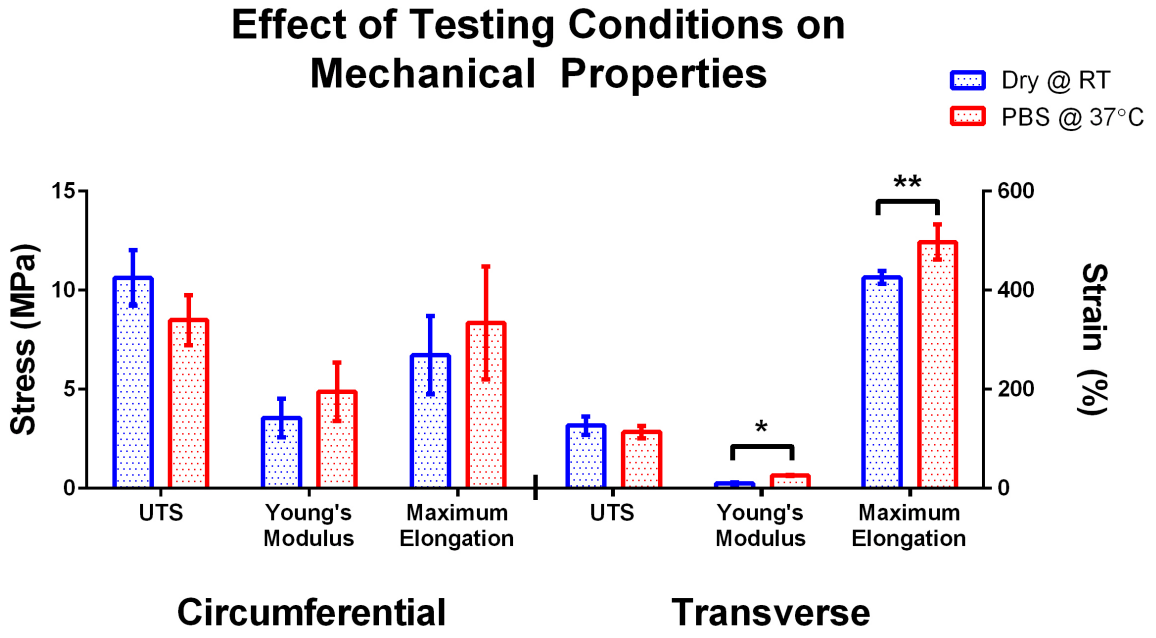

Figure 4.17: Effect of physiological conditions on PU scaffolds (n=4). *$p<0.0001$, **$p<0.01$. RT = 22°±2°C. Water bath maintained at 37°±1°C

4.3 Heparin Surface Modification

This section provides details of the qualitative and quantitative verifications and effects of the heparin surface modification. Note that going forward thin type (PEO/EtOH) sacrificial fibres had been selected for further study due to their ability to produce higher porosity constructs and so thick type (PEO/DCM) composites were not studied further. Qualitative and quantitative measures of heparinization efficacy are initially provided in Section 4.3.1 and 4.3.2, respectively. The effects of the heparinization process on the scaffold morphology are then presented in Section 4.3.3 followed by an analysis of the effects on scaffold mechanical properties in Section 4.3.4

4.3.1 Qualitative Results

Figure 4.18 depicts the results of the heparin binding verification assay.

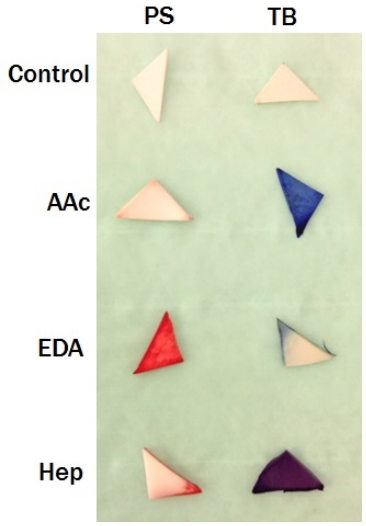

Figure 4.18: Qualitative verification of heparinization: PU controls were not stained by either Ponceau S (PS) or Toluidine Blue (TB). Samples that had undergone the acrylic acid grafting step were dyed blue by TB indicating the presence of negatively charged carboxyl groups. After the amination process samples were stained red by PS, and were no longer stained by TB, indicating the presence of positively charged amines and depletion of carboxyls, respectively. Finally, after heparinization the samples stained bright purple by TB and were no longer stained by PS, indicating the presence of highly negatively charged heparin molecules and depletion of amines on the surface of the fibres, respectively.

4.3.2 Quantitative Results

Scaffolds of a range of fibre fractions (20% - 100%), heparinized for mechanical testing, were also analysed for heparin content by MBTH assay, Figure 4.19 below summarises the data obtained from the experiment. No correlation was noted between heparin content and fibre fraction ($r = -0.4$, $p = 0.25$) and thus an average heparin content could be calculated per sample, after deducting the background reading (control values), to be 7.5±0.7 mg/g.

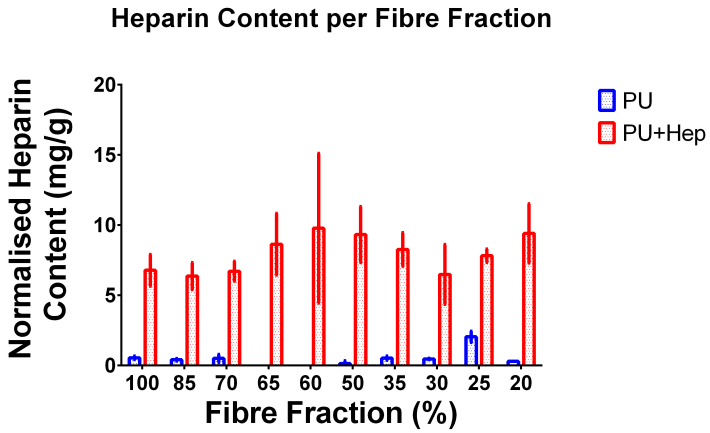

Figure 4.19: Quantitative assessment of heparinization: significantly more ($p<0.0001$) heparin detected per unit mass in heparinized groups than control groups. No significant differences detected across fibre fractions ($p=0.66$, $n = 3$). Mean heparin content = 7.5±0.7 mg/g.

4.3.3 Visualisation of Heparin Hydrogel Grafting

Figure 4.20 provides SEM images of samples before and after the heparinization process, note the "cobblestone" appearance of the dehydrated (in order obtain SEM images) heparin hydrogel layer on the surface of the PU fibres. A full study of the effects of the heparinization process on scaffold morphology will be described in Section 4.4.1.

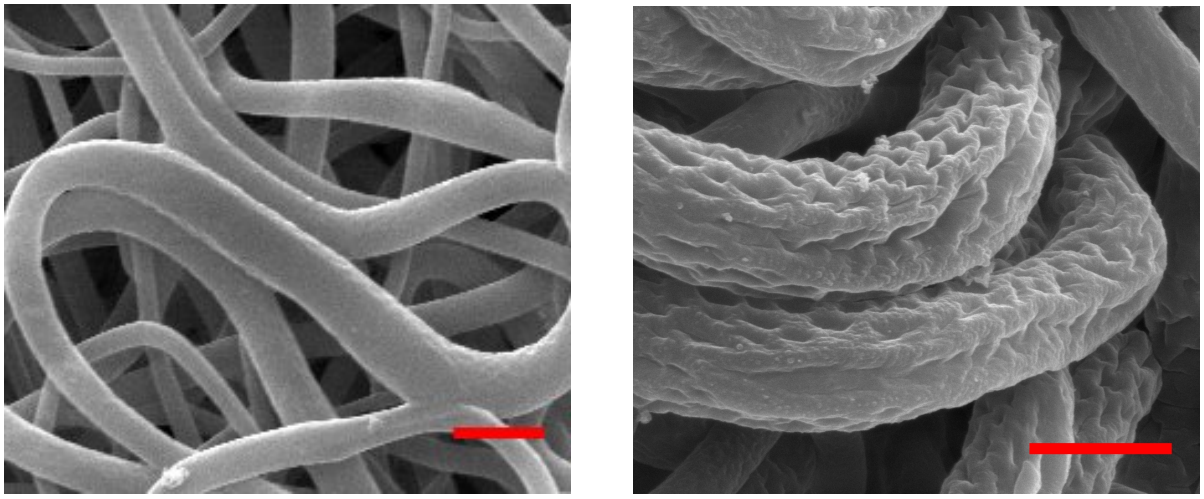

(a) PU (b) PU-HEP

Figure 4.20: SEM images of PU surface before and after the heparinization process. Scale bars represent 5µm

4.3.4 Effect on Mechanical Properties

Figure 4.21 and 4.22 provide typical stress/strain curves (circumferential direction) and summaries of the experiment's results, respectively.

The effect of the heparinization process on scaffold strength was observed to be dependant on the fibre fraction of the scaffold for both CD and TD groups, where the slopes were significantly different ($p<0.0001$) between heparinized and non-heparinized groups. The effect was most pronounced in the circumferential direction where 100% PU samples endured decreases of 7.6±0.8 MPa versus 2.5±0.6 MPa for 30% PU samples. For heparinized samples in the transverse direction, strength was not observed to be dependant on fibre fraction ($m = 0.002\pm0.001$ MPa/PU%, $r^2 = 0.21$, $p=0.11$).

Heparinized constructs were observed to be slightly more rigid in both the circumferential ($p<0.0001$) and transverse ($p<0.01$) directions than their non-heparinized counterparts with statistically parallel but distinct fitted lines. Slopes for CD ($r^2 = 0.79$ (PU) / 0.39 (Hep), $p<0.0001$) and TD groups ($r^2 = 0.75$ (PU) / 0.73 (Hep) ,$p<0.001$) were found to increase linearly with increases in fibre fraction.

The relationship between maximum strain and fibre fraction for heparinized and non-heparinized samples was not well described with the linear regression and no dependency was observed (r^2 <0.09, p>0.37); except for transversely oriented heparinized samples where maximum elongation was observed to decrease linearly with increasing fibre fractions (r^2 = 0.82, p<0.0001). Non-heparinized samples consistently endured greater strains than their heparinized counterparts with mean differences of 337%±24% (p<0.0001) and 366%±48% (p<0.0001) in the circumferential and transverse directions, respectively. Note that in the transverse direction the difference in maximum elongation between groups increased with increasing fibre fractions (p<0.0001).

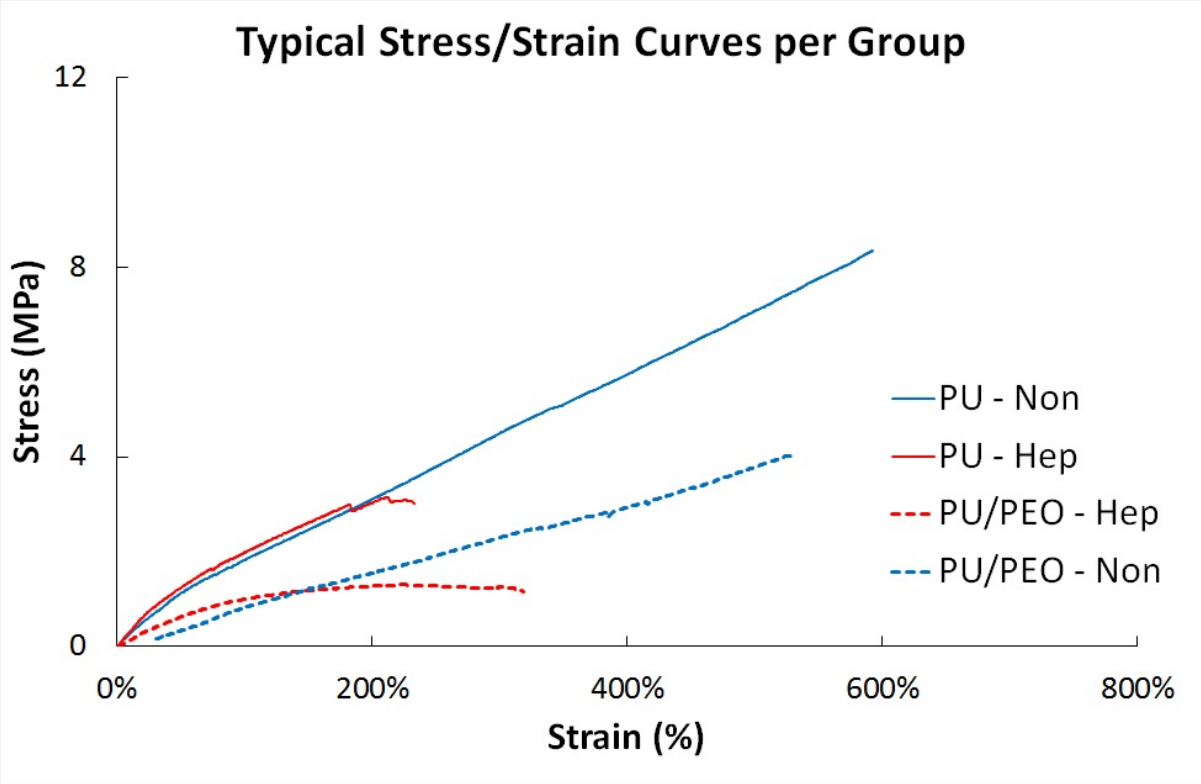

Figure 4.21: Typical stress/strain curves for heparinized and non-heparinized constructs. Note the decrease in maximum strain as well as UTS for pure PU samples, PU/PEO (45% fibre fraction, PEO removed) does not exhibit such large UTS losses.

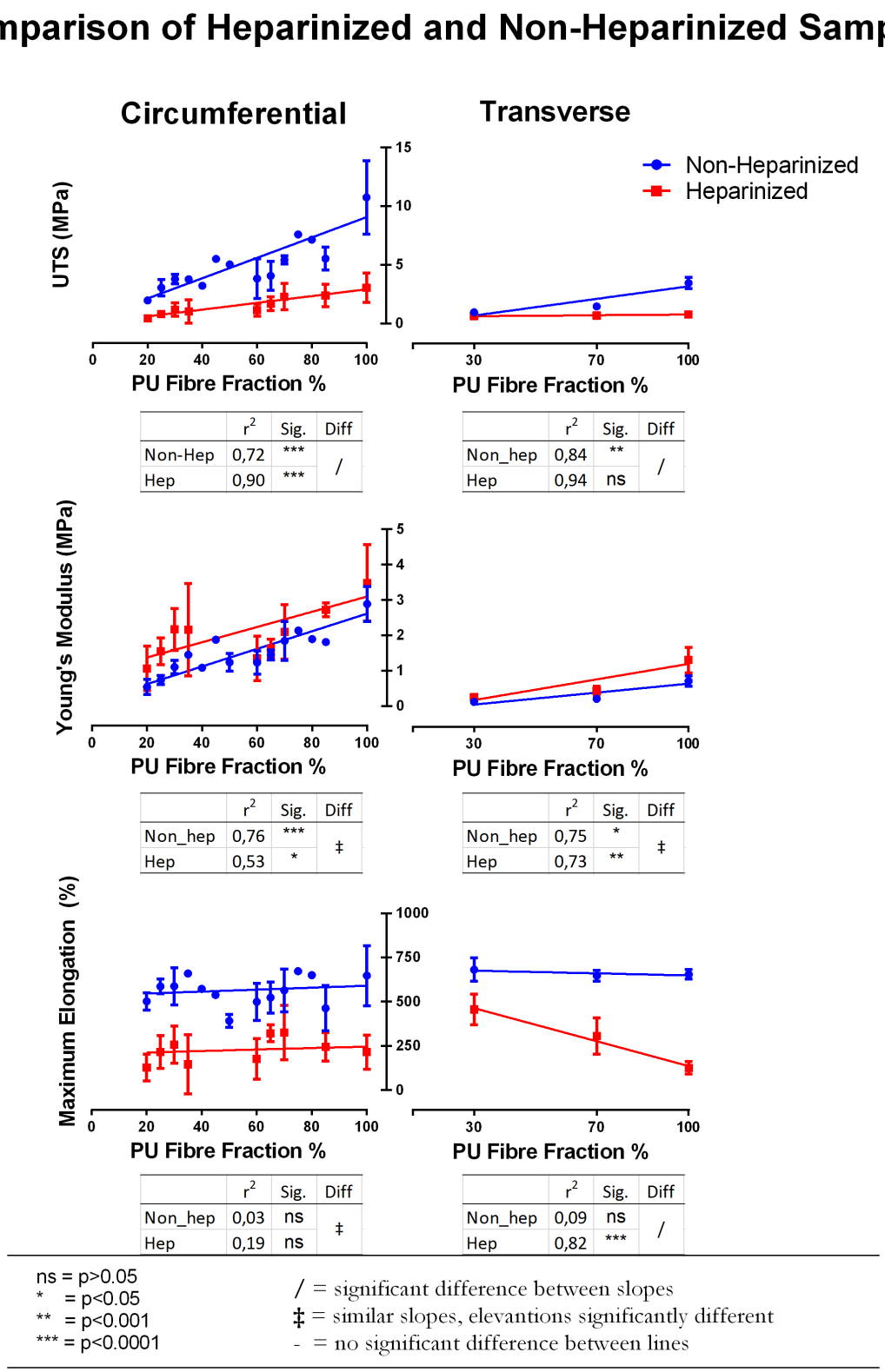

	r^2	Sig.	Diff
Non-Hep	0,72	***	/
Hep	0,90	***	

	r^2	Sig.	Diff
Non_hep	0,84	**	/
Hep	0,94	ns	

	r^2	Sig.	Diff
Non_hep	0,76	***	‡
Hep	0,53	*	

	r^2	Sig.	Diff
Non_hep	0,75	*	‡
Hep	0,73	**	

	r^2	Sig.	Diff
Non_hep	0,03	ns	‡
Hep	0,19	ns	

	r^2	Sig.	Diff
Non_hep	0,09	ns	/
Hep	0,82	***	

Figure 4.22: Mechanical effects of heparin surface modification process. Total sample sizes per group were: n_{CD}=45 and n_{TD}=10 for Non-Hep and n_{CD}=42 and n_{TD}=13) for Hep groups in the circumferential and transverse orientations, respectively. "Sig." denotes non-zero significance of fitted slopes. "Diff." expresses the difference between fitted slopes.

4.3.5 Compliance and Burst Pressure

Tensile testing data from Section 4.3.4 was transformed into equivalent theoretical burst pressures and compliance values for 6mm diameter, 0.5mm thick vascular grafts. Figure 4.23 depicts the results of the transformation. Compliance was calculated to linearly decrease with increasing fibre fractions for both PU ($C_d = -0.078 \pm 0.015 FF_{PU} + 10.3 \pm 0.92$ %/100mmHg, $r^2 = 0.72$, $p<0.001$) and PU+Hep ($C_d = -0.038 \pm 0.016 FF_{PU} + 6.93 \pm 0.98$ %/100mmHg, $r^2 = 0.45$, $p<0.05$) where the slope of the PU line was steeper than the PU+Hep line (p=0.0025)

Burst pressure was calculated to increase linearly with increasing fibre fraction for PU ($BP = 76 \pm 13 FF_{PU} + 1443 \pm 775$ mmHg, $r^2 = 0.74$, $p<0.0001$) and PU+Hep ($BP = 33 \pm 5 FF_{PU} - 87 \pm 312$ mmHg, $r^2 = 0.83$, p=0.0002) where the slope of the PU line was steeper than the PU+Hep line ($p<0.0001$)

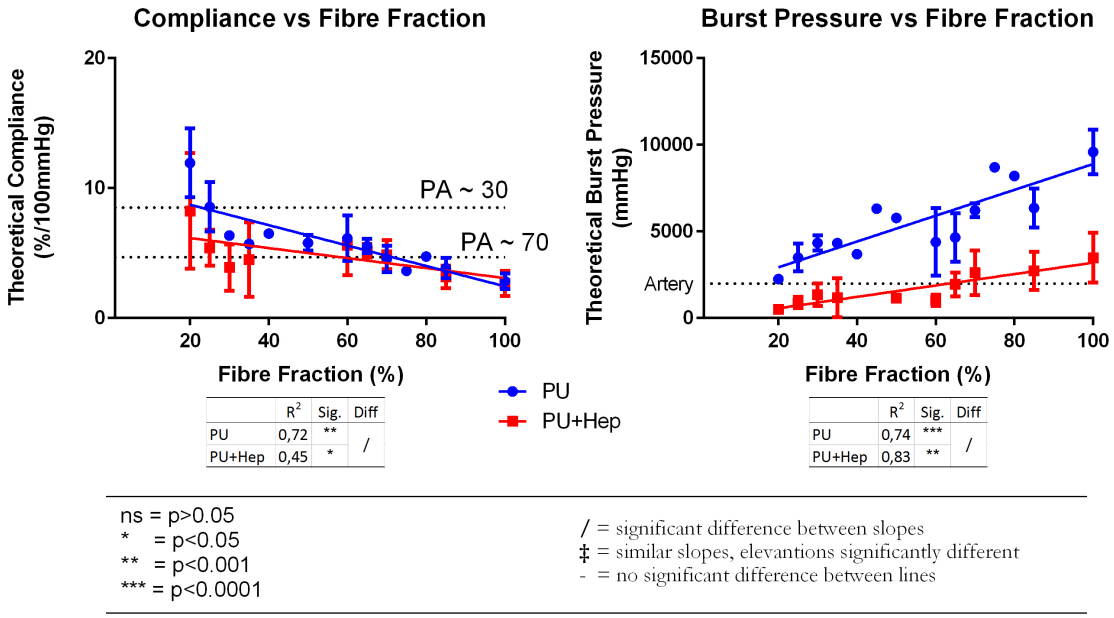

	R^2	Sig.	Diff
PU	0,72	**	/
PU+Hep	0,45	*	

	R^2	Sig.	Diff
PU	0,74	***	/
PU+Hep	0,83	**	

Figure 4.23: Calculated compliance and burst pressures of 6mm diameter, 0.5mm thick imaginary constructs. Compliance was observed to decrease linearly with increasing fibre fractions and heparinized constructs were less compliant than their non-heparinized counterparts at low fibre fractions. Burst pressures were observed to increase linearly with fibre fraction for both groups although heparinized groups were consistently weaker. PA 30 and PA 70 are compliance values of the human popliteal artery measured in patients at ages of 29±4 and 69±10 years of age, respectively [102]. *Artery* refers to the minimum burst pressure of 2000mmHg commonly sought in literature [127, 238, 239]

4.4 *In Vivo* Subcutaneous Study

This section provides details on the results of the *in Vivo* subcutaneous rat study investigating the effect of porosity and the heparin surface modification on tissue ingrowth, collagen deposition, vascularisation and inflammatory response. Firstly, the scaffold groups implanted were analysed for porosity, fibre diameter and pore-size prior to implantation in Section 4.4.1 followed by a full histological analyses post explanation in Section 4.4.2. All animals survived until their scheduled explant time.

4.4.1 Scaffold Morphology

Low, medium and high porosity scaffolds, along with heparinized (Hep) versions of each were analysed for fibre diameter, fibre alignment, pore-size, porosity and scaffold thickness. Figure 4.24 provides typical SEM images of each group and Figure 4.25 summarises the results of their analyses graphically.

Fibre diameter did not vary between porosity classifications ($p=0.95$) but heparinized fibres were significantly thicker on average than their unheparinized counterparts ($3.6\pm0.2\mu m$ vs $1.8\pm0.1\mu m$, $p<0.0001$). Similarly, fibre alignment was not significantly influenced by fibre fraction ($p=0.7$) but the heparinized groups exhibited a lesser degree of anisotropy than unheparinized groups (0.07 ± 0.02 vs 0.33 ± 0.04, $p<0.0001$).

Pore-size measurements were found to have a log-normal distribution (Figure 4.4.1c) and thus were transformed onto a logarithmic axis (Figure 4.4.1d) prior to statistical analysis. No statistical differences were found between Hep and non-Hep groups ($p=0.67$) but significant increases were observed between low and medium ($p<0.0001$), low and high ($p<0.0001$) but not medium and high ($p=0.54$) groups. Low, medium and high groups had mean pore-sizes of $4.0\pm2.1\mu m$, $9.6\pm4.2\mu m$ and $10.3\pm5.2\mu m$, respectively.

The measured porosity values of low, medium and high classification scaffolds was $76\%\pm0.2\%$, $83\%\pm0.5\%$ and $90\%\pm1.0\%$, respectively ($p<0.0001$); no statistical differences were detected in porosity between Hep and non-Hep groups ($p=0.27$).

Scaffold thickness did not deviated significantly between porosity classifications before implantation ($p>0.1$, $n=12$) and only a slight, non-significant, increase was observed between non-heparinized and heparinized groups (0.09 ± 0.04 mm, $p=0.09$), thus a mean scaffold thickness of 1.0 ± 0.05 mm was calculated.

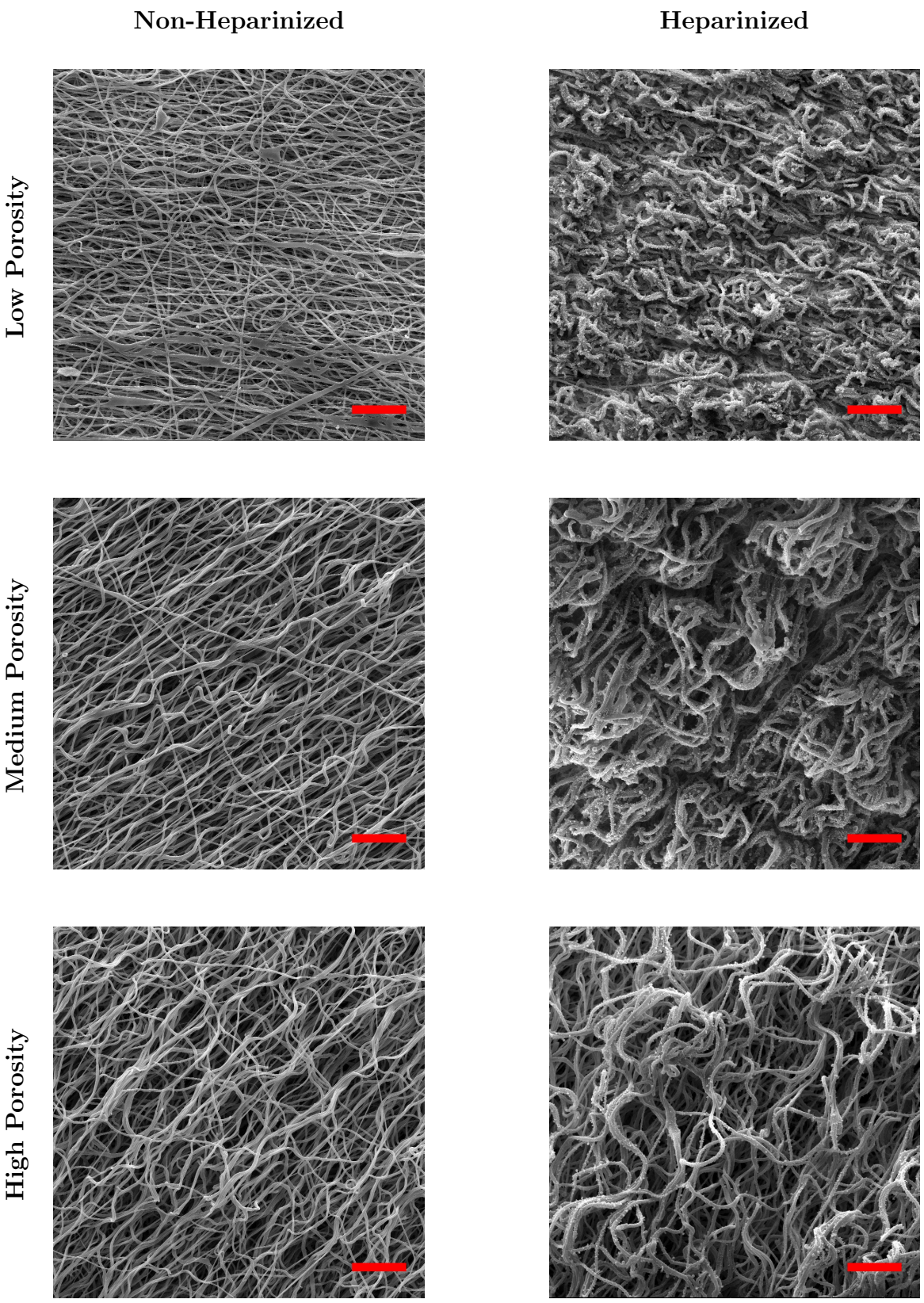

Figure 4.24: SEM images of scaffolds for *in Vivo* study: low, medium and high porosity scaffolds with heparinized versions of each. Scale bars represent 50µm

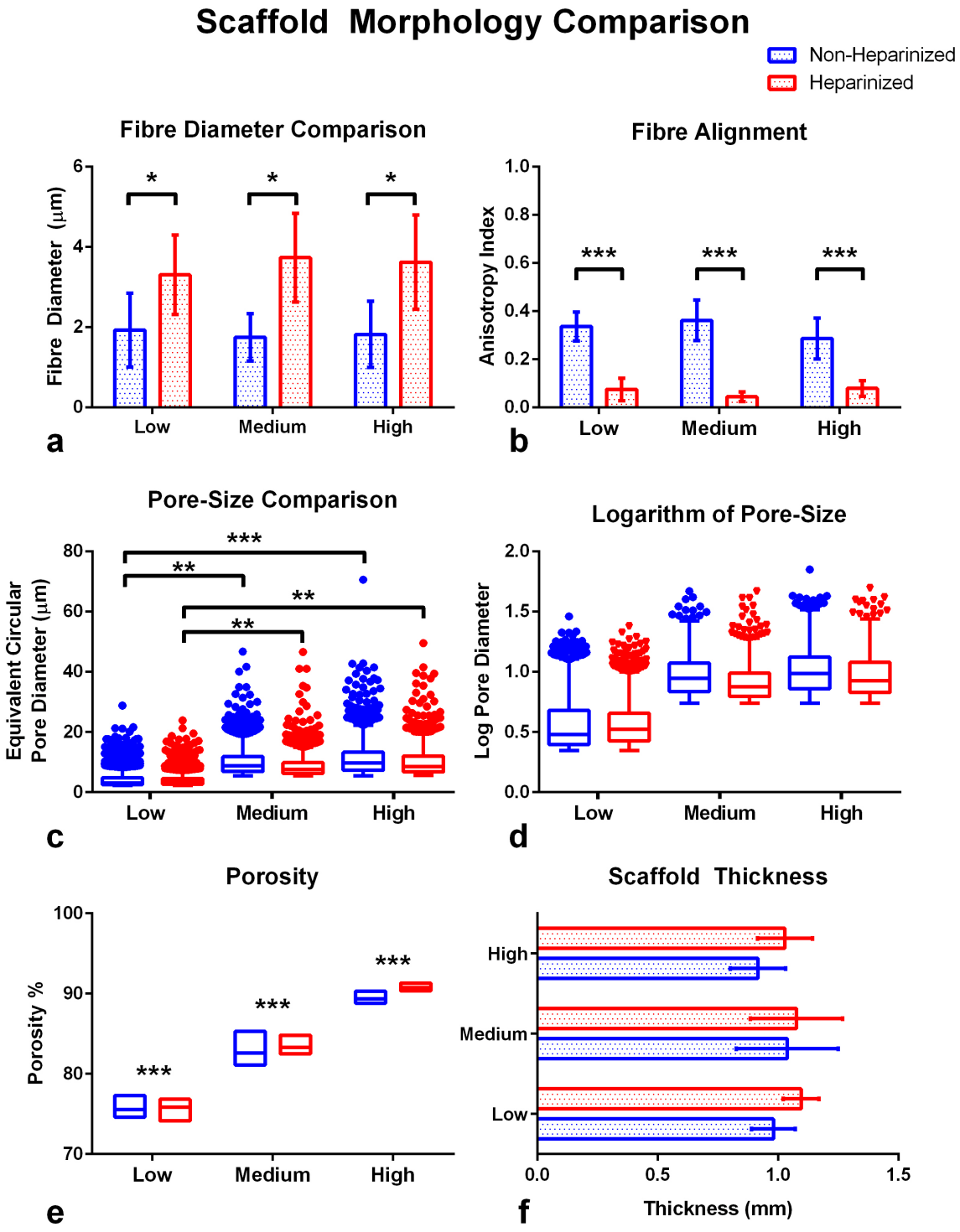

Figure 4.25: Morphological comparison of scaffold groups for implant: **a**) fibre diameter (n=4 samples x 2 images per sample), **b**) fibre alignment (n=4), **c**)& **d**) Tukey box & whiskers plots of pore-size and logarithm of pore-size (n=4 samples x 2 images per sample), **e**) low-high plot of scaffold porosity (n=12) (*** denotes significance between porosity classifications) and **f**) scaffold thickness (n=12). *, **, *** Denote statistical significance between groups with p-values less than 0.05, 0.001 and 0.0001, respectively (uncorrected multiple comparisons)

4.4.1.1 NanoCT Scan

Low and high porosity scaffolds (non-heparinized) were scanned by NanoCT at a resolution of 500nm and rendered in 3D. The results of the scan, while not sufficient for statistical analysis due to low sample size (n=1), are still interesting to compare to morphological measures obtained through SEM image analysis and porosity values calculated by the gravimetric method. Table 4.2 below summarises the results of each for comparison and Figure 4.26 provides 3D and cross-sectional images of the resultant NanoCT scans.

Table 4.2: Comparison of NanoCT Results to SEM Results

	NanoCT		SEM/Gravimetric	
Measure	Low	High	Low	High
Porosity	59%	79%	76±0,2%	90±1,0%
Fibre Diameter	2,36µm	1,94µm	1,9±1,0µm	1,8±0,8µm
Pore-size	3,37µm	7,38µm	4,0±2,3µm	11,1±5,5µm
Anisotropy	0,28	0,23	0,34±0,06	0,29±0,09

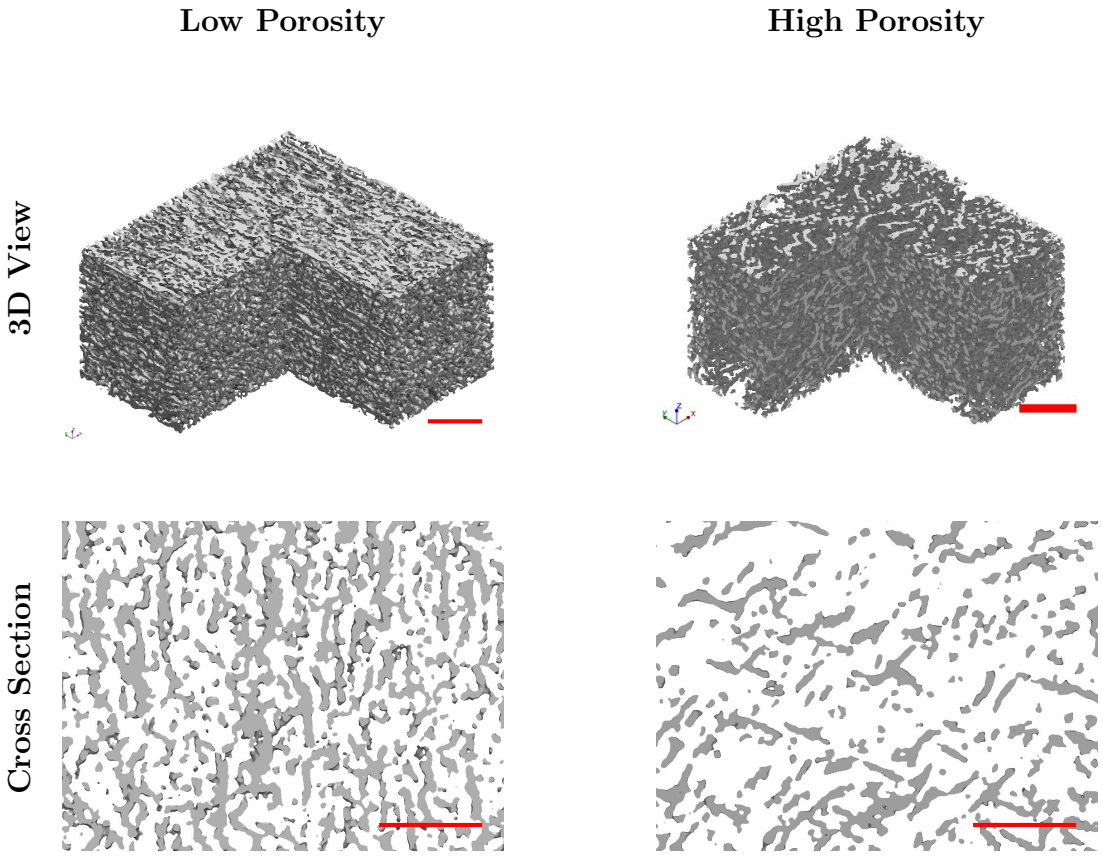

Figure 4.26: NanoCT renders of low and high porosity classification scaffolds, note the palpable difference in density. Scale bars represent 50µm

4.4.2 Histological Analysis

Low, medium, high and heparinized versions of each were explanted at 7, 14 and 28 days and compared for tissue ingrowth, collagen deposition, vascularisation and inflammatory response within the scaffold boundaries.

Tissue ingrowth was observed to increase over implant duration ($p<0.05$) for all groups but at different rates (low = 28±19 μm/week, medium = 60±14 μm/week, high = 155±23 μm/week, $p=0.0002$), where low, medium and high porosity scaffolds exhibited minimal (33±1%), moderate (71±9%) and complete (96±4%) ingrowth by day 28 ($p<0.001$). See Figure 4.28a and accompanying table for a complete statistical comparison of the different groups and Figure 4.27 for representative H&E stained micrographs of each porosity group over time.

No statistically significant differences were observed between heparinized and non-heparinized groups in tissue ingrowth (Figure 4.29), collagen deposition, vascularisation or inflammatory response (Figure 4.31 and Figure 4.32). Large differences were noted between porosity classes for collagen deposition and vascularisation (presented individually below) but not for inflammatory response where no significant differences were observed between groups or time points ($p>0.05$).

Collagen deposition area was observed to increase over time ($p<0.0001$) and with increasing porosity ($p<0.0001$) when measured as a fraction of the total scaffold area; however, when adjusted for available ingrowth area (calculated from H&E sections) collagen deposition per available ingrowth area was observed to be statistically independent of time with all groups having similar slopes ($p=0.52$) but with high porosity groups having higher elevations ($p<0.001$) than other groups. See Figure 4.28b&c.

Significantly more vascularisation was observed in high porosity scaffolds (27±12 vessels/mm^2) than low (2±3 vessels/mm^2, $p<0.0001$) and medium (where vascularisation was only observed after 28 days, 19±13 vessels/mm^2, $p=0.06$) porosity scaffolds. See Figure 4.28d.

No significant differences were observed in inflammatory response between groups or implant duration ($p>0.5$) where inflammatory response was measured as the area of ED1 tagged macrophages and foreign body giant cells (FBGC) per scaffold area. See Figure 4.28e.

High porosity scaffolds were observed to increase in thickness over time, starting at 243±43μm and 455±205μm at 7 days and ending at 881±307μm and 1290±357μm at 28 days for non-heparinized and heparinized versions, respectively; other groups did not change significantly in thickness over time ($p>0.07$). All groups appeared thinner in histological sections than measured before implantation with exception of high porosity scaffolds. See Figure 4.30.

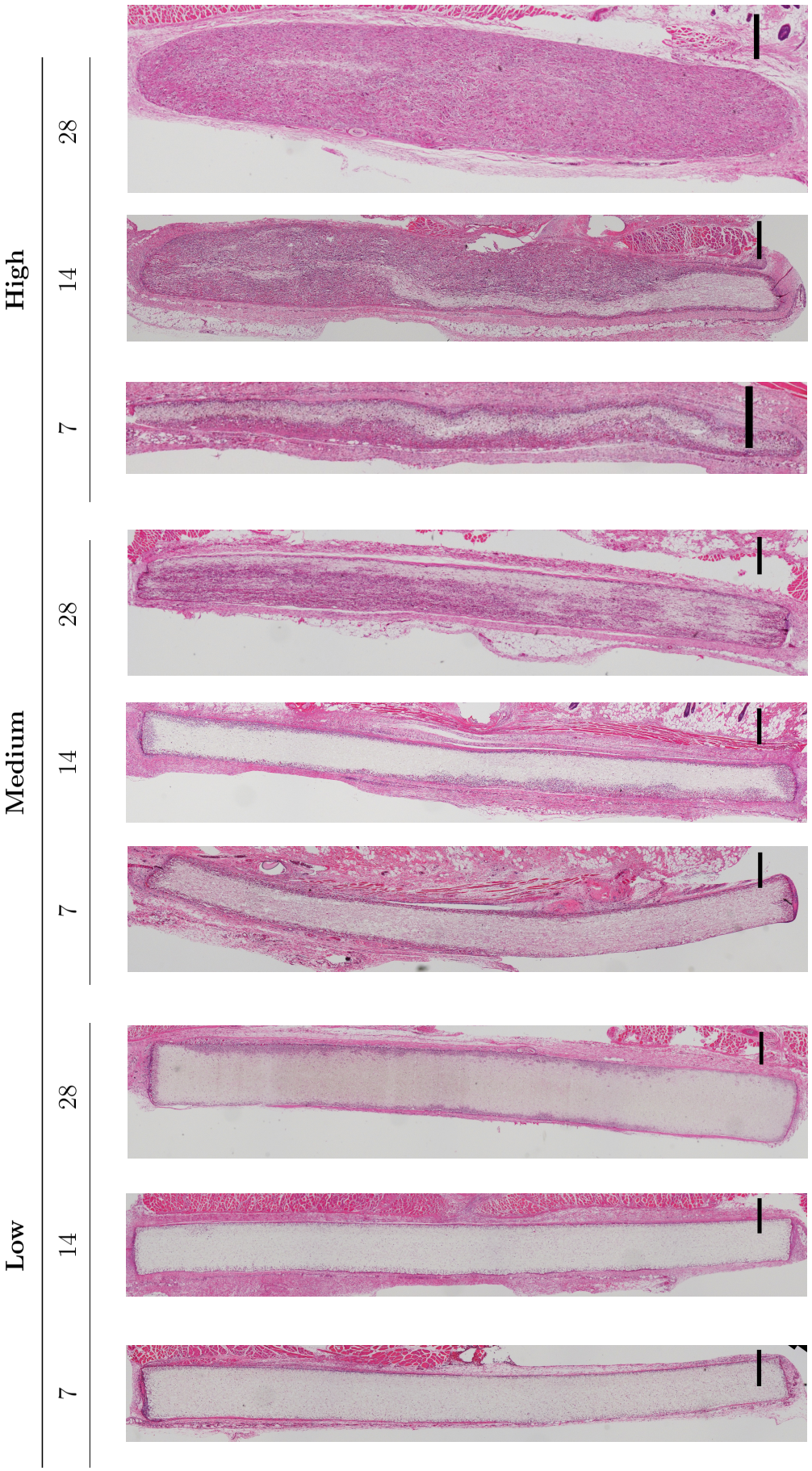

Figure 4.27: H&E Results of low, medium and high classification scaffolds (non-heparinized) at 7, 14 and 28 days showing cellular and tissue ingrowth over time. Scale bars represent 500µm

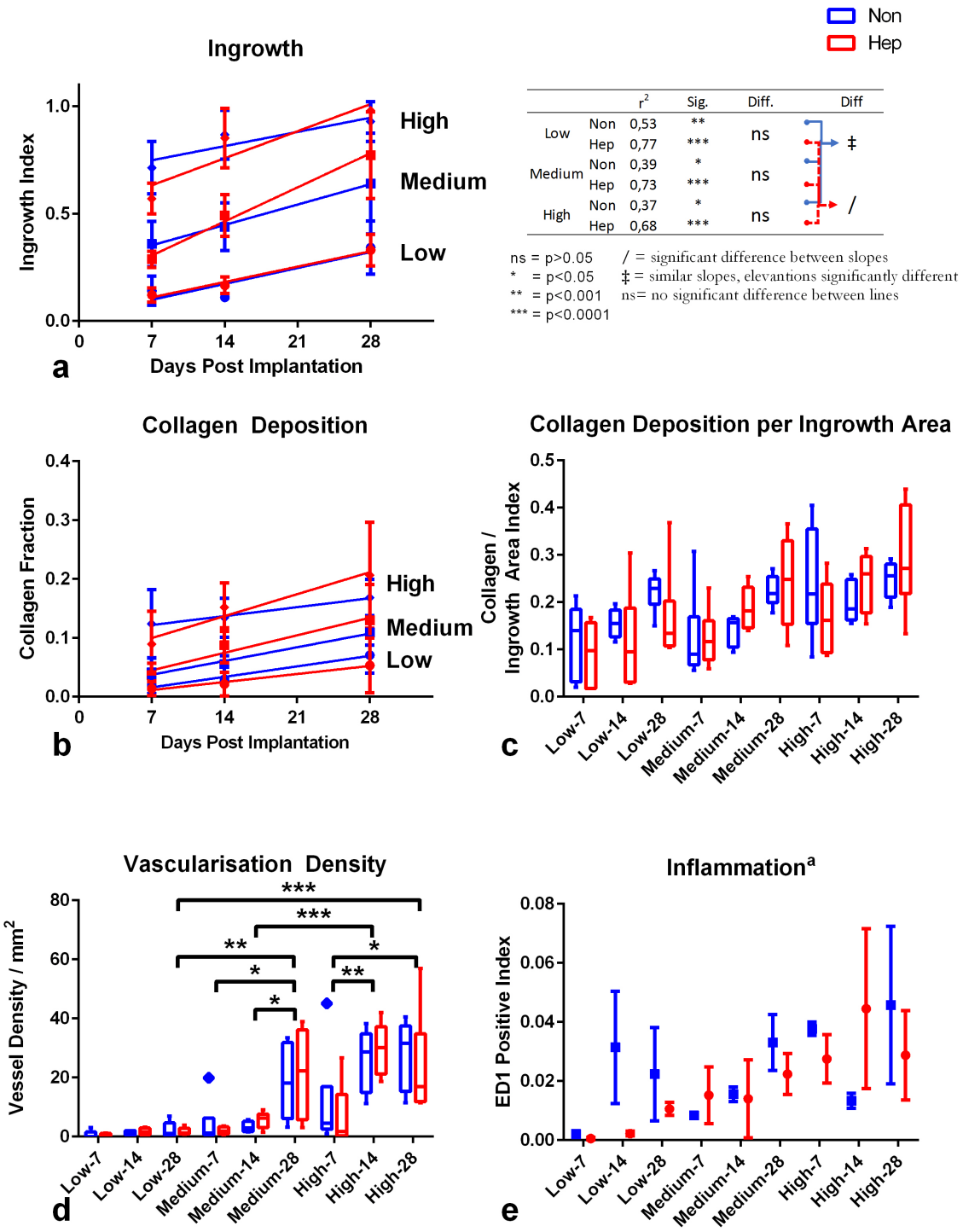

Figure 4.28: Summary of *in Vivo* results (n=6): **a**) linear regression analysis of groups over implant time, **b**) linear regressions of collagen area over time, **c**) collagen area normalised to tissue populated area (no significant differences between groups), **d**) density of vessels ($\geq$100µm^2) per mm^2, **e**) area of ED1 stained macrophages/FBGC per scaffold area. *, **, *** Denote statistical significance between groups with p-values less than 0.05, 0.001 and 0.0001, respectively (Tukey corrected multiple comparisons). **a**: 7&14 days→n=2; 28 days→n=6

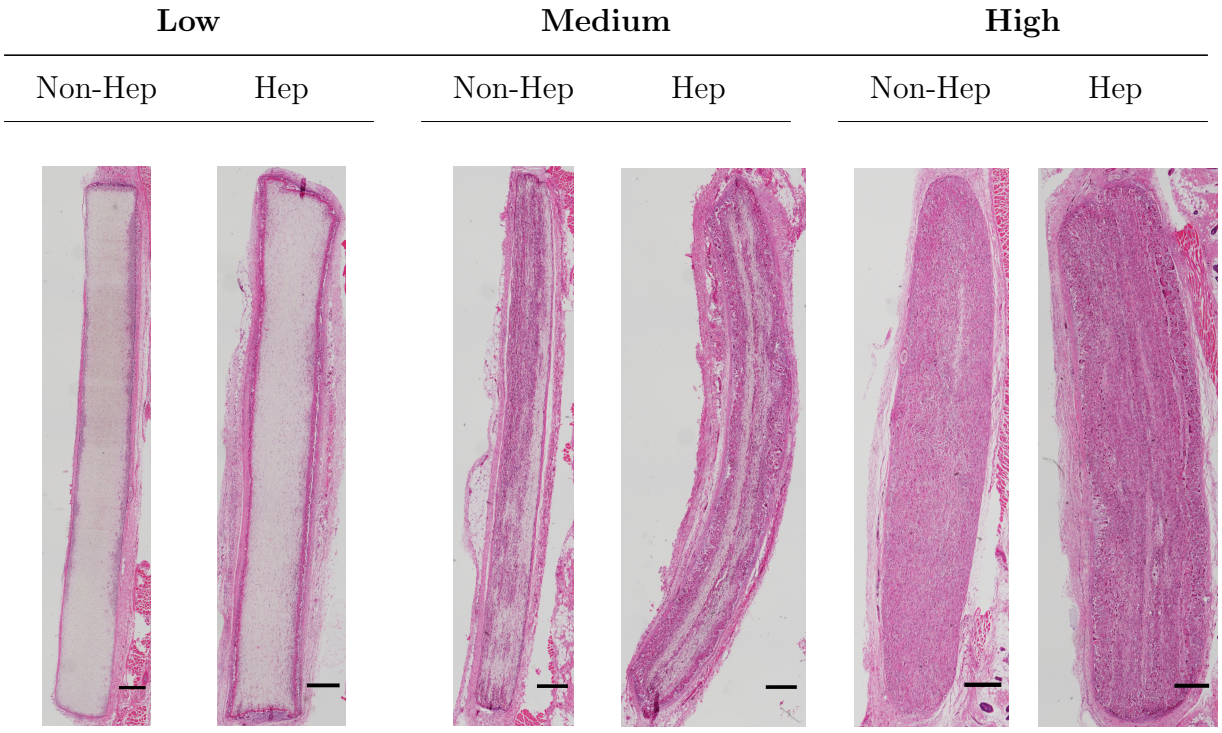

Figure 4.29: H&E stained micrographs of low, medium and high classification scaffolds and their heparinized versions at 28 days post implantation, no noticeable differences in tissue infiltration between heparinized and non-heparinized groups. Scale bars represent 500µm

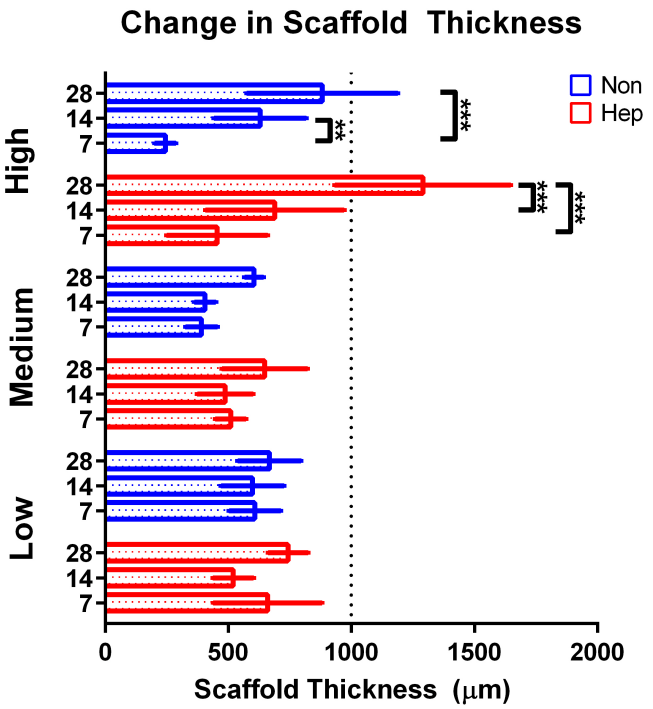

Figure 4.30: Thickness measurements from histological images (H&E) were consistently smaller than recorded before implant. Low and medium class scaffolds did not undergo significant changes over time but high type scaffolds almost tripled in width. *, **, *** Denote statistical significance between groups with p-values less than 0.05, 0.001 and 0.0001, respectively (Tukey corrected multiple comparisons) (n=6)

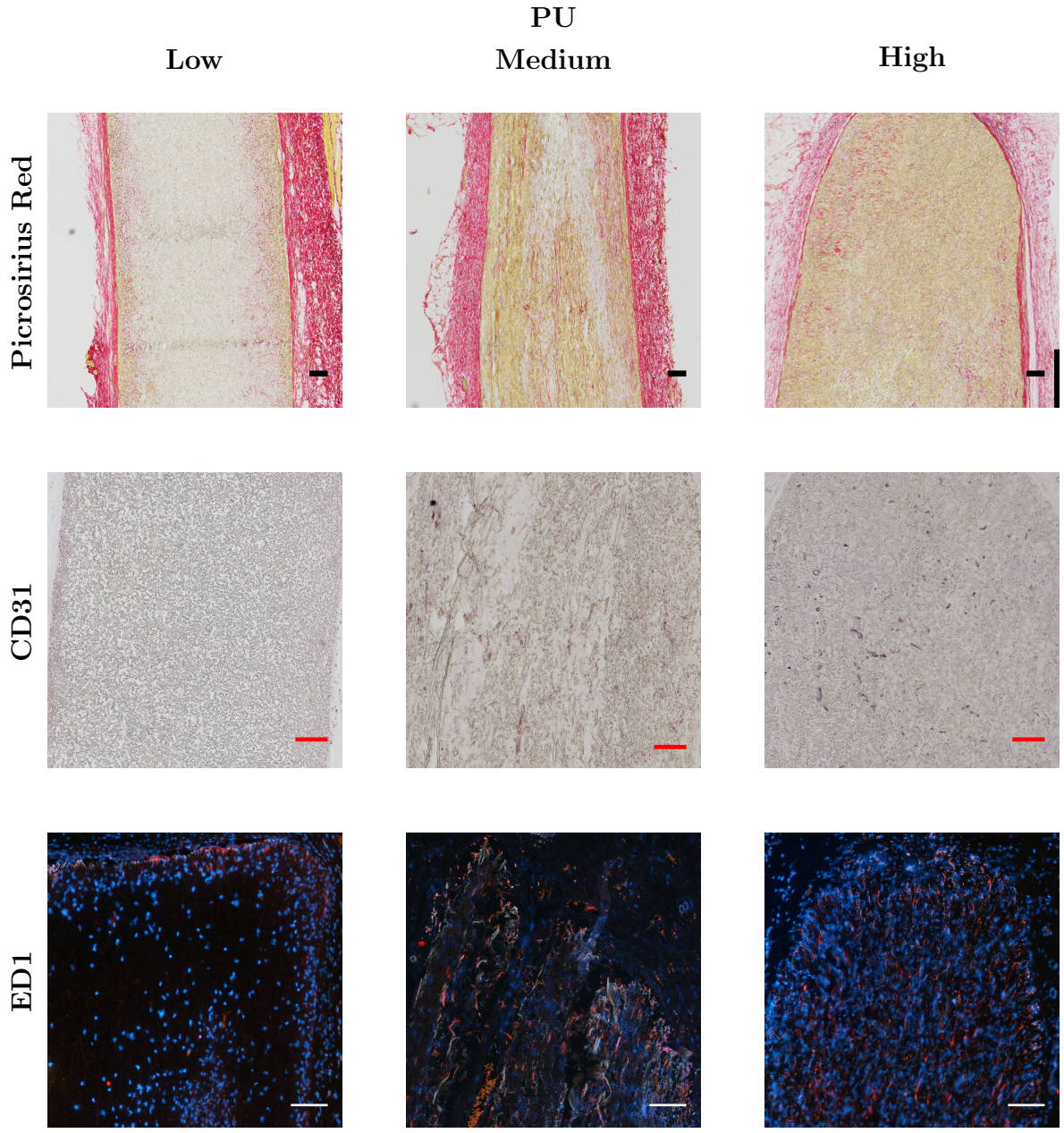

Figure 4.31: Typical histological results of Picroserius red (PSR), CD31 and ED1 stains for non-heparinized groups. PSR stains collagen red. CD31 stains endothelial cells purple. ED1-Cy3 bound macrophage cells and FBGCs fluoresce red/orange, DAPI tagged nuclei fluoresce blue. Scale bars represent 100µm

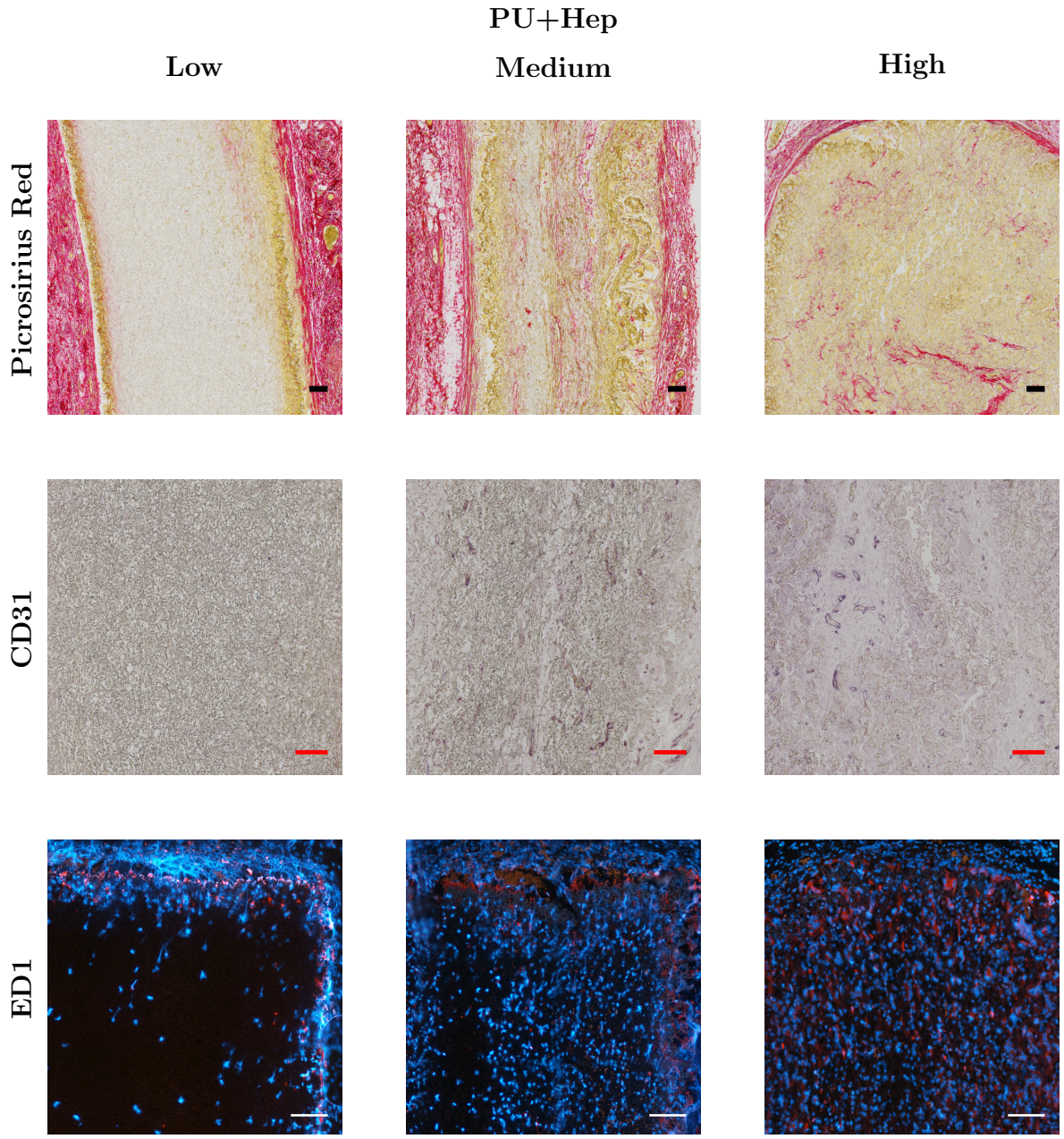

Figure 4.32: Typical histological results of Picroserius red (PSR), CD31 and ED1 stains for heparinized groups. PSR stains collagen red. CD31 stains endothelial cells purple. ED1-Cy3 bound macrophage cells and FBGCs fluoresce red/orange, DAPI tagged nuclei fluoresce blue. Scale bars represent 100µm

Chapter 5

Discussion

This chapter will discuss in detail the results observed in Chapter 4 in the same order, with the initial results obtained from single spinneret electrospinning (Section 5.1) being covered first followed by a discussion of the various results obtained during dual electrospinning in Section 5.2. A separate examination (Section 5.3) of the effects of the heparinization process will be provided and finally the implications of the *in Vivo* study (Section 5.4) will be discussed.

5.1 Single Spinneret Electrospinning

5.1.1 PU Fibre Optimization

PU fibres spun from THF:DMF co-solvent solutions were thinner, less aligned and were deposited over a wider area of the collector (all other parameters held constant). The observed reduction in fibre diameter when spinning from THF:DMF when compared to THF can be attributed to an increase in net charge density, due to the higher dielectric constant of the co-solvent mix, thereby increasing the tensile force on the solution yielding thinner fibres [183,189]. These observations are in agreement with current literature where both Wang *et al* (2013) and Feng *et al* (2013) concluded that PU solutions spun with a co-solvent mix of THF:DMF (1:1) yielded the smaller diameter fibres with less defects than when spinning from THF or DMF alone [190, 228]. The same mechanism can also be used to explain why fibre alignment and deposition were affected by the THF:DMF solvent system; the increased charge density of the solution causes increased repulsion forces between adjacent segments of the fibrous jet, resulting in a pronounced whipping effect, causing a larger radius for fibre deposition and more variation in fibre angle. These effects are also well documented in literature [148, 188, 228].

For the purposes of vascular grafts complete fibre alignment, as observed in PU/THF, is not desirable due to the lack of strength in the transverse direction resulting in inability to endure surgical handling and poor suture retention [127]. Additionally, as will be discussed later in Section 5.2.4 a degree of fibre isotropy and a wide fibre deposition band is desired for inter-dispersion with the sacrificial fibres.

5.1.2 PEO Fibre Diameter

Two distinctly different fibre diameter distributions were electrospun from the two solvents, where PEO/DCM produced much larger fibres than PEO/EtOH for the flow rates investigated. Interestingly, fibre diameter did not increase significantly with increasing flow rate for PEO/EtOH as it did for PEO/DCM and as is commonly reported in literature [148, 182, 188]; however Son *et al* (2004), who spun PEO fibres from solvents of Chloroform, EtOH, DMF and water, noted that flow rate did not have consistent effects on fibre diameter across all solvents. It is a possibility that the effects of the flow rate on fibre diameter are negated by the effects of the dielectric constant properties for the EtOH solvent system, whereas for DCM, with much weaker dielectric properties, the effects of the flow rate are more pronounced.

The overwhelming majority of work in electrospinning is focussed on controlling process parameters to reduce fibre diameter, to either better mimic the ECM (tissue engineering/regenerative medicine) or to increase surface-area/volume ratio (filtration), thus no established techniques for creating large diameter fibres have been published, in this author's knowledge, to date. In an attempt to create large diameter fibres DCM was selected as a solvent for its high vapour pressure and low dielectric constant which would allow spinning at short working distances (shown to increase fibre diameter) to the collector and reduce the tensile force acting to elongate the fibrous jet (reducing fibre diameter). While large fibre diameters were produced they were not uniform and many small diameter jets were observed to extrude perpendicularly to the large diameter fibres. This phenomenon, first observed by Reneker *et al* (2000), was proposed by Yarin *et al* (2005) to be due to static undulations in the fibrous jet resulting in adjacent segments repelling the local peaks into smaller diameter fibres, branching away perpendicularly from the primary jet [114, 181]. These anomalies are observed to be more common with large diameter fibres being spun at electric field strengths well above the minimum required for producing a Taylor cone [110]. While the large diameter fibres had morphological defects, they were still sufficient for the purposes of this study as they occupied a sufficiently larger volume per fibre than fibres spun from PEO/EtOH.

5.2 Dual Electrospinning

5.2.1 Tailoring the Electric Field for Dual Electrospinning

Introducing a second jet to the electrospinning process creates new issues that need to be addressed in order to effectively control the process. The most prominent side-effect of the dual spinning process is the electrostatic interaction between the charged polymer jets as they traverse towards the collector. By charging the two spinnerets with opposing polarities an attractive force will result between the two fibrous jets as they near the collector. In the case of the large diameter mandrel the fibres' trajectories are impeded by the positioning of the collector between them. However, for the small diameter mandrel the electrostatic attraction force between the two jets caused them to collide in mid-air or collect on the opposite spinneret, with little-to-no deposition occurring on the collector. This has also been observed by Ekaputra *et al* (2008) who noted that deposition efficiency decreased markedly with decreases in collector diameter while co-electospraying/electrospinning with opposing polarity spinnerets [216]. For the purposes of small diameter vascular grafts, with mandrels less than 6mm in diameter, this is an unacceptable result and so like-polarity charged spinnerets were investigated.

When both spinnerets are charged with a positive polarity the resultant jets act to repel one another. This is also an undesirable feature for this study as the sacrificial fibre and structural fibre are required to inter-disperse for facilitation of homogeneous void space creation (post sacrificial fibre removal). In an attempt to forcibly direct the deposition of the two fibres in the middle of the mandrel (transverse axis) electrostatic shields (guides) were erected in parallel on either side of the collector. This worked to improve the inter-deposition of the two fibre types but simultaneously acted to reduce the elongation forces acting on each solution at the capillary tip (towards the collector), requiring higher electric field strengths to initiate a stable Taylor cone. For this purpose the collector was charged with an opposing polarity to the spinnerets, instead of being grounded, thereby increasing the net potential difference between the spinnerets and the collector, promoting jet formation. However, the magnitude of the applied voltage to the collector was limited, as high voltages ($|>3$ kV$|$) caused arcing to the mandrel's electric motor.

5.2.2 Drying Process Post PEO Extraction

Lyophilization (freeze drying) was necessary for preserving the void volume left by the sacrificial fibres post removal, especially for very low PU fibre fractions. This could be due to PU's low stiffness and hence its inability to resist the weight and surface tension forces of the water in its liquid form (when vacuum dried), resulting in its collapse over the

newly generated voids where the PEO fibres had been removed. In contrast, lyophilization better preserved the void spaces created by the removal of the PEO fibres through the process of sublimation. It is important to retain the scaffolds bulk volume whilst removing the PEO fibres or else the void space obtained by removal of the sacrificial fibres will be lost to collapse of the bulk structure of the scaffold. While not explicitly reported in literature, sacrificial fibre authors utilizing a hydration step followed by vacuum drying report instability of low fibre fraction ($< 50\%$) constructs post PEO removal [71, 212]. However, studies that freeze dried constructs post PEO removal were able to facilitate structural stability at lower fibre fractions [213, 215]. This is supported by the increasing difference in bulk volume reduction between freeze dried samples and vacuum dried samples as fibre fraction is decreased (Figure 4.6).

5.2.3 Porosity Determination

The equivalence of the two porosity determination techniques, in this case, indicates that the density of electrospun PU remained unchanged from its bulk form. This result indicates that no micro-porosity exists within the PU fibres which would otherwise implicate negative effects on scaffold strength. An additional benefit of this result is that it negated the need to use the more labour intensive densitometric method.

5.2.4 Thin vs Thick Sacrificial Fibres

Composite scaffolds of PU with two distinctly different types of sacrificial PEO fibres were created, verified for inclusion and removal and then studied for their effects on porosity and mechanical properties of the remaining scaffold. It was found that the inclusion and subsequent removal of thin sacrificial fibres produced constructs with higher porosities than those where thick sacrificial fibres had been included/removed. This section aims to discuss the mechanisms behind the observed differences between the two groups by discussing the effects on porosity and mechanical properties separately.

5.2.4.1 Effect on Porosity

Visualisation of the inter-dispersion of thick or thin sacrificial fibres was verified separately by both SEM and confocal microscopy (with fluoroscein and rhodamine fluorescent dyes added to PU and PEO). Visualisation of the removal of the sacrificial fibre by confocal microscopy was confounded by the indiscriminate removal of both dyes during the PEO removal process. However, complete PEO removal was confirmed by washing to constant

mass, where the mass loss was also compared to the predicted mass loss as calculated by equation 3.12, a technique that has also been used by Milleret *et al* (2011) [71].

Surface SEM images of PU constructs (with thin, thick or no sacrificial fibre types) visualised before and after the PEO removal process showed that inclusion and subsequent removal of sacrificial fibres produced lower density architectures, with noticeably larger void spaces between PU fibres, than scaffolds produced by the standard electrospinning technique (100% PU). Note that the fibre packing density of pure PU scaffolds was unchanged after undergoing the PEO removal process indicating that the process itself was not responsible for the observed increases in void volume. Counter-intuitively, thick sacrificial fibres produced less void space between PU fibres than thin sacrificial fibres (same fibre fraction, Figure 4.9). These observations were confirmed during the porosity analysis of the scaffolds post PEO removal, where all groups (thin, thick and no sacrificial fibres) were equivalent in porosity before PEO removal, but post removal those constructs fabricated with thin sacrificial fibres possessed significantly higher porosities on average than those with thick and no sacrificial fibres (Figure 4.12a).

Figure 4.12b, hints at a possible mechanism for the observed reduction in porosity created by thick sacrificial fibres compared to thin sacrificial fibres: thick groups lost four-times more bulk volume than thin groups post PEO removal, resulting a large proportion of the potential void space created being lost to the collapsing or compacting of the PU fibres. This is visualized in Figure 4.10 where thick groups showed large, flattened-out voids in-between dense layers of PU, in contrast to the low density mesh observed from thin groups. Three mechanisms behind the collapse of void space observed in thick groups are offered: 1) PU fibres are not stiff enough to resist bending over the long distances associated with the voids created by thick sacrificial fibres (during removal process); 2) the high momentum associated with the thicker PEO fibres causes the hybrid mesh already present on the collector to be compacted on impact, causing PU fibres to form compact meshes in between PEO fibres; and 3) the productivity (fibres deposited per unit area per unit time) difference between PEO/DCM and PU/THF:DMF causes spatially distinct structural and sacrificial fibre populations. These mechanisms will now be discussed in more detail.

The PEO removal process involves high energy mixing in water/EtOH solutions, resulting in unavoidable hydrodynamic stresses acting on the PU fibres. In the case where there are large gaps of support between dense layers of elastic PU fibres (caused by the removal of large sacrificial fibres) the hydrodynamic forces may cause collapse of the PU sheets into the void spaces created by PEO removal. For thin sacrificial fibres, the span distance between adjacent fibres is not as large due to the diameter of both the sacrificial and structural fibre being in the same order of scale, thus void spaces are preserved. The collapse of the PU fibres into the newly created void spaces could also be due to residual

stresses in the elastic PU fibres, which form as they deposit and bend around large PEO fibres. When the large PEO fibres are removed the PU fibres are allowed to relax and straighten, thereby reducing the volume of the newly created voids. Whether due to external or internal stresses, the results of Figure 4.12b showed that scaffolds spun with PEO/DCM as a sacrificial fibre lost significantly more of their bulk volume in the extraction process than scaffolds spun with PEO/EtOH. Nam *et al* (2007), who added large NaCl particles simultaneously while electrospinning PCL, found that washing out the NaCl crystals caused large delaminations in their place [217], similar to the delaminations caused by the large sacrificial fibres seen in Figure 4.10a and Figure 4.10d.

The second mechanism offered as explanation for the reduced void space observed in thick groups is based on the premise that thicker jets have greater mass than thinner jets; resulting in greater impact energy when colliding with the collector, thus compacting the existing mesh. This effect would be even more pronounced in the case where complete evaporation of the solvent had not occurred, resulting in an even higher energy impact due to the weight of the solvent. However, it could be argued that the momentum gained from increased mass is balanced by the reduction in fibre velocity due to the lower Coulomb force as a result of the low dielectric constant of DCM when compared to EtOH (thin fibres); however, Reneker *et al* 2000 observed that the axial velocity of a jet undergoing large whipping instabilities actually slowed down, from 1.1 m/s to 0.8 m/s, as it traversed towards the collector (the radial component of velocity increased as it neared the collector) [114]. Thus, for PEO/EtOH, the high charge density leads to thinner fibres with larger whipping radii, in turn reducing the impact energy on the collector when compared to PEO/DCM. The relationship between jet velocity and solvent dielectric constant/conductivity has not been studied in great detail in existing literature so more work is needed to verify the assumptions of this mechanism.

Finally, the third mechanism is that a productivity mismatch occurs between PEO/DCM and PU/THF:DMF where an order of magnitude more PU fibres are deposited in an area per unit time than PEO fibres, thus dense sheets of PU are formed around scantly deposited, large PEO fibres. This is in contrast to the match in productivity between PEO/EtOH and PU/THF:DMF where equivalent amounts of fibres are deposited in an area simultaneously, leading to a homogeneous mixture of the two fibre types. Productivity has been shown to be dependant on solvent conductivity and dielectric constant where solutions with high values of these properties (DMF and EtOH) are observed to be more productive [183].

The observed differences in void space between scaffolds fabricated with PEO/EtOH and PEO/DCM are more likely due to a combination of the three mechanisms described above, where productivity mismatch between PEO/DCM and PU/THF:DMF causes dense layers of PU to be distributed over large, amorphous, scantly-distributed PEO fibres, which

are subsequently compacted by layer-upon-layer of massive PEO jets. This is in sharp contrast to the thin PEO fibres, which due to their matched productivity and fibre diameter to the PU fibres, deposit in an interspersed manner with no observable laminations. The deposition of partially evaporated thick fibres does confound the comparison of the two groups, however, even if perfectly formed thick fibres were produced, the issue of spatial separation of the two fibre type populations would still remain; where void spaces cannot be created between two structural fibres if sacrificial fibre does not occupy the space between them. It appears that in order to obtain interconnected void spaces inside the scaffold structure the productivity of the two polymeric solutions should be matched to ensure homogeneous interspersion of the two fibre types. Additionally, the whipping radii of the two polymeric jets should be large enough so as to ensure that the two polymers co-deposit simultaneously on the same area of the collector mandrel.

5.2.4.2 Effect on Mechanical Properties

Ultimate tensile stress (UTS), Young's modulus and maximum elongation have been studied for scaffolds produced from thick and thin sacrificial fibres over a range of fibre fractions. This section will describe and compare the trends observed with regard to fibre fraction both before and after sacrificial fibre removal.

Before PEO removal, thin and thick sacrificial fibre inclusion appears to have opposing effects on scaffold UTS, with a positive correlation observed for thin groups compared to a negative correlation for thick groups (Figure 4.16). It is important to note that the extrapolated y-intercept (UTS) of the fitted line (linear regression) through thick groups was observed to be significantly higher than for thin groups, while the difference at a PU fibre fraction of 55% was not; resulting in lines with large y-intercept differences progressing towards a common y-value at high PU fibre fractions. This observation correlated well with the observed trend in Figure 4.5, where it was observed that PEO/DCM (thick) produced stronger scaffolds at higher flow rates than PEO/EtOH (thin); thus for low PU fibre fraction scaffolds (where PEO flow rate is high) the strength provided by thick (PEO/DCM) PEO fibres is much higher than for thin (PEO/EtOH). Soliman *et al* (2011) also observed that micron-scale PCL fibres produced stronger scaffolds than nanometre-scale fibres, showing the influence of fibre diameter on resultant scaffold strength [132].

Both thin and thick groups exhibited similar responses to PU fibre fraction increases for scaffold stiffness (Young's modulus) where low fibre fraction scaffolds displayed the high stiffness values of PEO, while high fibre fraction scaffolds where PU fibres were in majority were dependant on the less stiff PU fibres. Interestingly, thick sacrificial fibres did not produce stiffer scaffolds than thin fibres (as was expected from Figure 4.5). Bel-

lan *et al* (2005) have shown that electrospun PEO fibres have higher Young's moduli than solvent-cast films which they hypothesize is due to molecular reorientation during the electrospinning process [240]. At high PEO flow rates (low PU fibre fractions), fibre deposition was observed to be "dry" for thin PEO/EtOH (thin groups) but "wet" for PEO/DCM (thick groups). Thus, according to Bellan's theory complete reorientation would occur in only the thin PEO groups, as the thick groups did not evaporate completely before deposition, creating a balance in stiffness between the two groups.

The almost two-fold increase in maximum elongation observed in thick sacrificial groups when compared to thin groups can be explained by the different deposition patterns observed in the two groups. Thick sacrificial fibre scaffolds were observed to be laminated, with separate layers of PEO and PU fibres, thus when uni-axially extended the fibrous layers would slide over each other, aligning themselves to the axis of the applied stress. For thin sacrificial fibre scaffolds the two fibre types intermeshed with each other which did not allow for the extent of reorganisation observed in thick sacrificial groups, resulting in lower strains-to-failure than thick groups. This theory is further reinforced by the observation that no significant differences were observed in maximum elongation before and after PEO removal for thick groups but large increases were observed for thin groups. For thin groups, the intermeshed PEO fibres that restricted the reorganisation of PU fibres were no longer present after PEO removal, resulting in higher attainable strains to failure. However, for thick groups, the PEO fibres did not restrict the reorganisation of the PU fibres in the first place, so PEO removal did not influence scaffold maximum elongation. Note that no significant differences were observed in fibre diameter or alignment between thin and thick groups post PEO removal, so the observed differences in maximum elongation could not be due to these factors (Figure 4.13).

After PEO removal, thin and thick groups exhibited similar increases in both UTS and Young's modulus values with increasing PU fibre fractions. The apparent superiority in strength and stiffness of thick groups when compared on the fibre fraction scale appears to be due to thin groups having higher porosities for a given fibre fraction; thus when compared on the porosity scale both groups exhibit equivalent strength and stiffness properties. This observation correlates well with the theory that thick groups create lower porosity due to their more severe bulk volume reductions post PEO removal. Removal of the PEO fibre causes large reductions in Young's modulus of the scaffold, this is expected as the stiffer PEO fibre is no longer present in the scaffold and only elastic PU fibre remain. These observations agree with those of Baker *et al* (2008) and Ifkovits *et al* (2010) who found that co-spun scaffolds inherited a proportion of the properties of each polymer depending on scaffold fibre fraction, similar to the observations in this text [212, 213].

Correlation between the mechanical properties measured and scaffold porosity was consistently stronger than the correlation between the same properties and fibre fraction. This is due to the porosity value taking into account the bulk volume changes which affect stress and strain calculations, whereas fibre fraction does not. For example, if a 20% fibre fraction scaffold was measured to undergo a large bulk volume reduction it would also have a thinner cross section, appearing stronger ($\sigma = F/A$) but it would also have a lower porosity ($P = V_{Voids}/V_{bulk}$), thus it would appear stronger than other 20% samples on the fibre fraction scale but would fit well with similar porosity scaffolds on the porosity scale.

Large decreases in UTS and Young's modulus but minor increases in maximum elongation were observed between circumferentially and transversely oriented scaffolds, respectively (Figure 4.15). This was expected due to the fibre alignment being prominently in the circumferential direction due to collector rotational velocity. This is in accordance with current literature [71, 212, 241].

5.2.4.3 Effect of Testing Conditions on PU Mechanical Properties

Immersion in PBS at 37°C did not significantly influence the mechanical properties of 100% PU scaffolds when tested in the circumferential direction. In transversely oriented samples, immersion resulted in slight increases in Young's modulus and maximum elongation. However, while the values obtained for Young's modulus were statistically significant, they were too small to be of clinical significance. The increase in maximum elongation for immersed samples has also been observed by Dempsey *et al* (2014), where they attributed the increases to reorganisation of hard domains in the PU structure [242]. However Dempsey's study immersed samples for much longer periods (36 days and 12 months) and still does not explain why differences were observed in the transverse but not circumferential directions, more testing is required to determine the mechanisms involved. Studies of the effects of physiological conditions on the mechanical properties of synthetic polymers in current literature are both sparse and dependant on the materials used: e.g. Lee *et al* found that PCL/collagen blends were significantly weaker with higher maximum elongations at break when tested immersed in PBS at 37°C than dry at RT [243]; whereas Thomas *et al* (2007) found that tensile strength was not affected by the same testing conditions for polyglyconate(Maxon®) and its blends with gelatin and elastin but tensile modulus was affected (differently for each blend) [244]. Thus, it can be concluded that effects of hydration and temperature on mechanical properties are polymer specific and should be tested to allow for effective, application-specific design.

5.2.4.4 Summary

Two distinct sacrificial fibre diameters were compared over a range of fibre fractions where thin sacrificial fibres, which exhibit electrospinning properties more closely matched to the properties of the structural fibre, were found to produce more porosity than thick sacrificial fibres, where moderate to severe delamination and bulk volume loss reduced porosity creation effectiveness. The mechanical properties of the PEO and PU composite scaffolds retained the properties of each individual material depending on the proportion (fibre fraction) of their inclusion. Post PEO removal, thin and thick sacrificial fibres were found to have equivalent, predictable reductions in strength and stiffness of the scaffolds, but laminations resulting from the inclusion and subsequent removal of thick sacrificial fibres resulted in higher maximum elongations in thick groups when compared to thin groups.

5.2.5 Fibre Fraction vs Scaffold Morphology

Scaffolds of PU co-spun with thin sacrificial fibres (PEO/EtOH) in low, medium and high porosity classifications were further evaluated before testing *in Vivo*. Low, medium and high classifications, fabricated by adjusting PEO flow rate to obtain fibre fractions of 100% (0ml/hr), 70% (1ml/hr) and 30%(6ml/hr), respectively. The observation of PEO fibre diameter being independent of flow rate (Figure 4.3 (EtOH)) worked in favour of producing scaffolds where the only variable varied by adjusting flow rate was fibre fraction. The measured values of porosity for all groups (low = 76±0.2%, medium = 83±0.5% and high = 90±1%) compared well with predicted values from the plotted linear regression (low = 75%, medium = 81% and high = 88%) indicating Equation 3.12 combined with the linear regression of fibre fraction vs porosity, as a useful tool for controlling porosity.

Average pore size was found to be significantly larger for sacrificial (medium/high) over pure PU constructs (low), however no statistically significant differences were observed between medium and high porosity scaffolds. This is a result of the distribution of pore size (depicted in the Tukey box and whisker plot of Figure 4.25c) which is severely positively skewed with the majority of small pores overwhelming any large pores present. However, it can be seen that high porosity scaffolds have abundantly more "outliers" or large pores than other groups, and while the average pore size stated is in fact the average; it is the large "outliers" that will dominate functional differences between scaffold groups, as they will provide the void-space for cellular infiltration and vascularisation. A computational study with electrospun, sacrificial fibres by Baker *et al* (2008) showed that only at very low fibre fractions (±10%) does the average pore-size start to shift towards a normal-shaped distribution, with large average pore sizes [212].

PU fibre diameter and alignment were shown to be unaffected by the sacrificial fibre inclusion and removal process (Figure 4.25a and Figure 4.25b) which was in accordance with similar studies in literature [212, 213].

NanoCT scans (Figure 4.26) of the low and high porosity scaffolds depicts the 3D density differences between the two. One must be cautious when drawing inferences from the single sample size scanned, but it can be seen that the software found similar results to those measured by SEM in terms of fibre diameter and anisotropy. However, the porosity and pore size results differed quite drastically for high porosity samples and could be due to a number of factors. For instance, the high porosity samples are very sensitive to handling and may have been compressed slightly when mounting for analysis, the scan section is also a very small portion ($1mm^3$) of the total scaffold size; thus more samples are required to be scanned before comparisons can be made between methods or groups. That being said, these scans are still of interest and show great promise for assessing the 3D morphological features of electrospun scaffolds.

5.2.5.1 Effects of Fibre Fraction on Compliance and Burst Pressure

Theoretical compliance, when calculated from the tensile testing data, was found to decrease linearly with increasing fibre fractions as expected when considering the associated increases in fibre density. Similarly, for the same reason, burst pressure was expected to increase linearly with increasing fibre fractions, as was observed. This is the first study that addresses compliance and burst pressure with scaffolds fabricated with sacrificial fibres for controllable porosity and as a result it is difficult to verify these findings. However, while care has been taken to not oversimplify the assumptions in the calculations (by using thick walled cylinder theory instead of thin walled), it is expected that cylindrical constructs tested specifically for these properties will exhibit greater compliance and lower burst pressure, due to un-modelled compression of the cylinder wall under radial stress. That being said, the results calculated are useful for designing the next set of experiments.

5.3 Heparin Surface Modification

PU scaffolds of various fibre fractions were successfully (covalently) grafted with heparin and quantified for heparin content and for its effect on the mechanical properties of the electrospun scaffold over a wide range of fibre fractions. Heparin content was found to be constant over the range of fibre fractions when normalised to scaffold mass, which, with constant average fibre diameter across fibre fractions (shown in Figure 4.25a), indicates

that heparin content is dependant on the available PU surface area, where low fibre fraction scaffolds have a lower total surface area than high fibre fraction scaffolds due to lower fibre density. The normalised heparin content calculated in this study (7.5±0.7 mg/g) is 10× less than values obtained by Steffens *et al* (2004) of 68±3µg/mg for heparin surface modified collagen matrices, however, their scaffolds had far greater surface-to-volume ratios due to the smaller diameter of collagen fibres [245].

Whether the concentration of surface immobilized heparin is sufficient to make a physiologically significant difference in blood clotting time and how long it will remain active requires more research. A similar study by Ye *et al* (2011), where they immobilized heparin on electrospun PCL fibrous scaffolds, had a concentration of 39.8µg/cm^2 (note the difference in units to those used in this study) [246]. They were able to show that this resulted in a significant increase in clotting time (in an activated thromboplastin time assay) with PCL controls clotting at 51.8±0.7s and PCL-Hep samples clotting at >300s. A separate study by Begovac *et al* (2003) monitored the heparin activity of Gore-tex® grafts with Carmeda® bioactive surface heparin immobilization and found that heparin activity did not reduce significantly over 12 weeks of *in vivo* implant (canine model, n=15) [94]. These questions require more in-depth investigation going forward.

The "cobblestone" appearance of the heparinized fibres when viewed under SEM was expected due to the stringent dehydration requirements for SEM visualisation, causing the heparin hydrogel layer to dimple. Figure 4.25a shows that the modification causes an average increase in diameter of 1.8µm (0.9µm thick) which correlates well with the previous study in this group which observed the surface modification thickness to be approximately 2µm (viewed hydrated, in its swollen form, under environmental SEM) [15]. However, the thickness of the heparin layer was not significant on the structural scales of the foamed PU scaffolds but resulted in doubling the fibre diameter of these electrospun PU fibres. Pore-size and porosity were not affected by the heparin surface modification (Figure 4.25c), again correlating with previous studies; however, the process of heparinization was found to severely affect fibre alignment, with reduced anisotropy resulting from wave-like fibrous morphologies (Figure 4.24). The reduced anisotropy is believed to be due to the heparinization process, which involved vigorous mixing in monomer solutions, causing the elastic PU fibres to deform under the hydrodynamic stresses.

In terms of mechanical properties, the heparinization process was observed to initially stiffen (higher Young's modulus) but eventually weaken (lower UTS) the PU scaffolds when pulled until failure under tensile loading. This observation was made in the transverse as well as the circumferential orientation, indicating that the process of heparinization caused the weakening of the fibres or more likely the weakening of the bonds between fibres. The increase in Young's modulus is suspected to be due to the hydrogel layer serv-

ing to thicken the fibre diameter, creating a larger surface area on average. The reduction in maximum elongation is also suspected to be due to weakening of the PU structure due to the various monomer solutions and high energy mixing in the heparinization process.

When this tensile testing data is transformed into compliance and burst pressure, the results show that the reductions in strength and increases in stiffness give heparinized constructs inferior burst pressure and compliance values, respectively, when compared to their PU counter-parts. However, when compared to the compliance of the popliteal artery (healthy patients 70 years old [102]) 60% fibre fraction, heparinized scaffolds are suitably matched for compliance while retaining sufficient burst pressure to meet the scientific standard of 2000mmHg [127, 238, 239].

5.4 *In Vivo* Subcutaneous Study

Porosity was shown to be a pivotal variable, strongly correlating with increased tissue ingrowth, vascularisation and collagen deposition. The most prominent result was that high porosity scaffolds allowed full ingrowth by day 14 compared with low porosity scaffolds where ingrowth barely penetrated the surface of the scaffold by day 28. This result agrees with previous studies in literature suggesting that cells require sufficiently sized pores to penetrate and populate the scaffold interior (*in vivo*: [67, 213, 215, 247] and *in vitro*: [71, 207, 216, 219]).

Heparin modified groups showed no significant differences in tissue ingrowth, collagen deposition, vascularisation or inflammation when compared to their unmodified counterparts. This result diverges from previous results in this group where heparin modified, porous, foamed PU scaffolds showed significantly more vascularisation *in Vivo* than non-heparinized versions [15]. However, the analysis of vascularisation in this study was confounded by the similarity in morphological features and low colour-contrast between CD31 stained microvessels and unstained PU fibres, causing a large degree of variation, reducing experimental power.

Expected wound healing response (i.e. recruitment of tissue macrophage cells, neovascularisation, collagen deposition, presence of foreign body giant cells and development of a fibrous capsule) was observed to progress with time at similar rates between porosity groups; but with different intensities, where high porosity scaffolds produced more vascularisation and collagen deposition at day 7 than low porosity groups by day 28. A similar observation was made by Bergmeister *et al* (2013) where high porosity PU scaffolds, facilitated by larger fibre diameters, showed increased collagen deposition when compared to low porosity scaffolds [67]. This increase in collagen deposition is suspected to be caused by the larger surface area exposed to host tissue as a result of the increased space

for cellular infiltration [248, 249]. Thus a collagen capsule for low porosity scaffolds will envelop the outer surfaces of the scaffold as a whole, while for high porosity scaffolds the capsule is required to surround each individual fibre, leading to the observed increases in collagen density. The increase in vascularisation observed with increased porosity is believed to be due to the increased space for vessel ingrowth, where the tightly packed fibres of low porosity scaffolds obstructed infiltration.

Another important observation was the apparent thickening of the high porosity scaffolds, where all other groups seemed to have been compacted by surrounding tissue (Figure 4.30). In high porosity groups fibres are packed less densely than other groups (with longer distances between inter-fibre connections) allowing cells to move individual, elastic PU fibres to make room for their own migration, proliferation and tissue deposition. This mechanism is suggested to be the cause of many similar observations where cellular infiltration has occurred in scaffolds with average pore-sizes known to be too small for penetration into more rigid scaffold types (foamed scaffolds) [67, 248, 250]. Thus, the initially observed compression of the scaffold is reversed into swelling as host cells infiltrate the loosely packed fibrous structure and begin to proliferate and form tissue.

Chapter 6

Conclusions

Cellular ingrowth was observed to be directly correlated to pore-size and porosity, which could be increased through the inclusion and removal of sacrificial fibres. The method presented in this study allows for porosity to be controlled by varying the fibre fraction of the sacrificial fibre through control of the sacrificial solution flow rate; furthermore, the compliance of cylindrical conduits are predicted to increase with porosity but must be balanced with associated decreases in burst pressure.

Different electric field configurations for the application of small diameter vascular grafts were explored, but like-charged spinnerets with the aid of electrostatic shields and an oppositely charged collector to help guide inter-deposition of the two fibres was the only viable option.

Scaffolds that included thin (PEO/EtOH) and thick (PEO/DCM) sacrificial fibres were compared and, counter-intuitively, it was found that thin fibres produced larger increases in porosity, believed to be due to mismatches in electrospinning solution properties between PEO/DCM and PU/THF:DCM (the latter of which produced laminations rather than interconnected pores).

Heparin was successfully grafted to the surface of the PU fibres and was found to have no negative impact on porosity or pore size but effectively doubled the fibre diameter and reduced local fibre alignment. When implanted *in vivo*, equivalent ingrowth, vascularisation and inflammatory response was observed between heparinized and non-heparinized groups.

Interestingly, it was observed that cells were able to deform the loosely packed, high porosity scaffolds to make space for their own infiltration, proliferation and ECM deposition, a characteristic that helps to explain why ingrowth is observed in fibrillar scaffolds where pore sizes are much smaller than those required of more rigid phase-inversion/porogen extraction type scaffolds.

Chapter 7

Recommendations

This work focussed on tailoring the dual electrospinning with sacrificial fibres technique for small diameter graft applications, where incorporation of Pellethane as the structural fibre was used for its model polyurethane properties. However, as with any study there are many recommendations for similar studies looking to take this work further:

- Utilization of degradable elastomers (e.g. Degrapol ®) to allow for tissue remodelling *in Vivo*. However, care should be taken during the extraction process to prevent hydrolytic degradation of the structural fibre.
- Utilization of a sacrificial fibre with biocompatible break-down products. This will allow for implantation of the scaffold as spun without the need for prior removal of the sacrificial fibre. Thus drugs could be loaded into the sacrificial fibre allowing for burst/sustained release over the degradation time of the polymer.
- Charging the sacrificial solution with high voltage alternating current (AC). While potentially dangerous, it has been shown that AC electrospinning produces neutrally charged fibrous jets, which offers a potential solution to the repulsion like-charged jets exhibited in this study [131]. However, the same study has also shown that AC electrospinning produces jets without whipping instabilities; the findings in this study indicate that this will impede inter-dispersion of the structural and sacrificial fibre thereby reducing porosity gains.
- Improving the manufacturable graft length. The current study was limited in the conduit lengths it could produce, this could be improved in further studies by extending the translation distance. Productivity could be improved by fitting multiple spinnerets of each type on each side, however, the repulsive forces between fibres will need to be accounted for in the electric field design.

- Quantification of the anti-coagulation properties of the heparinized conduits in an *in vitro* model. While scaffold heparin content was quantified in this study, the effects of the bound layer on blood clotting time were not. This would be a useful study to perform before proceeding to a circulatory model.

- Implantation of low, medium and high porosity grafts in a circulatory model. This thesis has shown that high porosity scaffolds allow for rapid tissue ingrowth and vascularisation whereas low porosity scaffolds prevented cellular penetration into the inner networks of its fibrous mesh. The logical next step is to determine whether the increased porosity will allow for transmural endothelialisation (which has been shown previously by our group in foamed PU scaffolds [16]). Figure 7.1 depicts the tool-set developed in this study which can be used to roughly predict the resultant porosity, compliance and burst pressure values of an electrospun graft with a given fibre fraction (manufactured by the method presented in this text). Note that some parameters may need to be adjusted for the smaller diameter collector, e.g. higher collector rotational speed in order to maintain surface velocity to achieve the same degree of fibre alignment.

- The effect of the heparin surface modification in high porosity grafts on transmural bleeding upon implantation needs to be investigated further. We have had some experience with heparinized high porosity foamed PU grafts in a rat aortic model and found that pre-clotting *in situ* managed to prevent bleeding but if necessary the injection of degradable hydrogels into the scaffold wall could be investigated as a method to prevent early bleeding.

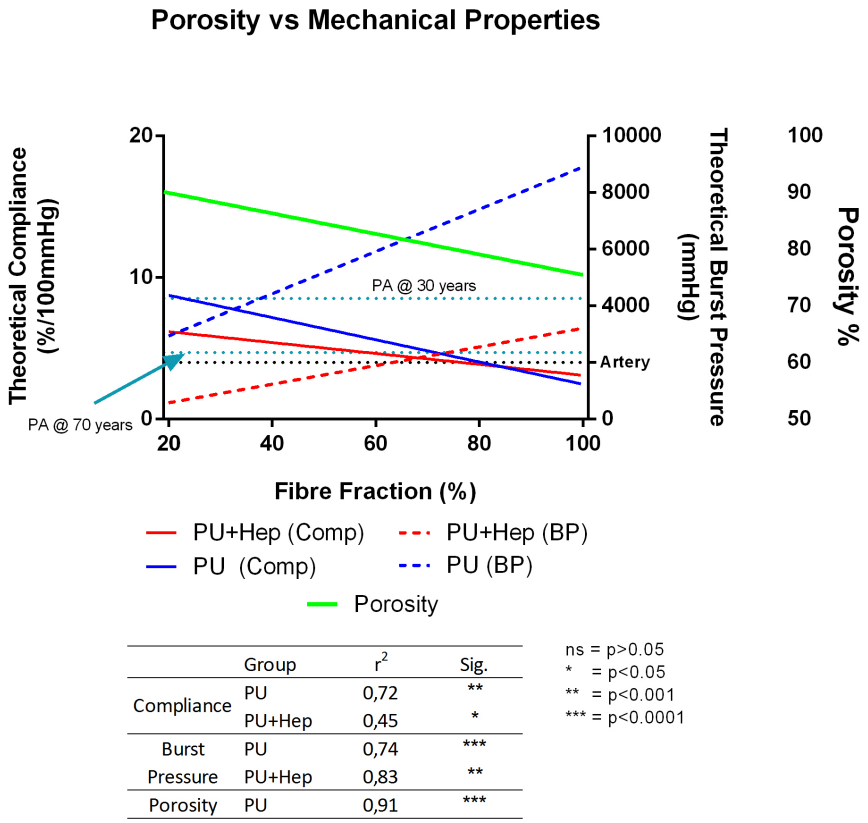

	Group	r^2	Sig.
Compliance	PU	0,72	**
	PU+Hep	0,45	*
Burst Pressure	PU	0,74	***
	PU+Hep	0,83	**
Porosity	PU	0,91	***

ns = p>0.05
* = p<0.05
** = p<0.001
*** = p<0.0001

Figure 7.1: Porosity and mechanical properties can be optimized by varying the fibre fraction of electrospun constructs. By varying the fibre fraction (through control of PEO solution flow rate), the porosity and compliance of the resulting conduit can be predicted. PA 30 and PA 70 are compliance values of the human popliteal artery measured in patients at ages of 29±4 and 69±10 years of age, respectively [102]. *Artery* refers to the minimum burst pressure of 2000mmHg commonly sought in literature, however this value should be used with discretion [127, 238, 239].

References

[1] Lloyd-Jones D, Adams R J, Brown T M, Carnethon M, Dai S *et al.* (2010). Heart disease and stroke statistics–2010 update: a report from the American Heart Association. *Circulation*, 121(7):46–215

[2] Chlupác J, Filová E, and Bacáková L (2009). Blood vessel replacement: 50 years of development and tissue engineering paradigms in vascular surgery. *Physiological research Academia Scientiarum Bohemoslovaca*, 58 Suppl 2(Ricotta 2005):S119–139

[3] Zilla P, Bezuidenhout D, and Human P (2007). Prosthetic vascular grafts: wrong models, wrong questions and no healing. *Biomaterials*, 28(34):5009–27

[4] Aronow W S (2005). Management of peripheral arterial disease. *Cardiology in review*, 13(2):61–8

[5] Bezuidenhout D and Zilla P (2004). Vascular Grafts. In G E Wnek and G L Bowlin, eds., *Encyclopedia of Biomaterials and Biomedical Engineering*. Marcel Dekker, pp. 1715–1725

[6] Popovic J R (2001). 1999 National Hospital Discharge Survey: annual summary with detailed diagnosis and procedure data. *Vital and health statistics Series*, 13(151):1–206

[7] Go A S, Mozaffarian D, Roger V L, Benjamin E J, Berry J D *et al.* (2013). Heart disease and stroke statistics–2013 update: a report from the American Heart Association. *Circulation*, 127(1):e6–e245

[8] Norman P E, Eikelboom J W, and Hankey G J (2004). Peripheral arterial disease: prognostic significance and prevention of atherothrombotic complications. *The Medical journal of Australia*, 181(3):150–4

[9] Hiatt W R (2001). Medical treatment of peripheral arterial disease and claudication. *The New England journal of medicine*, 344(21):1608–21

[10] Newman A B, Shemanski L, Manolio T a, Cushman M, Mittelmark M *et al.* (1999). Ankle-Arm Index as a Predictor of Cardiovascular Disease and Mortality in the Cardiovascular Health Study. *Arteriosclerosis, Thrombosis, and Vascular Biology*, 19(3):538–545

[11] Paul A, Mash B, and Rupesinghe G (2007). Peripheral arterial diseasehigh prevalence in rural black South Africans. *South African Medical Journal*, 97(4)

[12] Steyn K and Fourie J M (2007). HEART DISEASE IN SOUTH AFRICA. Technical Report July, Medical Research Council, Cape Town

[13] Rooke T W, Hirsch A T, Misra S, Sidawy A N, Beckman J a *et al.* (2011). 2011 ACCF/AHA Focused Update of the Guideline for the Management of Patients With Peripheral Artery Disease (updating the 2005 guideline): a report of the American College of Cardiology Foundation/American Heart Association Task Force on Practice Guidelin. *Journal of the American College of Cardiology*, 58(19):2020–45

[14] Allaire M, Clowes M, and Alexander W (1997). Endothelial cell injury in cardiovascular surgery: the intimal hyperplastic response. *The Annals of thoracic surgery*

[15] Bezuidenhout D, Davies N, Black M, Schmidt C, Oosthuysen A *et al.* (2010). Covalent surface heparinization potentiates porous polyurethane scaffold vascularization. *Journal of biomaterials applications*, 24(5):401–18

[16] Pennel T, Zilla P, and Bezuidenhout D (2013). Differentiating transmural from transanastomotic prosthetic graft endothelialization through an isolation loop-graft model. *Journal of vascular surgery*:1–9

[17] Nieponice A, Soletti L, Guan J, Hong Y, Gharaibeh B *et al.* (2010). In vivo assessment of a tissue-engineered vascular graft combining a biodegradable elastomeric scaffold and muscle-derived stem cells in a rat model. *Tissue Engineering: Part A*, 16(4):1215–23

[18] Trainor N, Pietak A, and Smith T (2014). Rethinking clinical delivery of adult stem cell therapies. *Nature biotechnology*, 32(8):729–35

[19] Wu W, Allen R a, and Wang Y (2012). Fast-degrading elastomer enables rapid remodeling of a cell-free synthetic graft into a neoartery. *Nature medicine*, 18(7):1148–53

[20] Allen R a, Wu W, Yao M, Dutta D, Duan X *et al.* (2014). Nerve regeneration and elastin formation within poly(glycerol sebacate)-based synthetic arterial grafts one-year post-implantation in a rat model. *Biomaterials*, 35(1):165–73

[21] Bezuidenhout D, Davies N, and Zilla P (2002). Effect of well defined dodecahedral porosity on inflammation and angiogenesis. *ASAIO journal*:465–471

[22] Wells M Y, Voute H, Bellingard V, Fisch C, Boulifard V *et al.* (2010). Histomorphology and vascular lesions in dorsal rat skin used as injection sites for a subcutaneous toxicity study. *Toxicologic pathology*, 38(2):258–66

[23] Friedman S (2008). *A history of vascular surgery.* Wiley-Blackwell, 2 edition

[24] Jr A V (1952). The use of tubes constructed from vinyon N cloth in bridging arterial defects: a preliminary report. *Annals of surgery*

[25] Blakemore A and Jr A V (1954). The use of tubes constructed from vinyon N cloth in bridging arterial defectsexperimental and clinical. *Annals of Surgery*

[26] Chlupác J, Filová E, and Bacáková L (2010). Vascular prostheses: 50 years of advancement from synthetic towards tissue engineering and cell therapy. *Rozhledy v chirurgii mesicnik Ceskoslovenske chirurgicke spolecnosti*, 89(1):85–94

[27] Vindigni V, Abatangelo G, and Bassetto F (2011). New Developments in Tissue Engineering of Microvascular Prostheses. In R Pignatello, ed., *Biomaterials Science and Engineering*, chapter 21. InTech

[28] Beijk M and Harskamp R (2013). Treatment of Coronary Artery Bypass Graft Failure. In W S Aronow, ed., *Artery Bypass*, chapter 13. InTech

[29] Sellke F, del Nido P J, and Swanson S J (2009). *Sabiston and Spencer's Surgery of the Chest: Expert Consult.* Elsevier Health Sciences

[30] Kachlik D, Baca V, and Stingl J (2007). Architectonic arrangement of the vasa vasorum of the human great saphenous vein. *Journal of vascular research*

[31] Fulton G J, Davies M G, and Hagen P O (1997). Preservation of the endothelium in venous bypass grafts: Relevance for graft patency gregory

[32] Osgood M J, Hocking K M, Voskresensky I V, Li F D, Komalavilas P *et al.* (2014). Surgical vein graft preparation promotes cellular dysfunction, oxidative stress, and intimal hyperplasia in human saphenous vein. In *Journal of Vascular Surgery*, volume 60. pp. 202–211

[33] Sarjeant J and Rabinovitch M (2002). Understanding and treating vein graft atherosclerosis. *Cardiovascular Pathology*

[34] Teebken O E and Haverich A (2002). Tissue Engineering of Small Diameter Vascular Grafts. *European Journal of Vascular and Endovascular Surgery*, 23(6):475–485

[35] Moore A M (1967). Tanned collagen arterial prosthesis of bovine carotid origin in man. *Plastic and Reconstructive Surgery*, 39(3):323

[36] Rosenberg N, Martinez A, Sawyer P N, Wesolowski S A, Postlethwait R W *et al.* (1966). Tanned collagen arterial prosthesis of bovine carotid origin in man. Preliminary studies of enzyme-treated heterografts. *Annals of surgery*, 164(2):247–256

[37] Schmidt C E and Baier J M (2000). Acellular vascular tissues: natural biomaterials for tissue repair and tissue engineering. *Biomaterials*, 21(22):2215–2231

[38] Conklin B, Richter E, Kreutziger K, Zhong D S, and Chen C (2002). Development and evaluation of a novel decellularized vascular xenograft. *Medical Engineering & Physics*, 24(3):173–183

[39] Teebken O E, Bader A, Steinhoff G, and Haverich A (2000). Tissue engineering of vascular grafts: human cell seeding of decellularised porcine matrix. *European Journal of Vascular and Endovascular Surgery*, 19(4):381–6

[40] Zhang W J, Liu W, Cui L, and Cao Y (2007). Tissue engineering of blood vessel. *Journal of cellular and molecular medicine*, 11(5):945–57

[41] Prevel C D, Eppley B L, McCarty M, Jackson J R, Voytik S L *et al.* (1994). Experimental evaluation of small intestinal submucosa as a microvascular graft material. *Microsurgery*, 15(8):586–591

[42] Nugent H M and Edelman E R (2003). Tissue engineering therapy for cardiovascular disease. *Circulation research*, 92(10):1068–78

[43] Wang X, Lin P, Yao Q, and Chen C (2007). Development of small-diameter vascular grafts. *World journal of surgery*, 31(4):682–9

[44] Sladen J, Gllmour J, and Wong R (1986). Cumulative patency and actual palliation in patients with claudication after aortofemoral bypass: prospective long-term follow-up of 100 patients. *The American journal of surgery*

[45] Takagi H, Goto S N, Matsui M, Manabe H, and Umemoto T (2010). A contemporary meta-analysis of Dacron versus polytetrafluoroethylene grafts for femoropopliteal bypass grafting. *Journal of vascular surgery*, 52(1):232–6

[46] Wang X, Lin P, Yao Q, and Chen C (2007). Development of small-diameter vascular grafts. *World journal of surgery*, 31(4):682–9

[47] Salzmann D and Kleinert L (1999). Inflammation and neovascularization associated with clinically used vascular prosthetic materials. *Cardiovascular Pathology*, 8(2):63–71

[48] Roll S, Müller-Nordhorn J, Keil T, Scholz H, Eidt D *et al.* (2008). Dacron vs. PTFE as bypass materials in peripheral vascular surgery–systematic review and meta-analysis. *BMC surgery*, 8(1):22

[49] Bos G and Poot A (1998). *Small-diameter vascular graft prostheses: current status.* Ph.D. thesis, University of Twente, Enschede, The Netherlands

[50] Abbott W M, Green R M, Matsumoto T, Wheeler J R, Miller N *et al.* (1997). Prosthetic above-knee femoropopliteal bypass grafting: Results of a multicenter randomized prospective trial. *Journal of Vascular Surgery*, 25(1):19–28

[51] Abbott W M (1997). Prosthetic above-knee femoral-popliteal bypass: indications and choice of graft. *Seminars in vascular surgery*, 10(1):3–7

[52] Pevec W C, Darling R, L'Italien G I, and Abbott W M (1992). Femoropopliteal reconstruction with knitted, nonvelour Dacron versus expanded polytetrafluoroethylene. *Journal of Vascular Surgery*, 16(1):60–65

[53] Xue L and Greisler H P (2003). Biomaterials in the development and future of vascular grafts. *Journal of vascular surgery*, 37(2):472–80

[54] Milleret V, Hefti T, Hall H, Vogel V, and Eberli D (2012). Influence of fiber diameter and surface roughness of electrospun vascular grafts on blood activation. *Acta Biomaterialia*, 8:4349–4356

[55] Heath D E and Cooper S L (2013). A. Polyurethanes. In B D Ratner, A S Hoffman, F J Schoen, and J E Lemons, eds., *Biomaterials Science*, chapter 1.2. Elsevier, 3 edition, pp. 79–82

[56] Kannan R Y, Salacinski H J, Butler P E, Hamilton G, and Seifalian A M (2005). Current status of prosthetic bypass grafts: a review. *Journal of biomedical materials research Part B, Applied biomaterials*, 74(1):570–81

[57] Tatai L, Moore T G, Adhikari R, Malherbe F, Jayasekara R *et al.* (2007). Thermoplastic biodegradable polyurethanes: the effect of chain extender structure on properties and in-vitro degradation. *Biomaterials*, 28(36):5407–17

[58] Seifalian A, Salacinski H, and Tiwari A (2003). In vivo biostability of a poly (carbonate-urea) urethane graft. *Biomaterials*

[59] Tiwari A, Cheng K S, Salacinski H, Hamilton G, and Seifalian A M (2003). Improving the patency of vascular bypass grafts: the role of suture materials and surgical techniques on reducing anastomotic compliance mismatch. *European journal of vascular and endovascular surgery : the official journal of the European Society for Vascular Surgery*, 25(4):287–95

[60] Hiratzka L F (1979). In Vivo Comparison of Replamineform, Silastic, and Bioelectric Polyurethane Arterial Grafts. *Archives of Surgery*, 114(6):698

[61] Zdrahala R J (1996). Small Caliber Vascular Grafts. Part II: Polyurethanes Revisited. *Journal of biomaterials applications*, 11(1):37–61

[62] Zdrahala R J (1999). Biomedical Applications of Polyurethanes: A Review of Past Promises, Present Realities, and a Vibrant Future. *Journal of biomaterials applications*, 14(1):67–90

[63] Kowligi R R, von Maltzahn W W, and Eberhart R C (1988). Fabrication and characterization of small-diameter vascular prostheses. *Journal of Biomedical Materials Research*, 22(S14):245–256

[64] Wintermantel E (1996). Tissue engineering scaffolds using superstructures. *Biomaterials*, 17(2):83–91

[65] Gupta B S and Kasyanov V A (1997). Biomechanics of human common carotid artery and design of novel hybrid textile compliant vascular grafts. *Journal of biomedical materials research*, 34(3):341–9

[66] Bergmeister H, Grasl C, Walter I, Plasenzotti R, Stoiber M *et al.* (2012). Electrospun small-diameter polyurethane vascular grafts: ingrowth and differentiation of vascular-specific host cells. *Artificial organs*, 36(1):54–61

[67] Bergmeister H, Schreiber C, Grasl C, Walter I, Plasenzotti R *et al.* (2013). Healing characteristics of electrospun polyurethane grafts with various porosities. *Acta biomaterialia*, 9(4):6032–40

[68] Grasl C, Bergmeister H, Stoiber M, Schima H, and Weigel G (2010). Electrospun polyurethane vascular grafts: in vitro mechanical behavior and endothelial adhesion molecule expression. *Journal of biomedical materials research Part A*, 93(2):716–23

[69] Stitzel J, Liu J, Lee S J, Komura M, Berry J *et al.* (2006). Controlled fabrication of a biological vascular substitute. *Biomaterials*, 27(7):1088–94

[70] Matsuda T, Ihara M, Inoguchi H, Kwon I K, Takamizawa K *et al.* (2005). Mechano-active scaffold design of small-diameter artificial graft made of electrospun segmented polyurethane fabrics. *Journal of biomedical materials research Part A*, 73(1):125–31

[71] Milleret V, Simona B, Neuenschwander P, and Hall H (2011). Tuning electrospinning parameters for production of 3D-fiber-fleeces with increased porosity for soft tissue engineering applications. *European cells & materials*, 21:286–303

[72] Leidner J, Wong E W, MacGregor D C, and Wilson G J (1983). A novel process for the manufacturing of porous grafts: process description and product evaluation. *Journal of biomedical materials research*, 17(2):229–47

[73] Wilson G J, MacGregor D C, Klement P, Lee J M, Nido P J D *et al.* (1983). Anisotropic polyurethane nonwoven conduits: a new approach to the design of a vascular prosthesis. *ASAIO journal*, 29(1):260–268

[74] Guarino V, Cirillo V, Taddei P, Alvarez-Perez M A, and Ambrosio L (2011). Tuning size scale and crystallinity of PCL electrospun fibres via solvent permittivity to address hMSC response. *Macromolecular bioscience*, 11(12):1694–705

[75] Kwon I K, Kidoaki S, and Matsuda T (2005). Electrospun nano- to microfiber fabrics made of biodegradable copolyesters: structural characteristics, mechanical properties and cell adhesion potential. *Biomaterials*, 26(18):3929–39

[76] Rnjak-Kovacina J and Weiss A (2011). Increasing the pore size of electrospun scaffolds. *Tissue Engineering Part B*, 17(5)

[77] Pennel T, Fercana G, Bezuidenhout D, Simionescu A, Chuang T H *et al.* (2014). The performance of cross-linked acellular arterial scaffolds as vascular grafts; pre-clinical testing in direct and isolation loop circulatory models. *Biomaterials*

[78] Tiwari A, Salacinski H, Seifalian A M, and Hamilton G (2002). New Prostheses for Use in Bypass Grafts with Special Emphasis on Polyurethanes. *Vascular*, 10(3):191–197

[79] Eberhart A, Zhang Z, Guidoin R, Laroche G, Guay L *et al.* (1999). A new generation of polyurethane vascular prostheses: rara avis or ignis fatuus? *Journal of biomedical materials research*, 48(4):546–58

[80] Zhang Z, Marois Y, Guidoin R, Bull P, Marois M *et al.* (1997). Vascugraft polyurethane arterial prosthesis as femoro-popliteal and femoro-peroneal bypasses in humans: pathological, structural and chemical analyses of four excised grafts. *Biomaterials*, 18(2):113–124

[81] Mathur A B, Collier T O, Kao W J, Wiggins M, Schubert M a *et al.* (1997). In vivo biocompatibility and biostability of modified polyurethanes. *Journal of biomedical materials research*, 36(2):246–57

[82] Tanzi M C, Mantovani D, Petrini P, Guidoin R, and Laroche G (1997). Chemical stability of polyether urethanes versus polycarbonate urethanes. *Journal of biomedical materials research*, 36(4):550–9

[83] Akiyama N, Esato K, Fujioka K, and Zempo N (1997). A comparison of CORVITA and expanded polytetrafluoroethylene vascular grafts implanted in the abdominal aortas of dogs. *Surgery Today*, 27(9):840–845

[84] Georg Y, Settembre N, Marchand C, Lejay A, Thaveau F *et al.* (2014). Poor long-term stability of the Corvita abdominal stentgraft. *European Journal of Vascular and Endovascular Surgery*, 47(2):160–163

[85] Xie X, Eberhart A, Guidoin R, Marois Y, Douville Y *et al.* (2010). Five types of polyurethane vascular grafts in dogs: the importance of structural design and material selection. *Journal of biomaterials science Polymer edition*, 21(8-9):1239–1264

[86] De Mel A, Punshon G, Ramesh B, Sarkar S, Darbyshire A *et al.* (2009). In situ endothelialisation potential of a biofunctionalised nanocomposite biomaterial-based small diameter bypass graft. *Bio-Medical Materials and Engineering*, 19(4-5):317–331

[87] Sarkar S, Burriesci G, Wojcik A, Aresti N, Hamilton G *et al.* (2009). Manufacture of small calibre quadruple lamina vascular bypass grafts using a novel automated extrusion-phase-inversion method and nanocomposite polymer. *Journal of Biomechanics*, 42(6):722–730

[88] Pathak Y, Shoen F J, and Levy R J (1996). Pathologic calcification of biomaterials. In B Ratner, ed., *Biomaterials Science, an Introduction to Materials in Medicine*. pp. 272–282

[89] Park J C, Song M J, Hwang Y S, and Suh H (2001). Calcification comparison of polymers for vascular graft. *Yonsei Medical Journal*, 42(3):304–310

[90] de Valence S, Tille J C, Mugnai D, Mrowczynski W, Gurny R *et al.* (2012). Long term performance of polycaprolactone vascular grafts in a rat abdominal aorta replacement model. *Biomaterials*, 33(1):38–47

[91] Kapadia M R, Popowich D a, and Kibbe M R (2008). Modified prosthetic vascular conduits. *Circulation*, 117(14):1873–82

[92] Salacinski H J, Goldner S, Giudiceandrea A, Hamilton G, Seifalian A M *et al.* (2001). The Mechanical Behavior of Vascular Grafts: A Review. *Journal of Biomaterials Applications*, 15(3):241–278

[93] Rashid S T, Salacinski H J, Fuller B J, Hamilton G, and Seifalian A M (2004). Engineering of bypass conduits to improve patency. *Cell proliferation*, 37(5):351–66

[94] Begovac P, Thomson R, Fisher J, Hughson A, and Gällhagen A (2003). Improvements in GORE-TEX vascular graft performance by Carmeda bioactive surface heparin immobilization. *European Journal of Vascular and Endovascular Surgery*, 25(5):432–437

[95] Devine C, Hons B, and McCollum C (2001). Heparin-bonded Dacron or polytetrafluoroethylene for femoropopliteal bypass grafting: A multicenter trial. *Journal of Vascular Surgery*, 33(3):533–539

[96] Akers D L, Du Y H, and Kempczinski R F (1993). The effect of carbon coating and porosity on early patency of expanded polytetrafluoroethylene grafts: an experimental study. *Journal of vascular surgery*, 18(1):10–5

[97] Kannan R Y, Salacinski H J, Butler P E, Hamilton G, and Seifalian A M (2005). Current status of prosthetic bypass grafts: a review. *Journal of biomedical materials research Part B, Applied biomaterials*, 74(1):570–81

[98] Zilla P, Deutsch M, Meinhart J, Puschmann R, Eberl T *et al.* (1994). Clinical in vitro endothelialization of femoropopliteal bypass grafts: An actuarial follow-up over three years. *Journal of Vascular Surgery*, 19(3):540–548

[99] Deutsch M, Meinhart J, Fischlein T, Preiss P, and Zilla P (1999). Clinical autologous in vitro endothelialization of infrainguinal ePTFE grafts in 100 patients: A 9-year experience. *Surgery*, 126(5):847–855

[100] Meinhart J G, Deutsch M, Fischlein T, Howanietz N, Fröschl A *et al.* (2001). Clinical autologous in vitro endothelialization of 153 infrainguinal ePTFE grafts. *The Annals of Thoracic Surgery*, 71(5):S327–S331

[101] Kawasaki T, Sasayama S, Yagi S I, Asakawa T, and Hirai T (1987). Non-invasive assessment of the age related changes in stiffness of major branches of the human arteries. *Cardiovascular Research*, 21(9):678–687

[102] Tai N R, Giudiceandrea A, Salacinski H J, Seifalian A M, and Hamilton G (1999). In vivo femoropopliteal arterial wall compliance in subjects with and without lower limb vascular disease. *Journal of Vascular Surgery*, 30(5):936–945

[103] Seifalian A, Giudiceandrea A, and Schmitz-Rixen T (1999). Noncompliance: The Silent Acceptance of a Villain. In P Zilla and P Greisler, eds., *Tissue Engineering of Vascular Prosthetic Grafts*. R G Landes Company Publishers, pp. 43–56

[104] Trubel W, Moritz A, Schima H, Raderer F, Scherer R *et al.* (1994). Compliance and formation of distal anastomotic intimal hyperplasia in Dacron mesh tube constricted veins used as arterial bypass grafts. *ASAIO journal (American Society for Artificial Internal Organs : 1992)*, 40(3):M273–M278

[105] Ballyk P D, Walsh C, Butany J, and Ojha M (1997). Compliance mismatch may promote graft-artery intimal hyperplasia by altering suture-line stresses. *Journal of Biomechanics*, 31(3):229–237

[106] Tai N R, Salacinski H J, Edwards A, Hamilton G, and Seifalian A M (2000). Compliance properties of conduits used in vascular reconstruction. *The British journal of surgery*, 87(11):1516–24

[107] Sun Z, Zussman E, aL Yarin, Wendorff J, and Greiner a (2003). Compound CoreShell Polymer Nanofibers by Co-Electrospinning. *Advanced Materials*, 15(22):1929–1932

[108] Taylor G (1969). Electrically Driven Jets. *Proceedings of the Royal Society A: Mathematical, Physical and Engineering Sciences*, 313(1515):453–475

[109] Reneker D H and Hou H (2004). Electrospinning. In *Encyclopedia of Biomaterials and Biomedical Engineering*. Marcel Dekker, pp. 543–550

[110] Reneker D H and Yarin A L (2008). Electrospinning jets and polymer nanofibers. *Polymer*, 49:2387–2425

[111] Yarin A L (1982). Dynamics of bending disturbances of nonlinear viscous liquid jets in air. *Journal of Applied Mechanics and Technical Physics*, 23(1):39–43

[112] Yarin A L (1987). Flexural perturbations of free jets of maxwell and Doi-Edwards liquids. *Journal of Applied Mechanics and Technical Physics*, 27(6):828–836

[113] Yarin A L, Oron A, and Rosenau P (1993). Capillary instability of thin liquid film on a cylinder. *Physics of Fluids A: Fluid Dynamics*, 5(1):91–98

[114] Reneker D H, Yarin A L, Fong H, and Koombhongse S (2000). Bending instability of electrically charged liquid jets of polymer solutions in electrospinning. *Journal of Applied Physics*, 87(9):4531

[115] Yarin A (2011). Coaxial electrospinning and emulsion electrospinning of core-shell fibers. *Polymers for Advanced Technologies*, 22(3):310–317

[116] Yu D G, Williams G R, Gao L D, Bligh S A, Yang J H *et al.* (2012). Coaxial electrospinning with sodium dodecylbenzene sulfonate solution for high quality polyacrylonitrile nanofibers. *Colloids and Surfaces A: Physicochemical and Engineering Aspects*, 396:161–168

[117] Huang W, Zou T, Li S, Jing J, Xia X *et al.* (2013). Drug-loaded zein nanofibers prepared using a modified coaxial electrospinning process. *AAPS PharmSciTech*, 14(2):675–81

[118] Liu J J, Wang C Y, Wang J G, Ruan H J, and Fan C Y (2011). Peripheral nerve regeneration using composite poly(lactic acid-caprolactone)/nerve growth factor conduits prepared by coaxial electrospinning. *Journal of biomedical materials research Part A*, 96(1):13–20

[119] Ji W, Yang F, van den Beucken J J J P, Bian Z, Fan M *et al.* (2010). Fibrous scaffolds loaded with protein prepared by blend or coaxial electrospinning. *Acta biomaterialia*, 6(11):4199–207

[120] Townsend-Nicholson A and Jayasinghe S N (2006). Cell electrospinning: a unique biotechnique for encapsulating living organisms for generating active biological microthreads/scaffolds. *Biomacromolecules*, 7(12):3364–9

[121] Moghe A K and Gupta B S (2008). Coaxial Electrospinning for Nanofiber Structures: Preparation and Applications. *Polymer Reviews*, 48(2):353–377

[122] Elahi M, Lu W, Guoping G, and Khan F (2013). Core-shell Fibers for Biomedical Applications-A Review. *Journal of Bioengineering & Biomedical Science*, 3(1):1–14

[123] Liu W, Ni C, Chase D, and Rabolt J (2013). Preparation of Multilayer Biodegradable Nanofibers by Triaxial Electrospinning. *ACS Macro Letters*:466–468

[124] Han D and Steckl A (2013). Triaxial electrospun nanofiber membranes for controlled dual release of functional molecules. *ACS applied materials & interfaces*

[125] Yarin A and Zussman E (2004). Upward needleless electrospinning of multiple nanofibers. *Polymer*, 45(9):2977–2980

[126] Migliaresi C, Ruffo G A, Volpato F Z, and Zeni D (2012). Advanced Electrospinning Setups and Special Fibre and Mesh Morphologies. In Nuno M Neves, ed., *Electrospinning for Advanced Biomedical Applications and Therapies*, chapter 2. Smithers Rapra Technology, pp. 23–68

[127] Drilling S, Gaumer J, and Lannutti J (2009). Fabrication of burst pressure competent vascular grafts via electrospinning: effects of microstructure. *Journal of biomedical materials research Part A*, 88(4):923–34

[128] Vaquette C and Cooper-White J J (2011). Increasing electrospun scaffold pore size with tailored collectors for improved cell penetration. *Acta biomaterialia*, 7(6):2544–57

[129] Simonet M, Schneider O D, Neuenschwander P, and Stark W J (2007). Ultraporous 3D polymer meshes by low-temperature electrospinning: Use of ice crystals as a removable void template. *Polymer Engineering & Science*, 47(12):2020–2026

[130] Supaphol P, Mit-Uppatham C, and Nithitanakul M (2005). Ultrafine electrospun polyamide-6 fibers: Effect of emitting electrode polarity on morphology and average fiber diameter. *Journal of Polymer Science Part B: Polymer Physics*, 43(24):3699–3712

[131] Kessick R, Fenn J, and Tepper G (2004). The use of AC potentials in electrospraying and electrospinning processes. *Polymer*, 45(9):2981–2984

[132] Soliman S, Sant S, Nichol J W, Khabiry M, Traversa E *et al.* (2011). Controlling the porosity of fibrous scaffolds by modulating the fiber diameter and packing density. *Journal of biomedical materials research Part A*, 96(3):566–74

[133] Nezarati R, Eifert M, and Cosgriff-Hernandez E (2013). Effects of Humidity and Solution Viscosity on Electrospun Fiber Morphology. *Tissue Engineering: Part C*, 19(10):810–819

[134] Sill T J and Von Recum H A (2008). Electrospinning : Applications in drug delivery and tissue engineering. *Biomaterials*, 29:1989–2006

[135] Rayleigh L (1882). On the equilibrium of liquid conducting masses charged with electricity. *Philosophical Magazine Series 5*, 14(87):184–186

[136] Zeleny J (1917). Instability of Electrified Liquid Surfaces. *Physical Review*, 10(1):1–6

[137] Taylor G (1964). Disintegration of Water Drops in an Electric Field. *Proceedings of the Royal Society A: Mathematical, Physical and Engineering Sciences*, 280(1382):383–397

[138] Formhals A (1934). Process and apparatus for preparing artificial threads

[139] Martin G E and Cockshott I D (1977). Fibrillar product of electrostatically spun organic material

[140] How T V (1985). Synthetic vascular grafts, and methods of manufacturing such grafts

[141] Bornat A (1982). Electrostatic spinning of tubular products

[142] Doshi J and Reneker D H (1995). Electrospinning process and applications of electrospun fibers. *Journal of Electrostatics*, 35(2-3):151–160

[143] Huang L, McMillan R A, Apkarian R P, Pourdeyhimi B, Conticello V P *et al.* (2000). Generation of Synthetic Elastin-Mimetic Small Diameter Fibers and Fiber Networks. *Macromolecules*, 33(8):2989–2997

[144] Stitzel J D, Pawlowski K J, Bowlin G L, Wnek G E, and Simpson D G (2001). Arterial Smooth Muscle Cell Proliferation on a Novel Biomimicking, Biodegradable Vascular Graft Scaffold. *Journal of Biomaterials Applications*, 16(1):22–33

[145] Boland E, Wnek G, Simpson D, Pawlowski K, and Bowlin G (2001). Tailoring Tissue Eengineering Scaffolds Using Eelectrostatic Processing Techniques: A Study of Poly(Glycolic acid) Electrospinning. *Journal of Macromolecular Science, Part A*, 38(12):1231–1243

[146] Anka F and Jr K B (2013). Novel Nanofiltration Hollow Fiber Membrane Produced via Electrospinning. *Industrial & Engineering Chemistry ...*

[147] Liu W, Thomopoulos S, and Xia Y (2012). Electrospun nanofibers for regenerative medicine. *Advanced healthcare materials*, 1(1):10–25

[148] Pham Q P, Sharma U, and Mikos A G (2006). Electrospinning of Polymeric Nanofibers for Tissue Engineering Applications : A Review. *TISSUE ENGINEERING*, 12(5):1197–211

[149] Bhardwaj N and Kundu S C (2010). Electrospinning: a fascinating fiber fabrication technique. *Biotechnology advances*, 28(3):325–47

[150] Hasan A, Memic A, Annabi N, Hossain M, Paul A *et al.* (2014). Electrospun scaffolds for tissue engineering of vascular grafts. *Acta Biomaterialia*, 10(1):11–25

[151] Karchin A, Simonovsky F I, Ratner B D, and Sanders J E (2011). Melt electrospinning of biodegradable polyurethane scaffolds. *Acta biomaterialia*, 7(9):3277–84

[152] Matthews J A, Wnek G E, Simpson D G, and Bowlin G L (2002). Electrospinning of Collagen Nanofibers. *Biomacromolecules*, 3(2):232–238

[153] Wise S G, Byrom M J, Waterhouse A, Bannon P G, Weiss A S *et al.* (2011). A multilayered synthetic human elastin/polycaprolactone hybrid vascular graft with tailored mechanical properties. *Acta biomaterialia*, 7(1):295–303

[154] Browning M B, Dempsey D, Guiza V, Becerra S, Rivera J *et al.* (2012). Multilayer vascular grafts based on collagen-mimetic proteins. *Acta biomaterialia*, 8(3):1010–21

[155] Simpson D G and Bowlin G L (2006). Tissue-engineering scaffolds: can we re-engineer mother nature? *Expert review of medical devices*, 3(1):9–15

[156] Chew S Y, Park T G, Sell S A, McClure M J, Garg K *et al.* (2009). Electrospinning of collagen/biopolymers for regenerative medicine and cardiovascular tissue engineering. *Advanced Drug Delivery Reviews*, 61(12):1007–1019

[157] McKenna K a, Hinds M T, Sarao R C, Wu P C, Maslen C L *et al.* (2012). Mechanical property characterization of electrospun recombinant human tropoelastin for vascular graft biomaterials. *Acta biomaterialia*, 8(1):225–33

[158] Innocente F, Mandracchia D, Pektok E, Nottelet B, Tille J C *et al.* (2009). Paclitaxel-eluting biodegradable synthetic vascular prostheses: a step towards reduction of neointima formation? *Circulation*, 120(11 Suppl):S37–45

[159] Kuwabara F, Narita Y, Yamawaki-Ogata A, Kanie K, Kato R *et al.* (2012). Novel small-caliber vascular grafts with trimeric Peptide for acceleration of endothelialization. *The Annals of thoracic surgery*, 93(1):156–63; discussion 163

[160] Zheng W, Wang Z, Song L, Zhao Q, Zhang J *et al.* (2012). Endothelialization and patency of RGD-functionalized vascular grafts in a rabbit carotid artery model. *Biomaterials*, 33(10):2880–91

[161] Ye L, Wu X, Duan H Y, Geng X, Chen B *et al.* (2012). The in vitro and in vivo biocompatibility evaluation of heparin-poly(ϵ-caprolactone) conjugate for vascular tissue engineering scaffolds. *Journal of biomedical materials research Part A*, 100(12):3251–8

[162] Lu G, Cui S, Geng X, Ye L, and Chen B (2013). Design and preparation of polyurethane-collagen/heparin-conjugated polycaprolactone double-layer bionic small-diameter vascular graft and its preliminary. *Chinese medical journal*, 126(2007):1310–1316

[163] Hashi C K, Derugin N, Janairo R R R, Lee R, Schultz D *et al.* (2010). Antithrombogenic modification of small-diameter microfibrous vascular grafts. *Arteriosclerosis, thrombosis, and vascular biology*, 30(8):1621–7

[164] Soletti L, Nieponice A, Hong Y, Ye S H, Stankus J J *et al.* (2011). In vivo performance of a phospholipid-coated bioerodable elastomeric graft for small-diameter vascular applications. *Journal of biomedical materials research Part A*, 96(2):436–48

[165] Tillman B W, Yazdani S K, Lee S J, Geary R L, Atala A *et al.* (2009). The in vivo stability of electrospun polycaprolactone-collagen scaffolds in vascular reconstruction. *Biomaterials*, 30(4):583–8

[166] Zhao J, Qiu H, Chen D l, Zhang W x, Zhang D c *et al.* (2013). Development of nanofibrous scaffolds for vascular tissue engineering. *International journal of biological macromolecules*, 56:106–13

[167] Heydarkhan-Hagvall S, Schenke-Layland K, Dhanasopon A P, Rofail F, Smith H *et al.* (2008). Three-dimensional electrospun ECM-based hybrid scaffolds for cardiovascular tissue engineering. *Biomaterials*, 29(19):2907–14

[168] Wang S, Mo X M, Jiang B J, Gao C J, Wang H S *et al.* (2013). Fabrication of small-diameter vascular scaffolds by heparin-bonded P(LLA-CL) composite nanofibers to improve graft patency. *International journal of nanomedicine*, 8:2131–9

[169] de Valence S, Tille J C, Giliberto J P, Mrowczynski W, Gurny R *et al.* (2012). Advantages of bilayered vascular grafts for surgical applicability and tissue regeneration. *Acta biomaterialia*, 8(11):3914–20

[170] Pektok E, Nottelet B, Tille J C, Gurny R, Kalangos A *et al.* (2008). Degradation and healing characteristics of small-diameter poly(epsilon-caprolactone) vascular grafts in the rat systemic arterial circulation. *Circulation*, 118(24):2563–70

[171] Rocco K a, Maxfield M W, Best C a, Dean E W, and Breuer C K (2014). In vivo applications of electrospun tissue-engineered vascular grafts: a review. *Tissue engineering Part B, Reviews*, 20(6):628–40

[172] Nottelet B, Pektok E, Mandracchia D, Tille J C, Walpoth B *et al.* (2009). Factorial design optimization and in vivo feasibility of poly(epsilon-caprolactone)-micro- and nanofiber-based small diameter vascular grafts. *Journal of biomedical materials research Part A*, 89(4):865–75

[173] Hashi C K, Zhu Y, Yang G Y, Young W L, Hsiao B S *et al.* (2007). Antithrombogenic property of bone marrow mesenchymal stem cells in nanofibrous vascular grafts. *Proceedings of the National Academy of Sciences of the United States of America*, 104(29):11915–11920

[174] He W, Ma Z, Teo W E, Dong Y X, Robless P A *et al.* (2009). Tubular nanofiber scaffolds for tissue engineered small-diameter vascular grafts. *Journal of biomedical materials research Part A*, 90(1):205–16

[175] Zhai W, Qiu L J, Mo X M, Wang S, Xu Y F *et al.* (2013). Coaxial electrospinning of P(LLA-CL)/heparin biodegradable polymer nanofibers: potential vascular graft for substitution of femoral artery. *Journal of biomedical materials research Part B, Applied biomaterials*:1–8

[176] Huang C, Wang S, Qiu L, Ke Q, Zhai W *et al.* (2013). Heparin loading and pre-endothelialization in enhancing the patency rate of electrospun small-diameter vascular grafts in a canine model. *ACS applied materials & interfaces*, 5(6):2220–6

[177] Hong Y, Ye S H, Nieponice A, Soletti L, Vorp D a *et al.* (2009). A small diameter, fibrous vascular conduit generated from a poly(ester urethane)urea and phospholipid polymer blend. *Biomaterials*, 30(13):2457–67

[178] Bergmeister H, Seyidova N, Schreiber C, Strobl M, Grasl C *et al.* (2015). Biodegradable, thermoplastic polyurethane grafts for small diameter vascular replacements. *Acta biomaterialia*, 11:104–13

[179] Zamani M (2013). Advances in drug delivery via electrospun and electrosprayed nanomaterials. *International journal of Nanomedicine*:2997–3017

[180] Deitzel J, Kleinmeyer J, Harris D, and Beck Tan N (2001). The effect of processing variables on the morphology of electrospun nanofibers and textiles. *Polymer*, 42(1):261–272

[181] Yarin A L, Kataphinan W, and Reneker D H (2005). Branching in electrospinning of nanofibers. *Journal of Applied Physics*, 98(6):064501

[182] Megelski S, Stephens J, Chase D, and Rabolt J (2002). Micro-and nanostructured surface morphology on electrospun polymer fibers. *Macromolecules*

[183] Wannatong L, Sirivat A, and Supaphol P (2004). Effects of solvents on electrospun polymeric fibers: preliminary study on polystyrene. *Polymer International*, 53(11):1851–1859

[184] Jaeger R and Bergshoef M (1998). Electrospinning of ultrathin polymer fibers. *Macromolecular Symposia*

[185] Gupta P, Elkins C, Long T, and Wilkes G (2005). Electrospinning of linear homopolymers of poly (methyl methacrylate): exploring relationships between fiber formation, viscosity, molecular weight and concentration. *Polymer*

[186] Gumbleton M, Barnes C P, Sell S A, Boland E D, Simpson D G *et al.* (2007). Nanofiber technology: Designing the next generation of tissue engineering scaffolds. *Advanced Drug Delivery Reviews*, 59(14):1413–1433

[187] Zeng J, Haoqing H, Schaper A, Wendorff J H, and Greiner A (2003). Poly-L-lactide nanofibers by electrospinning Influence of solution viscosity and electrical conductivity on fiber diameter and fiber morphology. *e-Polymers*, 3(1):102–110

[188] Zong X, Kim K, Fang D, Ran S, Hsiao B S *et al.* (2002). Structure and process relationship of electrospun bioabsorbable nanofiber membranes. *Polymer*, 43(16):4403–4412

[189] Son W K, Youk J H, Lee T S, and Park W H (2004). The effects of solution properties and polyelectrolyte on electrospinning of ultrafine poly(ethylene oxide) fibers. *Polymer*, 45(9):2959–2966

[190] Feng Y, Meng F, Xiao R, Zhao H, and Guo J (2010). Electrospinning of polycarbonate urethane biomaterials. *Frontiers of Chemical Science and Engineering*, 5(1):11–18

[191] Luo C, Nangrejo M, and Edirisinghe M (2010). A novel method of selecting solvents for polymer electrospinning. *Polymer*, 51(7):1654–1662

[192] H R D, Yarin A, Zussman E, Koombhongse S, and Kataphinan W (2006). Nanofiber manufacturing : Toward better process control. *ACS symposium series*, 918:7–20

[193] Baker B M and Mauck R L (2007). The Effect of Nanofiber Alignment on the Maturation of Engineered Meniscus Constructs. *Biomaterials*, 28(11):1967–1977

[194] Xu C, Inai R, Kotaki M, and Ramakrishna S (2004). Electrospun nanofiber fabrication as synthetic extracellular matrix and its potential for vascular tissue engineering. *Tissue engineering*, 10(7-8):1160–8

[195] Zhu Y, Cao Y, Pan J, and Liu Y (2010). Macro-alignment of electrospun fibers for vascular tissue engineering. *Journal of biomedical materials research Part B, Applied biomaterials*, 92(2):508–16

[196] Uttayarat P, Perets A, Li M, Pimton P, Stachelek S J *et al.* (2010). Micropatterning of three-dimensional electrospun polyurethane vascular grafts. *Acta biomaterialia*, 6(11):4229–37

[197] Xie J, Li X, Lipner J, Manning C N, Schwartz A G *et al.* (2010). "Aligned-to-random" nanofiber scaffolds for mimicking the structure of the tendon-to-bone insertion site. *Nanoscale*, 2(6):923–6

[198] Yang D, Lu B, Zhao Y, and Jiang X (2007). Fabrication of Aligned Fibrous Arrays by Magnetic Electrospinning. *Advanced Materials*, 19(21):3702–3706

[199] Fennessey S F and Farris R J (2004). Fabrication of aligned and molecularly oriented electrospun polyacrylonitrile nanofibers and the mechanical behavior of their twisted yarns. *Polymer*, 45(12):4217–4225

[200] Balguid A, Mol A, van Marion M H, Bank R A, Bouten C V *et al.* (2009). Tailoring Fiber Diameter in Electrospun Poly(-Caprolactone) Scaffolds for Optimal Cellular Infiltration in Cardiovascular Tissue Engineering. *Tissue engineering Part A*, 15(2)

[201] Lowery J L, Datta N, and Rutledge G C (2010). Effect of fiber diameter, pore size and seeding method on growth of human dermal fibroblasts in electrospun poly(epsilon-caprolactone) fibrous mats. *Biomaterials*, 31(3):491–504

[202] Milleret V, Hefti T, Hall H, Vogel V, and Eberli D (2012). Influence of the fiber diameter and surface roughness of electrospun vascular grafts on blood activation. *Acta biomaterialia*, 8(12):4349–56

[203] Ju Y M, Choi J S, Atala A, Yoo J J, and Lee S J (2010). Bilayered scaffold for engineering cellularized blood vessels. *Biomaterials*, 31(15):4313–21

[204] Pham Q P, Sharma U, and Mikos A G (2006). Electrospun poly (e-caprolactone) microfiber and multilayer nanofiber/microfiber scaffolds: Characterization of scaffolds and measurement of cellular infiltration. *Biomacromolecules*, 7(10):2796–2805

[205] Zhu X, Cui W, Li X, and Jin Y (2008). Electrospun fibrous mats with high porosity as potential scaffolds for skin tissue engineering. *Biomacromolecules*, 9:1795–1801

[206] McClure M J, Wolfe P S, Simpson D G, Sell S A, and Bowlin G L (2012). The use of air-flow impedance to control fiber deposition patterns during electrospinning. *Biomaterials*, 33(3):771–9

[207] Blakeney B a, Tambralli A, Anderson J M, Andukuri A, Lim D J *et al.* (2011). Cell infiltration and growth in a low density, uncompressed three-dimensional electrospun nanofibrous scaffold. *Biomaterials*, 32(6):1583–90

[208] Simonet M, Stingelin N, Wismans J G F, Oomens C W J, Driessen-Mol A *et al.* (2014). Tailoring the void space and mechanical properties in electrospun scaffolds towards physiological ranges. *Journal of Materials Chemistry B*, 2(3):305

[209] Gupta P and Wilkes G L (2003). Some investigations on the fiber formation by utilizing a side-by-side bicomponent electrospinning approach. *Polymer*, 44(20):6353–6359

[210] Madhugiri S and Dalton A (2003). Electrospun MEH-PPV/SBA-15 composite nanofibers using a dual syringe method. *Journal of the American Chemical Society*, 125(47):14531–8

[211] Kidoaki S, Kwon I K, and Matsuda T (2005). Mesoscopic spatial designs of nano- and microfiber meshes for tissue-engineering matrix and scaffold based on newly devised multilayering and mixing electrospinning techniques. *Biomaterials*, 26(1):37–46

[212] Baker B M, Gee A O, Metter R B, Nathan A S, Marklein R a *et al.* (2008). The potential to improve cell infiltration in composite fiber-aligned electrospun scaffolds by the selective removal of sacrificial fibers. *Biomaterials*, 29(15):2348–58

[213] Ifkovits J L, Wu K, Mauck R L, and Burdick J A (2010). The influence of fibrous elastomer structure and porosity on matrix organization. *PloS one*, 5(12):e15717

[214] Phipps M C, Clem W C, Grunda J M, Clines G A, and Bellis S L (2012). Increasing the pore sizes of bone-mimetic electrospun scaffolds comprised of polycaprolactone, collagen I and hydroxyapatite to enhance cell infiltration. *Biomaterials*, 33(2):524–34

[215] Baker B M, Shah R P, Silverstein A M, Esterhai J L, Burdick J a *et al.* (2012). Sacrificial nanofibrous composites provide instruction without impediment and enable functional tissue formation. *Proceedings of the National Academy of Sciences of the United States of America*, 109(35):14176–81

[216] Ekaputra A K, Prestwich G D, Cool S M, and Hutmacher D W (2008). Combining electrospun scaffolds with electrosprayed hydrogels leads to three-dimensional cellularization of hybrid constructs. *Biomacromolecules*, 9(8):2097–103

[217] Nam J, Huang Y, Agarwal S, and Lannutti J (2007). Improved cellular infiltration in electrospun fiber via engineered porosity. *Tissue engineering*, 13(9):2249–57

[218] Cai S, Xu H, Jiang Q, and Yang Y (2013). Novel 3D electrospun scaffolds with fibers oriented randomly and evenly in three dimensions to closely mimic the unique architectures of extracellular matrices in soft tissues: fabrication and mechanism study. *Langmuir : the ACS journal of surfaces and colloids*, 29(7):2311–8

[219] Lee J B, Jeong S I, Bae M S, Yang D H, Heo D N *et al.* (2011). Highly porous electrospun nanofibers enhanced by ultrasonication for improved cellular infiltration. *Tissue engineering Part A*, 17(21-22):2695–702

[220] Gupta B, Revagade N, and Hilborn J (2007). Poly(lactic acid) fiber: An overview. *Progress in Polymer Science*, 32(4):455–482

[221] Zhuo H, Hu J, Chen S, and Yeung L (2008). Preparation of polyurethane nanofibers by electrospinning. *Journal of Applied Polymer Science*, 109(1):406–411

[222] Lee B L P, Jeon H, Wang A, Yan Z, Yu J *et al.* (2012). Femtosecond laser ablation enhances cell infiltration into three-dimensional electrospun scaffolds. *Acta biomaterialia*, 8(7):2648–58

[223] Nedjari S, Schlatter G, and Hébraud A (2014). Thick electrospun honeycomb scaffolds with controlled pore size. *Materials Letters*, 142:180–183

[224] Yin A, Li J, Bowlin G L, Li D, Rodriguez I a *et al.* (2014). Fabrication of cell penetration enhanced poly (l-lactic acid-co--caprolactone)/silk vascular scaffolds utilizing air-impedance electrospinning. *Colloids and surfaces B, Biointerfaces*, 120:47–54

[225] Lavielle N, Hébraud A, Schlatter G, Thöny-Meyer L, Rossi R M *et al.* (2013). Simultaneous electrospinning and electrospraying: a straightforward approach for fabricating hierarchically structured composite membranes. *ACS applied materials & interfaces*, 5(20):10090–7

[226] Wang K, Xu M, Zhu M, Su H, Wang H *et al.* (2013). Creation of macropores in electrospun silk fibroin scaffolds using sacrificial PEO-microparticles to enhance cellular infiltration. *Journal of biomedical materials research Part A*, 101(12):3474–81

[227] Wang K, Zhu M, Li T, Zheng W, Xu L L *et al.* (2014). Improvement of Cell Infiltration in Electrospun Polycaprolactone Scaffolds for the Construction of Vascular Grafts. *Journal of Biomedical Nanotechnology*, 10(8):1588–1598

[228] Wang N, Burugapalli K, and Song W (2013). Tailored fibro-porous structure of electrospun polyurethane membranes, their size-dependent properties and trans-membrane glucose diffusion. *Journal of Membrane Science*:207–217

[229] Riesenfeld J and Rodén L (1990). Quantitative analysis of N-sulfated, N-acetylated, and unsubstituted glucosamine amino groups in heparin and related polysaccharides. *Analytical biochemistry*, 188(2):383–9

[230] Rezakhaniha R, Agianniotis A, Schrauwen J T C, Griffa A, Sage D *et al.* (2012). Experimental investigation of collagen waviness and orientation in the arterial adventitia using confocal laser scanning microscopy. *Biomechanics and modeling in mechanobiology*, 11(3-4):461–73

[231] Fonck E, Feigl G G, Fasel J, Sage D, Unser M *et al.* (2009). Effect of aging on elastin functionality in human cerebral arteries. *Stroke; a journal of cerebral circulation*, 40(7):2552–6

[232] Schindelin J, Arganda-Carreras I, Frise E, Kaynig V, Longair M *et al.* (2012). Fiji: an open-source platform for biological-image analysis. *Nature methods*, 9(7):676–82

[233] Sage D (2012). OrientationJ. http://bigwww.epfl.ch/demo/orientation/, [Accessed 10/12/14]

[234] Weissler A M, Harris W S, and Schoenfeld C D (1968). Systolic Time Intervals in Heart Failure in Man. *Circulation*, 37(2):149–159

[235] Jose A D and Collison D (1970). The normal range and determinants of the intrinsic heart rate in man. *Cardiovascular research*, 4(2):160–7

[236] Beckstead J H (1994). A simple technique for preservation of fixation-sensitive antigens in paraffin-embedded tissues. *Journal of Histochemistry & Cytochemistry*, 42(8):1127–1134

[237] Falstad P. Electrostatics Simulation. http://www.falstad.com/emstatic/, [Accessed: 12/12/14]

[238] L'Heureux N, Dusserre N, Konig G, Victor B, Keire P *et al.* (2006). Human tissue-engineered blood vessels for adult arterial revascularization. *Nature medicine*, 12(3):361–5

[239] Yang J, Motlagh D, R Webb A, and A Ameer G (2005). Novel biphasic elastomeric scaffold for small-diameter blood vessel tissue engineering. *Tissue engineering*, 11(11):1876–1886

[240] Bellan L M, Kameoka J, and Craighead H G (2005). Measurement of the Youngs moduli of individual polyethylene oxide and glass nanofibres. *Nanotechnology*, 16(8):1095–1099

[241] Wan-Ju L, Mauck R L, Cooper J A, Yuan X, and Tuan R S (2007). Engineering controllable anisotropy in electrospun biodegradable nanofibrous scaffolds for musculoskeletal tissue engineering. *Journal of Biomechanics*, 40(8):1686–1693

[242] Dempsey D K, Carranza C, Chawla C P, Gray P, Eoh J H *et al.* (2014). Comparative analysis of in vitro oxidative degradation of poly(carbonate urethanes) for biostability screening. *Journal of biomedical materials research Part A*, 102(10):3649–65

[243] Lee S J, Liu J, Oh S H, Soker S, Atala A *et al.* (2008). Development of a composite vascular scaffolding system that withstands physiological vascular conditions. *Biomaterials*, 29(19):2891–8

[244] Thomas V, Zhang X, Catledge S a, and Vohra Y K (2007). Functionally graded electrospun scaffolds with tunable mechanical properties for vascular tissue regeneration. *Biomedical materials (Bristol, England)*, 2(4):224–32

[245] Steffens G C M, Yao C, Prével P, Markowicz M, Schenck P *et al.* (2004). Modulation of angiogenic potential of collagen matrices by covalent incorporation of heparin and loading with vascular endothelial growth factor. *Tissue engineering*, 10(9-10):1502–9

[246] Ye L, Wu X, Mu Q, Chen B, Duan Y *et al.* (2011). Heparin-Conjugated PCL Scaffolds Fabricated by Electrospinning and Loaded with Fibroblast Growth Factor 2. *Journal of Biomaterials Science, Polymer Edition*, 22(1-3):389–406

[247] Leong M F, Chan W Y, Chian K S, Rasheed M Z, and Anderson J M (2010). Fabrication and in vitro and in vivo cell infiltration study of a bilayered cryogenic electrospun poly(D,L-lactide) scaffold. *Journal of biomedical materials research Part A*, 94(4):1141–9

[248] Cao H, McHugh K, Chew S Y, and Anderson J M (2010). The topographical effect of electrospun nanofibrous scaffolds on the in vivo and in vitro foreign body reaction. *Journal of biomedical materials research Part A*, 93(3):1151–9

[249] Tang L, Ugarova T P, Plow E F, and Eaton J W (1996). Molecular determinants of acute inflammatory responses to biomaterials. *The Journal of clinical investigation*, 97(5):1329–34

[250] Boland E D, Telemeco T A, Simpson D G, Wnek G E, and Bowlin G L (2004). Utilizing acid pretreatment and electrospinning to improve biocompatibility of poly(glycolic acid) for tissue engineering. *Journal of biomedical materials research Part B, Applied biomaterials*, 71(1):144–52